



BNXXXX-v0.0
December 15, 2022

Measurement of inclusive $B \rightarrow \Lambda_c$ branching fractions using Belle data and hadronic Full Event Interpretation

Leonardo Benjamin Rizzato¹.

¹*Institute Jožef Stefan, Ljubljana, Slovenia*

Abstract

Inclusive $B \rightarrow \Lambda_c$ branching fractions were measured most recently by BaBar collaboration. However, the measurement still presented a poor accuracy. A more precise measurement of inclusive $B \rightarrow \Lambda_c$ branching fraction could be useful to gain a better confidence on B meson weak decays treatment. With help of the Full Event Interpretation algorithm, it is possible to perform a more precise measurement of inclusive $B \rightarrow \Lambda_c$ branching fractions using Belle data set.

Changelog

Version 1.0

Version for first review

- introduced the argumentation about the crossfeed ratio parametrization in Sec.4.2
- updated Fig. 34 in Sec.4.2, Table 1, Fig. 36 and Fig. 37 (adjusting the comments)
- changed the linearity tests plots for charged correlated decays (Fig. 38 - Fig. 39 and Fig. 82 and Fig. 83 for anticorrelated decays)
- updated the systematics for chargeed correlated decays: summary Table 2, Sec. 4.8 updated with the results from the 2D fit (having the crossfeed ratio param.), same for Sec. 4.9. And for charged anticorrelated decays: summary Table 13 and Sections 6.8 -6.9.
- added the section about the systematics deriving from the parametrization of crossfeed normalization in the 2D fit (Sec. 4.10 and in charged anticorrelated decays Sec. 6.10), which takes into account the statistical uncertainties of the parameters.
- added the sections about the crossfeed peaking fraction in the 2D fit for anticorrelated decays (Sec. 4.11 and Sec. 6.11)
- Updated Table 12 for anticorrelated decays and also the corresponding plots.
- updated Table 17 for BR values of charged anticorrelated decays
- in the control sample chapter, updated Section 5.6 for the 2D fit on data, just adding the 2D fit performed on data using the parametrized normalization of crossfeed background, with results. And in the last section Sec. 5.13 added the new BR measured value for data.

Contents

1	Introduction	1
1.1	Analysis Setup	1
1.2	Datasets	1
2	Event selection and reconstruction	2
2.1	B_{tag} reconstruction	2
2.2	Λ_c reconstruction	2
2.3	Wrongly reconstructed B_{tag} candidates	3
3	Signal selection optimization	4
4	$B^- \rightarrow \Lambda_c^+$ decays	6
4.1	Probability Density Functions (PDFs) for the two dimensional fit	11
4.2	Two dimensional fit	27
4.3	Probability Density Functions (PDFs) for the B_{tag}	33
4.4	B_{tag} fit	35
4.5	Λ_c and FEI efficiency	36
4.6	Studies of Systematic Effects	38
4.7	Continuum background modeling	38
4.8	Crossfeed background modeling	40
4.9	Crossfeed ratio	40
4.10	Parametrization of crossfeed normalization in the 2D fit	41
4.11	Crossfeed peaking fraction in the 2D fit	41
4.12	Efficiencies	42
4.13	Fit biases	42
4.14	PID efficiency correction	43
4.15	crossfeed peak fraction	43
4.16	Sideband fit on data	44
4.17	Measured $B^+ \rightarrow \bar{\Lambda}_c^- X$ inclusive Branching Fraction	45
5	$B^- \rightarrow D^0$ control decay	46
5.1	Dataset used	46
5.2	Event selection and reconstruction	46
5.3	Signal selection optimization	46
5.4	Probability Density Functions (PDFs) for two dimensional fit	47
5.5	2D Fit on Monte Carlo simulated data	51
5.6	2D Fit on data	52
5.7	Probability Density Functions (PDFs) for the B_{tag}	54
5.8	B_{tag} Fit on Monte Carlo simulated data	55
5.9	B_{tag} Fit on data	57
5.10	PID efficiency correction	58
5.11	D^0 and FEI efficiency	58

5.12	Studies of Systematic Effects	59
5.13	Measured $B^+ \rightarrow \bar{D}^0 X$ inclusive Branching Fraction	59
6	$B^- \rightarrow \bar{\Lambda}_c^-$ decays	61
6.1	Probability Density Functions (PDFs) for the two dimensional fit	61
6.2	Two dimensional fit	67
6.3	Probability Density Functions (PDFs) for the B_{tag}	72
6.4	B_{tag} fit	74
6.5	Λ_c and FEI efficiency	75
6.6	Studies of Systematic Effects	76
6.7	Continuum background modeling	76
6.8	Crossfeed background modeling	78
6.9	Crossfeed ratio	78
6.10	Parametrization of crossfeed normalization in the 2D fit	79
6.11	Crossfeed peaking fraction in the 2D fit	79
6.12	Efficiencies	79
6.13	Fit biases	79
6.14	Measured $B^+ \rightarrow \Lambda_c^+$ inclusive Branching Fraction	79
Appendix		81
.1	$B^- \rightarrow \Lambda_c^+$ decays: additional plots	83
.2	$B^- \rightarrow D^0$ decays: additional plots	89
.3	$B^- \rightarrow \bar{\Lambda}_c^-$ decays: additional plots	93

¹ 1 Introduction

² Inclusive B meson baryonic decays with a Λ_c baryon in the final state are the most
³ abundant, due to a relatively large V_{cb} element of the CKM matrix. The *BaBar* experiment
⁴ measured their branching fractions to be around the percent level (see ref. [1]). However, the
⁵ branching fractions were determined with big uncertainties: nearly 50% on the measured
⁶ values or, in the case of the $B^0 \rightarrow \Lambda_c^+$ decay, only an upper limit could be established.
⁷ A more precise measurement of inclusive $B \rightarrow \Lambda_c$ branching fractions may shed light on
⁸ the appropriateness of B meson weak decays treatment, particularly of strong interaction
⁹ effects modelling. Predictions for inclusive branching fractions are given, for example, in
¹⁰ ref. [2].

¹¹ Exploiting the Full Event Interpretation (FEI) algorithm, developed for the Belle
¹² II experiment, it may be possible to perform a more precise measurement of inclusive
¹³ $B \rightarrow \Lambda_c$ branching fractions, using the full Belle data set. A more precise measurement
¹⁴ may also trigger further research on currently scarce theory predictions for B meson decays
¹⁵ to charm baryons.

¹⁶ 1.1 Analysis Setup

¹⁷ The reconstruction is performed with BASF2 release 05-02-03 together with the `b2bii`
¹⁸ package in order to convert the *Belle* MDST files (BASF data format) to *Belle II* MDST files
¹⁹ (`BASF2` data format). The FEI version used is `FEI_B2BII_light-2012-minos`.

²⁰ 1.2 Datasets

²¹ The Belle detector acquired a dataset of about $L_0 \approx 710 fb^{-1}$ of integrated luminosity in
²² its lifetime at the $\Upsilon(4S)$ energy of 10.58 GeV, which corresponds to about $771 \times 10^6 B\bar{B}$
²³ meson pairs. Additionally, several streams of Monte-Carlo (MC) samples were produced,
²⁴ where each stream of MC corresponds to the same amount of data that was taken with
²⁵ the detector. No specific signal MC was used: instead of producing dedicated signal MC
²⁶ samples, the samples were obtained by filtering the decays of interest from the generic
²⁷ on-resonance MC samples. The following samples were used in this analysis:

- ²⁸ • data
- ²⁹ • MC - 10 streams of B^+B^- and $B^0\bar{B}^0$ (denoted as `charged` and `mixed`) for signal
³⁰ decays and backgrounds.
 - ³¹ - 6 streams of $q\bar{q}$ produced at $\Upsilon(4S)$ resonance energy
 - ³² - 6 streams of $q\bar{q}$ produced at 60 MeV below $\Upsilon(4S)$ resonance energy, where each
³³ stream corresponds to $1/10 \times L_0$.

35 2 Event selection and reconstruction

36 In this chapter the procedure for reconstruction of the events where one B meson decays
37 inclusively to a Λ_c baryon and the accompanying B meson decays hadronically.

38 2.1 B_{tag} reconstruction

39 The FEI is an exclusive tagging algorithm that uses machine learning to reconstruct
40 B meson decay chains and calculates the probability that these decay chains correctly
41 describe the true process. In this analysis only hadronically reconstructed decay chains
42 are considered. The training called `FEI_B2BII_light-2012-minos` is used. Tag-side B
43 meson candidates are required to have a beam-constrained mass greater than $5.22 \text{ GeV}/c^2$
44 and $-0.15 < \Delta E < 0.07 \text{ GeV}$.

45 In the case of multiple candidates in the same event, the candidate with the highest
46 SignalProbability (the signal probability calculated by FEI using FastBDT) is chosen. To
47 suppress the background consisting of B^0 events misreconstructed as B^+ (and vice-versa)
48 from neutral (charged) decays also a B^0 (B^+) candidate is reconstructed with FEI and if
49 its SignalProbability is higher than the charged (neutral) reconstructed B meson, the event
50 is discarded. This constitutes a sort of crossfeed-veto, rejecting part of events belonging
51 to the other typology of decays of interest: for example in the case one is interested
52 in reconstructing $B^{+/-}$ decays and the event actually contains B^0/\bar{B}^0 decays, the FEI
53 reconstructed neutral B meson candidate most likely presents a higher SignalProbability
54 than the charged FEI reconstructed candidate.

55 2.2 Λ_c reconstruction

56 In the *rest of event* (ROE) of the reconstructed B_{tag} meson, to select $\Lambda_c \rightarrow pK\pi$ signal
57 candidates, the following event selection criteria are applied. Charged tracks with the
58 impact parameters perpendicular to and along the nominal interaction point (IP) are
59 required to be less than 2 cm and 4 cm respectively ($dr < 2 \text{ cm}$ and $|dz| < 4 \text{ cm}$).

60 The pion tracks are required to be identified with $\frac{\mathcal{L}_\pi}{\mathcal{L}_K + \mathcal{L}_\pi} > 0.6$. The kaon tracks are
61 required to be identified with $\frac{\mathcal{L}_K}{\mathcal{L}_K + \mathcal{L}_\pi} > 0.6$, and the proton/anti-proton tracks are
62 required to be identified with $\frac{\mathcal{L}_{p/\bar{p}}}{\mathcal{L}_K + \mathcal{L}_{p/\bar{p}}} > 0.6$ and $\frac{\mathcal{L}_{p/\bar{p}}}{\mathcal{L}_\pi + \mathcal{L}_{p/\bar{p}}} > 0.6$, where the $\mathcal{L}_{\pi,K,p/\bar{p}}$ are the
63 likelihoods for pion, kaon, proton/anti-proton, respectively, determined using the ratio of
64 the energy deposit in the ECL to the momentum measured in the SVD and CDC, the
65 shower shape in the ECL, the matching between the position of charged track trajectory
66 and the cluster position in the ECL, the hit information from the ACC and the dE/dx
67 information in the CDC.

68 For the Λ_c candidates a vertex fit is performed with `TreeFitter`, requiring it to converge.
69 If there are more than one Λ_c combination, then the best candidate based on the χ^2
70 probability is chosen. The Λ_c signal region is defined to be $|M_{\Lambda_c} - m_{\Lambda_c}| < 20 \text{ MeV}/c^2$ (\sim
71 3σ), here m_{Λ_c} is the nominal mass of m_{Λ_c} .

72

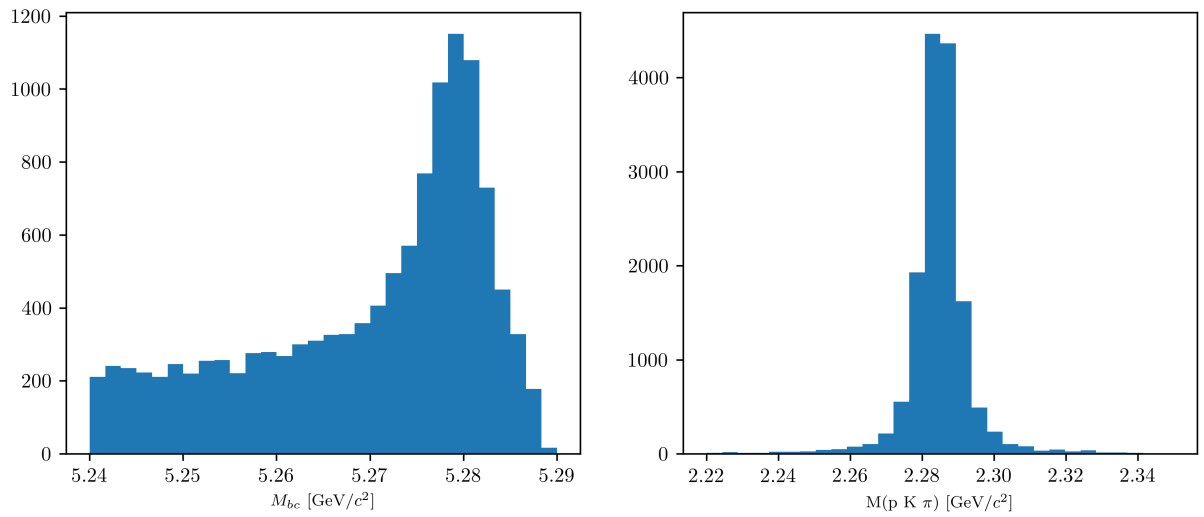


Figure (1) M_{bc} and $M(pK\pi)$ distributions of B_{tag} and Λ_c candidates reconstructed in the signal sample.

73 2.3 Wrongly reconstructed B_{tag} candidates

74 In the case of the signal sample the distributions for the beam-constrained mass M_{bc} and
75 for the correctly reconstructed Λ_c candidates, look like in Fig. 1. If one then investigates
76 the M_{bc} distribution of the B_{tag} candidates reconstructed with FEI, it can be seen that
77 there is a peaking structure for wrongly reconstructed B mesons (as in Fig. 2), according
78 to the BASF2 internal truth matching variable **isSignal**. It is obvious from this that the
79 BASF2 internal truth matching variable cannot be used to separate properly the signal
80 events in correctly and wrongly reconstructed B mesons. In the study BELLE2-NOTE-TE-
81 2021-026 <https://docs.belle2.org/record/2711/files/BELLE2-NOTE-TE-2021-026.pdf> a possible solution was found developing new variables that can be used for an
82 improved truth matching for the FEI (those variables were added to a newer BASF2
83 release than the one used for this study). In the present study instead a more "traditional"
84 approach was adopted: fitting the M_{bc} distribution with a sum of PDFs that account for the
85 flat (background) component and the peaking (signal) component. The first component
86 represents the combinatorial background, i.e. B mesons that were mis-reconstructed,
87 and therefore those events are denoted from now on as "**misreconstructed signal**".
88 The peaking component represents the correctly reconstructed signal events in M_{bc} and
89 therefore denoted from now on as "**reconstructed signal**". Only the second one is then
90 considered for the signal yield, while the first is counted as a background. To validate this
91 method a control decay study was performed on the flavor correlated $B^+ \rightarrow \bar{D}^0$ channel.
92

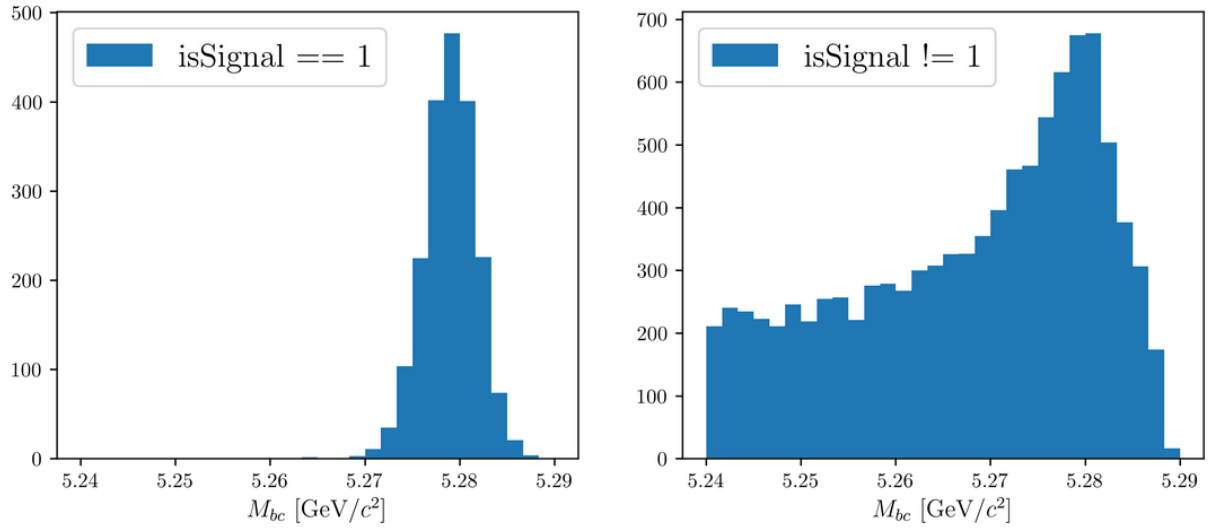


Figure (2) M_{bc} distribution of B_{tag} candidates reconstructed in the signal sample, truth-matched (on the left) and not (on the right).

93 3 Signal selection optimization

94 To further enhance the purity of the signal decays, an optimization procedure is adopted
 95 to determine optimal cuts for a set of variables for each decay mode under investigation
 96 by this study. The cuts on the following variables are optimized:

- 97 • *foxWolframR2*: the event based ratio of the 2-nd to the 0-th order Fox-Wolfram
 98 moments
- 99 • *SignalProbability*: the already mentioned signal probability calculated by FEI using
 100 FastBDT
- 101 • $p_{CMS}^{\Lambda_c}$: momentum of the Λ_c candidates in the center of mass system

102 The optimization is based on the Figure Of Merit (FOM): $FOM = \frac{S}{\sqrt{S+B}}$
 103 Where S and B are respectively signal and background events in the signal region:
 104 $M_{bc} > 5.27 \text{ GeV}/c^2$, $2.2665 < M(pK\pi) < 2.3065 \text{ GeV}/c^2$.

105 Due to the issue reported in Sec. 2.3, to separate signal events that peak in M_{bc} from
 106 the ones that are not (which are then categorized as background events), the events
 107 reconstructed in the signal sample are fitted with a sum of Crystal Ball function and
 108 Argus for each cut value on the corresponding variable to optimize (as in Fig. 3).

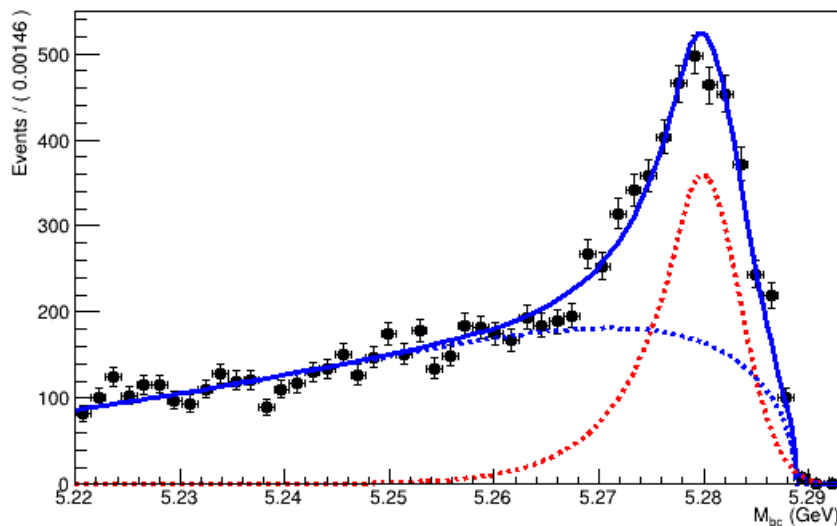


Figure (3) Example of a fit used to separate the correctly reconstructed B mesons (described by the red dotted Crystal Ball function) from the wrongly reconstructed ones (described by the blue dotted Argus function).

¹⁰⁹ **4 $B^- \rightarrow \Lambda_c^+ \text{ decays}$**

¹¹⁰ First, in order to suppress the continuum background the cut on *foxWolframR2* is
¹¹¹ optimized. Fig. 4 shows the *foxWolframR2* distributions for signal and continuum
events.

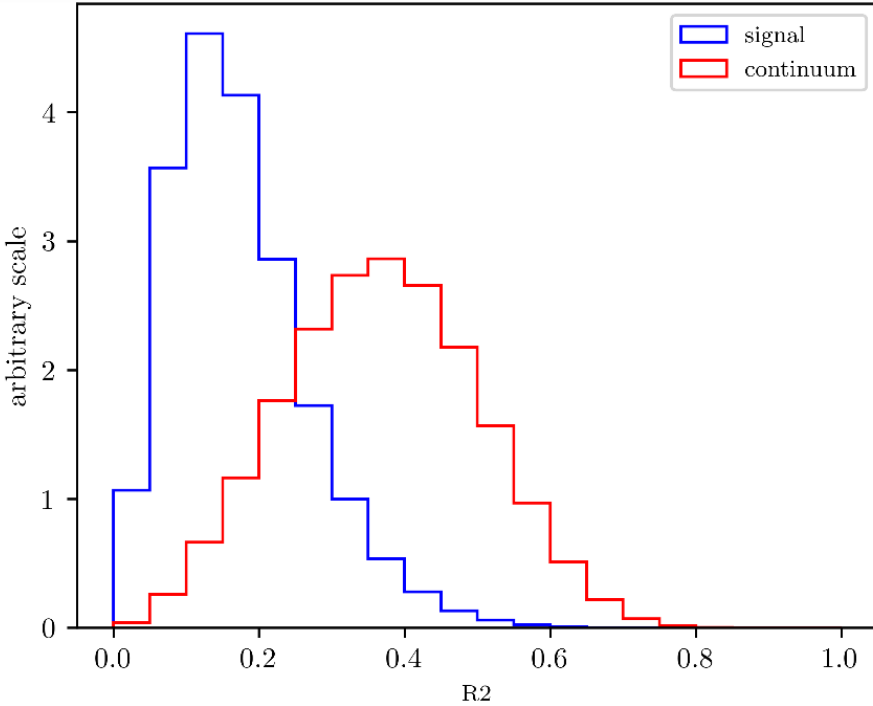


Figure (4) Distribution of the *foxWolframR2* variable for signal and continuum background events.

¹¹²
¹¹³ With the optimized cut $\text{foxWolframR2} < 0.27$, the cut on SignalProbability is
¹¹⁴ optimized in the same way (see Fig. 7).

¹¹⁵
¹¹⁶ With the optimized cut SignalProbability > 0.01 , the cut on *foxWolframR2* variable is
¹¹⁷ rechecked (Fig. 8). Being the maximum values fluctuating around *foxWolframR2* < 0.3 ,
this cut is the one finally chosen for this variable.

¹¹⁸
¹¹⁹ With the optimized cuts on SignalProbability and *foxWolframR2* variable, the cut
on $p_{CMS}^{\Lambda_c}$ is optimized

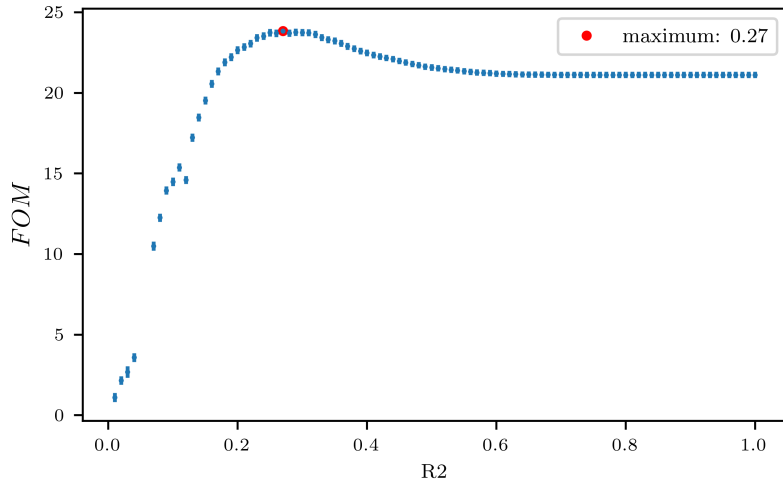


Figure (5) Figure of Merit values calculated at several cuts on the *foxWolframR2* variable

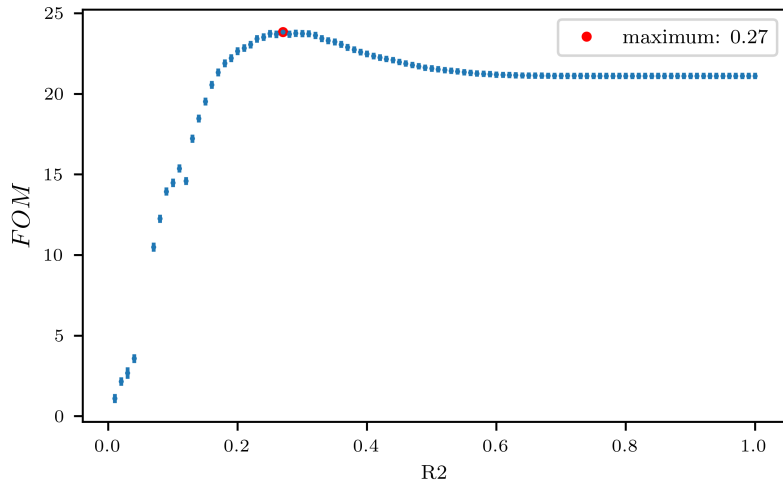


Figure (6) Figure of Merit values calculated at several cuts on the *foxWolframR2* variable

121 From Fig. 9 one can see that with values of the cut above $p_{CMS}^{\Lambda_c} < 1.8 \text{ GeV}/c^2$ a
 122 plateau of maximum FOM values is reached. But such a cut would still be useful to reject
 123 some background events as one can see from Fig. 10.

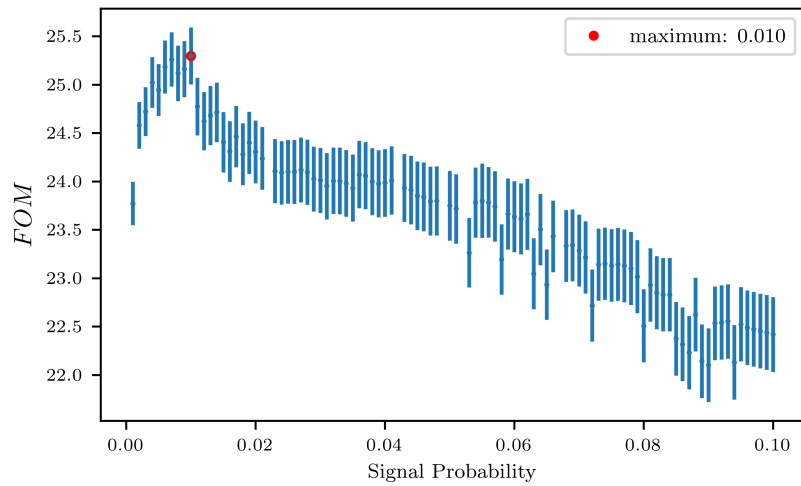


Figure (7) Figure of Merit values calculated at several cuts on the SignalProbability variable

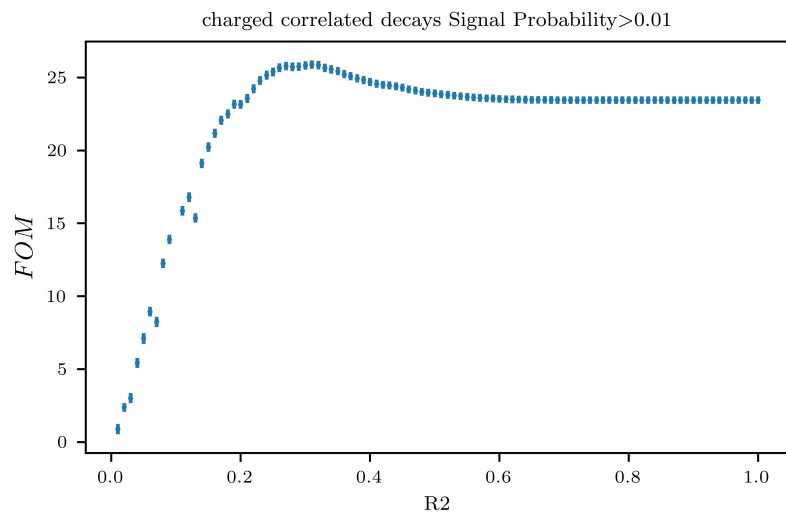


Figure (8) Figure of Merit values calculated at several cuts on the *foxWolframR2* variable

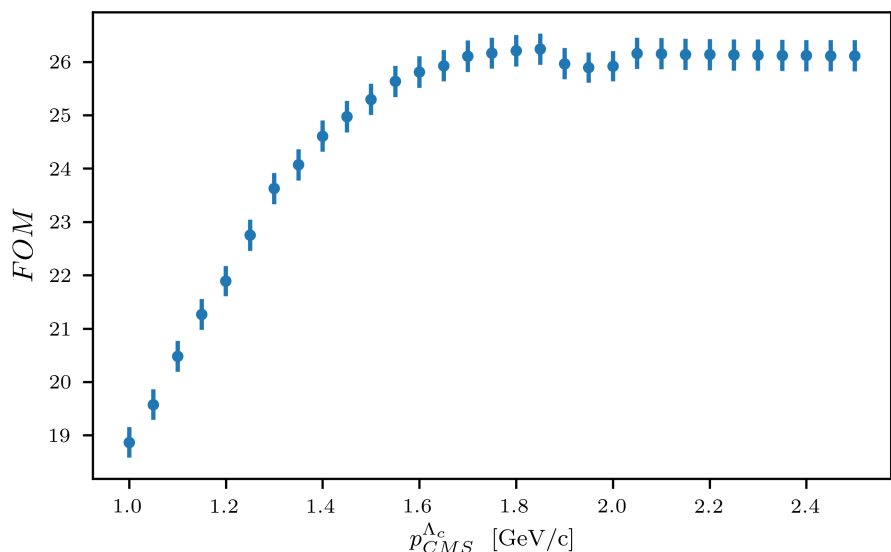


Figure (9) Figure of Merit values calculated at several cuts on the momentum of the Λ_c candidates in the center of mass system

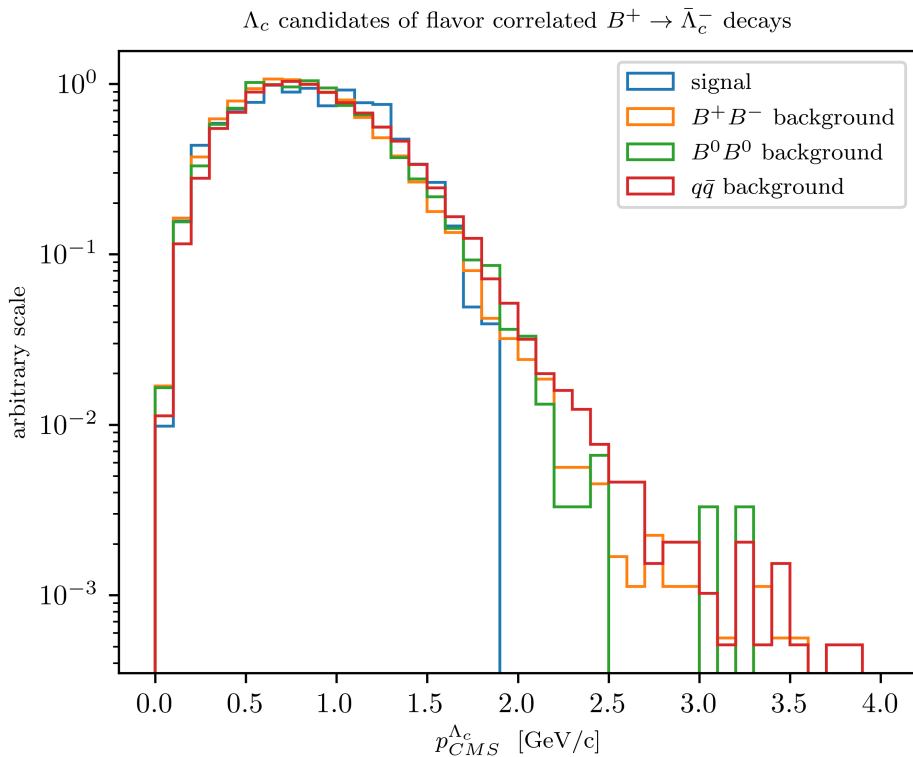


Figure (10) Distribution of Λ_c candidates momenta in the center of mass system

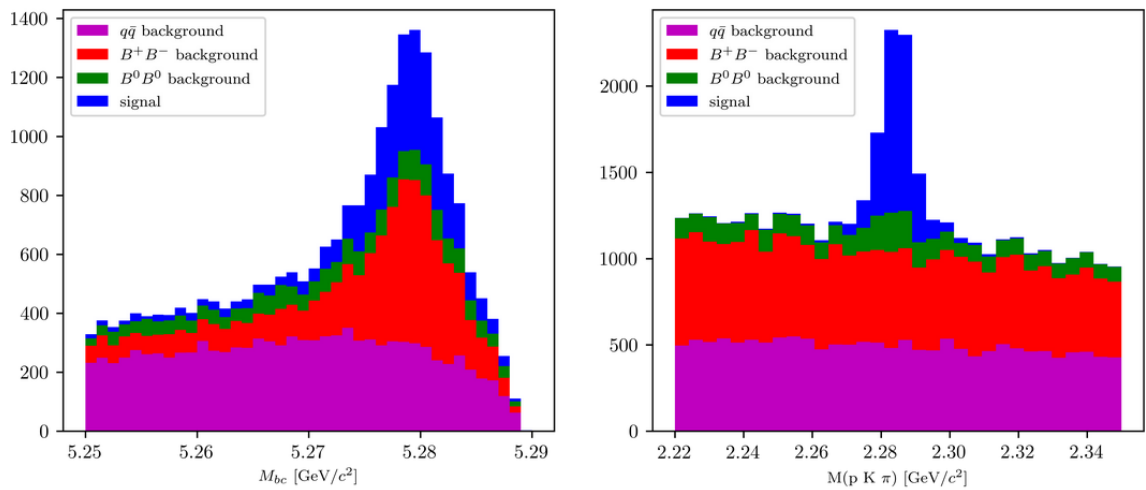


Figure (11) Distribution of M_{bc} (left) and invariant mass of charged correlated Λ_c candidates (right), in the signal region after the above mentioned selection cuts.

128 To measure the inclusive branching fraction of $B^- \rightarrow \Lambda_c^+ X$ the following quantities
 129 need to be known:

$$Br(B^- \rightarrow \Lambda_c^+ X) = \frac{N_{tag,\Lambda_c} \cdot \epsilon_{FEI}^+}{N_{tag} \cdot Br(\Lambda_c^+ \rightarrow pK^-\pi^+) \epsilon_{\Lambda_c} \epsilon_{FEI,sig}^+} \quad (1)$$

130

131 Where

- 132 • N_{tag,Λ_c} is the reconstructed signal yield obtained from a two dimensional fit of M_{bc}
 133 and $M(pK\pi)$ in the final sample.
- 134 • N_{tag} is the reconstructed signal yield obtained from the M_{bc} fit of all the tagged B
 135 mesons in the final sample.
- 136 • ϵ_{Λ_c} is the Λ_c reconstruction efficiency.
- 137 • ϵ_{FEI}^+ represents the hadronic tag-side efficiency for generic B^+B^- events.
- 138 • $\epsilon_{FEI,sig}^+$ represents the hadronic tag-side efficiency for B^+B^- events where the tagged
 139 B meson decays hadronically and the accompanying meson decays inclusively into
 140 the studied signal channel.
- 141 • $Br(\Lambda_c^+ \rightarrow pK^-\pi^+)$: the branching fraction of the decay mode used to reconstruct
 142 the Λ_c baryon.

143 Here a decision was made not to rely on the estimated number of B meson pair, as it is
 144 usually done, and the absolute FEI efficiency, since the latter shows large discrepancy
 145 between MC and data (see i.e. the results reported in the PhD Thesis by M. Gelb [3] and
 146 also by J. Schwab [4]) and also it depends strongly on the signal-side (i.e. $\epsilon_{FEI}^+ \neq \epsilon_{FEI,sig}^+$).
 147 Instead, to limit the systematics, the branching ratio normalization is obtained using the
 148 fitted tagged B mesons and the ratio $\epsilon_{FEI,sig}^+/\epsilon_{FEI}^+$ measured on MC, which is expected to
 149 be described much better rather than the absolute FEI efficiency.

150 The final samples contain both signal and background candidates from various sources
 151 and in order to extract N_{tag,Λ_c} and N_{tag} unbinned extended maximum-likelihood fits are
 152 performed.

153 In the next sections the methods used to determine the above mentioned quantities are
 154 described. First the fit model that accurately describes the distributions in the $B_{tag} + \Lambda_c$
 155 final sample will be described.

156 4.1 Probability Density Functions (PDFs) for the two dimensional 157 fit

158 The PDFs used to describe the signal distributions are discussed first. The final sample of
 159 total signal events presents a peak around the expected B meson mass and a tail at low
 160 M_{bc} values.

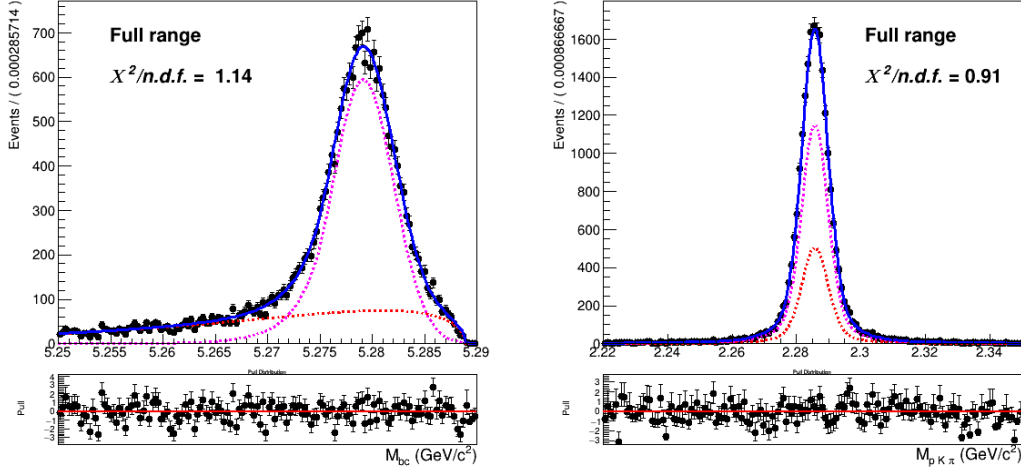


Figure (12) Two dimensional fit of total signal events in M_{bc} and $M(pK\pi)$

161 The 2D fit shown in Fig. 12 is performed on five streams of signal MC with a sum of
 162 the following probability density functions:

$$P_{B,\Lambda_c}^{recSig}(M_{bc}, M(pK\pi)) = \Gamma_{CB}(M_{bc}) \times \rho_G(M(pK\pi)) \quad (2)$$

163

$$P_{B,\Lambda_c}^{misSig}(M_{bc}, M(pK\pi)) = \Gamma_{ARG}(M_{bc}) \times \rho_G(M(pK\pi)) \quad (3)$$

164 The first is used to fit the reconstructed signal and $\Gamma_{CB}(M_{bc})$ is a Crystal Ball function.
 165 The second is used to model the misreconstructed signal and $\Gamma_{ARG}(M_{bc})$ is an Argus
 166 function. In both cases a sum of three Gaussian functions $\rho_G(M(pK\pi))$ describes the
 167 mass of the Λ_c baryon.
 168

169 As already said in Sec. 2.3, only the reconstructed signal considered for the signal
 170 yield, while the misreconstructed signal is considered as background. Other background
 171 components that will be discussed in the next pages are:

- 172
- **generic** (charged B) background

173

 - **crossfeed** (neutral B) background

174

 - **continuum** background

175 **Generic background**

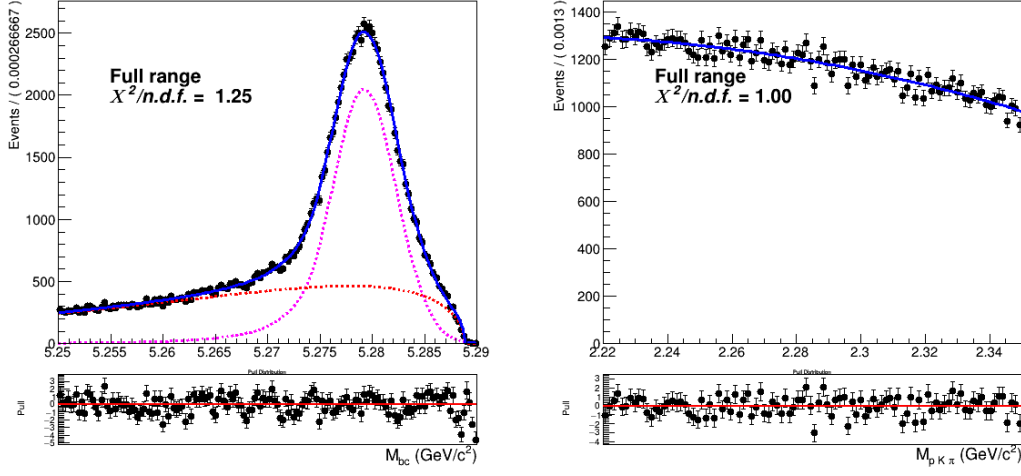


Figure (13) Two dimensional fit of generic (B^+B^-) events in M_{bc} and $M(pK\pi)$.

176 The generic background deriving from other B^+B^- events presents a similar shape of the
 177 distribution in M_{bc} (see Fig. 13): the probability density functions used for it are again a
 178 Crystal Ball and an Argus. For both functions the parameters differ from the ones used in
 179 Eq. 2-4.1. Instead, the flat background in $M(pK\pi)$ can be described with a second order
 180 Chebychev polynomial function. The two dimensional PDF in this case is given by:

$$P_{B,\Lambda_c}^{GenBkg}(M_{bc}, M(pK\pi)) = [\Gamma_{CB}(M_{bc}) + \Gamma_{ARG}(M_{bc})] \times \rho_{Cheb2}(M(pK\pi)) \quad (4)$$

181 **Crossfeed background**

182 The contamination of misreconstructed B^0 events in the B^+ signal (and vice-versa) induces
 183 a background which peaks near the B meson mass, as one can see in Fig. 14, independently
 184 from the category of events in the Λ_c mass (see Figures 15- 16). Since among the
 185 misreconstructed B^0 events there are also $B^0 \rightarrow \Lambda_c$ decays (peaking at the Λ_c mass, see
 186 e.g. Fig. 15), this background contribution is also named "crossfeed background".

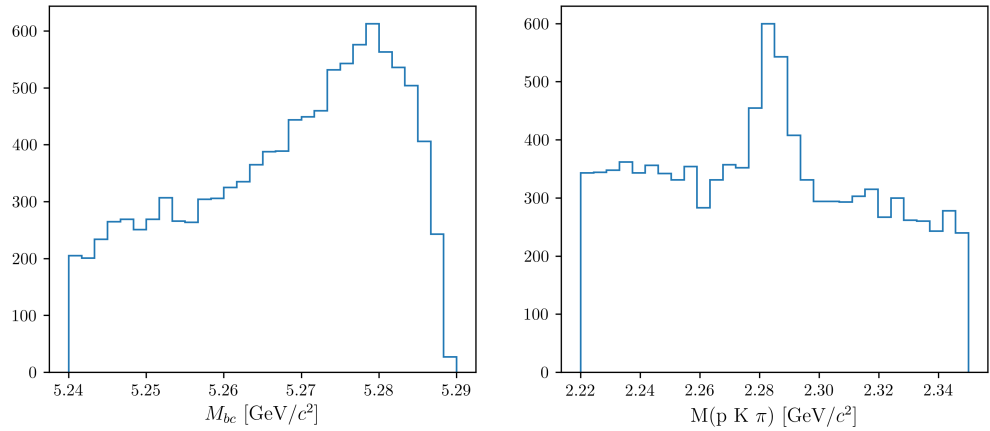


Figure (14) M_{bc} and $M(pK\pi)$ distributions of crossfeed background events.

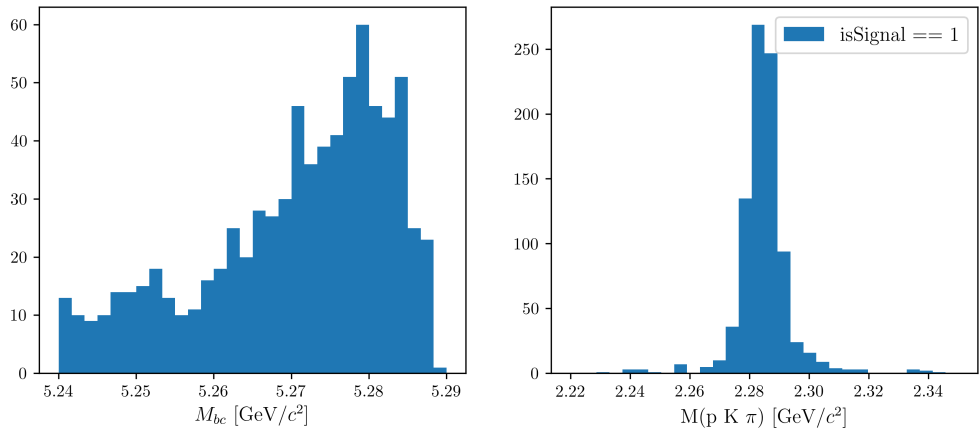


Figure (15) M_{bc} and $M(pK\pi)$ of crossfeed events peaking at the Λ_c mass, i.e.: where true Λ_c baryons were correctly reconstructed.

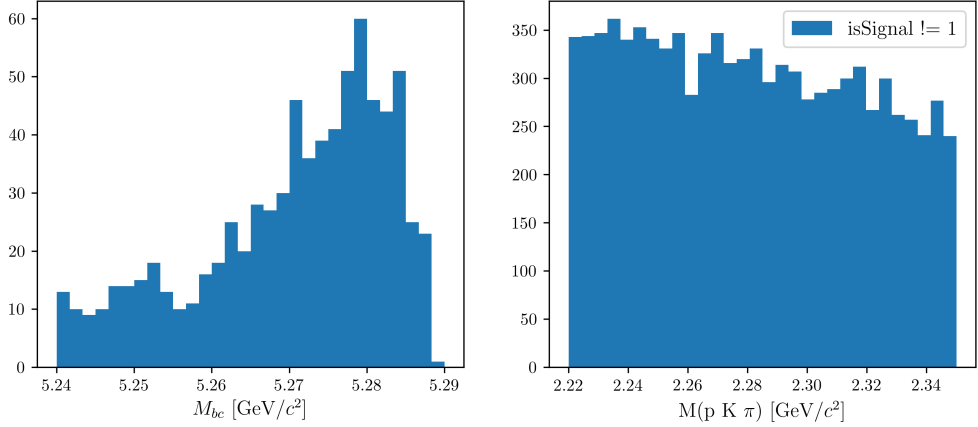


Figure (16) M_{bc} and $M(pK\pi)$ of crossfeed events without Λ_c peak, i.e.: where Λ_c baryons were not present or not correctly reconstructed.

Fig. 17 shows the projections in M_{bc} and $M(pK\pi)$ of the two dimensional fit of this type of background. The M_{bc} is modelled with a sum of Novosibirsk (colored in magenta) and Argus function (colored in red). Whereas the $M(pK\pi)$ distribution is described by the sum of a first order Chebychev polynomial and the peak by the same sum of three Gaussian functions used to describe the signal peak. In fact the latter is the result of the reconstruction of crossfeed events $B^0 \rightarrow \Lambda_c$. Therefore the 2D PDF can be written as:

193

$$P_{B,\Lambda_c}^{CrossBkg}(M_{bc}, M(pK\pi)) = [\Gamma_{Nov}(M_{bc}) + \Gamma_{ARG}(M_{bc})] \times [\rho_{Cheb1}(M(pK\pi)) + \rho_G(M(pK\pi))] \quad (5)$$

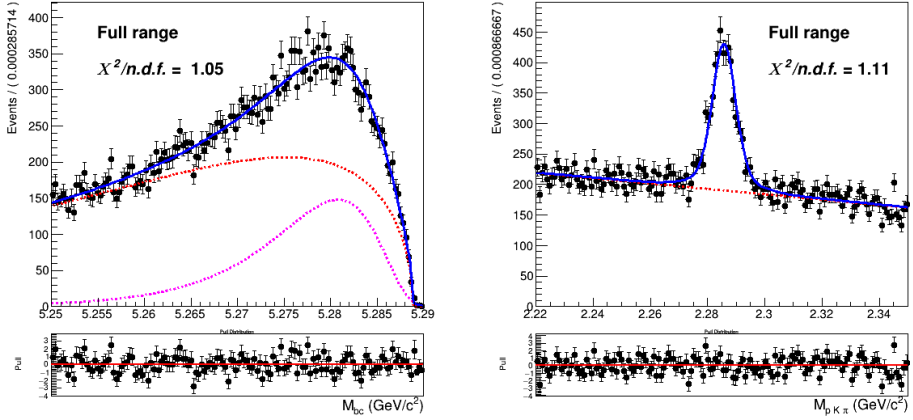


Figure (17) Two dimensional fit of crossfeed ($B^0 \bar{B}^0$) events in M_{bc} and $M(pK\pi)$.

From the projections plotted in Fig. 17 the distributions appear to be well described by the PDF discussed above. Though the agreement in the Λ_c invariant mass is not fully

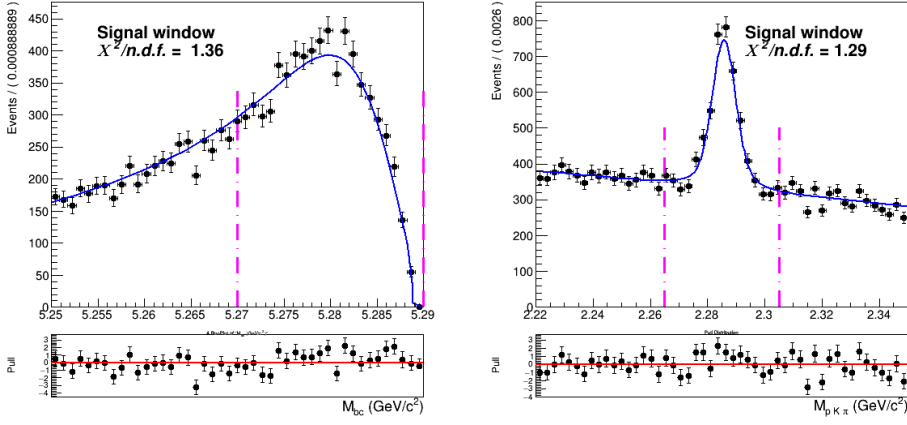


Figure (18) Signal region projections in M_{bc} and $M(pK\pi)$.

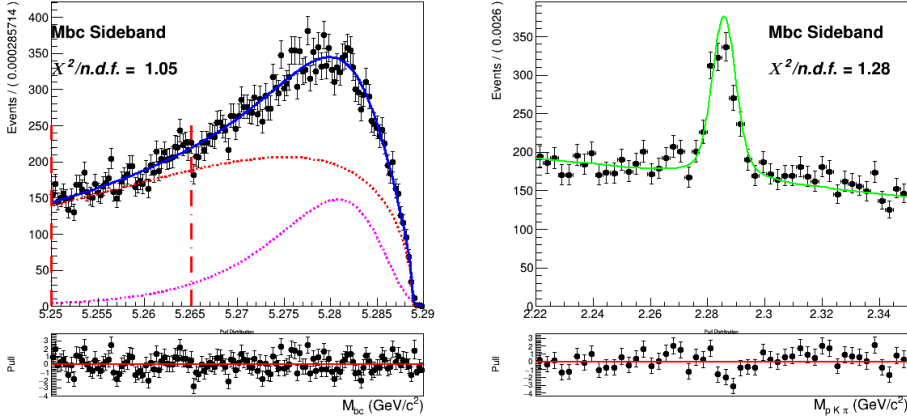


Figure (19) M_{bc} sideband region projection.

respected when different regions of M_{bc} are considered, as one can see from Fig. 18 and Fig. 19. The fraction of the amount of peaking events is not uniform among different M_{bc} regions. Since this background typology is peaking in both the observables of the fit, the potential correlation between them could have an impact on the signal yield extraction in the total fit.

To minimize this effect, and to avoid possible biases deriving from this feature, a correction is attempted. The M_{bc} is divided in 5 different regions. As shown in Figures ??-21e, for each of these regions a fit on the projected Λ_c invariant mass is performed to extract 5 values of the fraction of peaking events in those regions (all other parameters are fixed). Those values are then used for a parametrization of this parameter as a function of M_{bc} .

From the plot shown in Fig. 20 one can see that it is possible to describe the trend with a linear dependence with a good approximation.

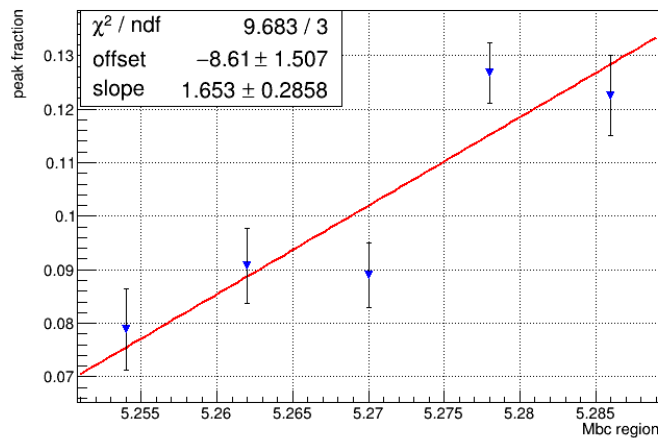


Figure (20) Invariant mass peak fraction as a function of M_{bc} .

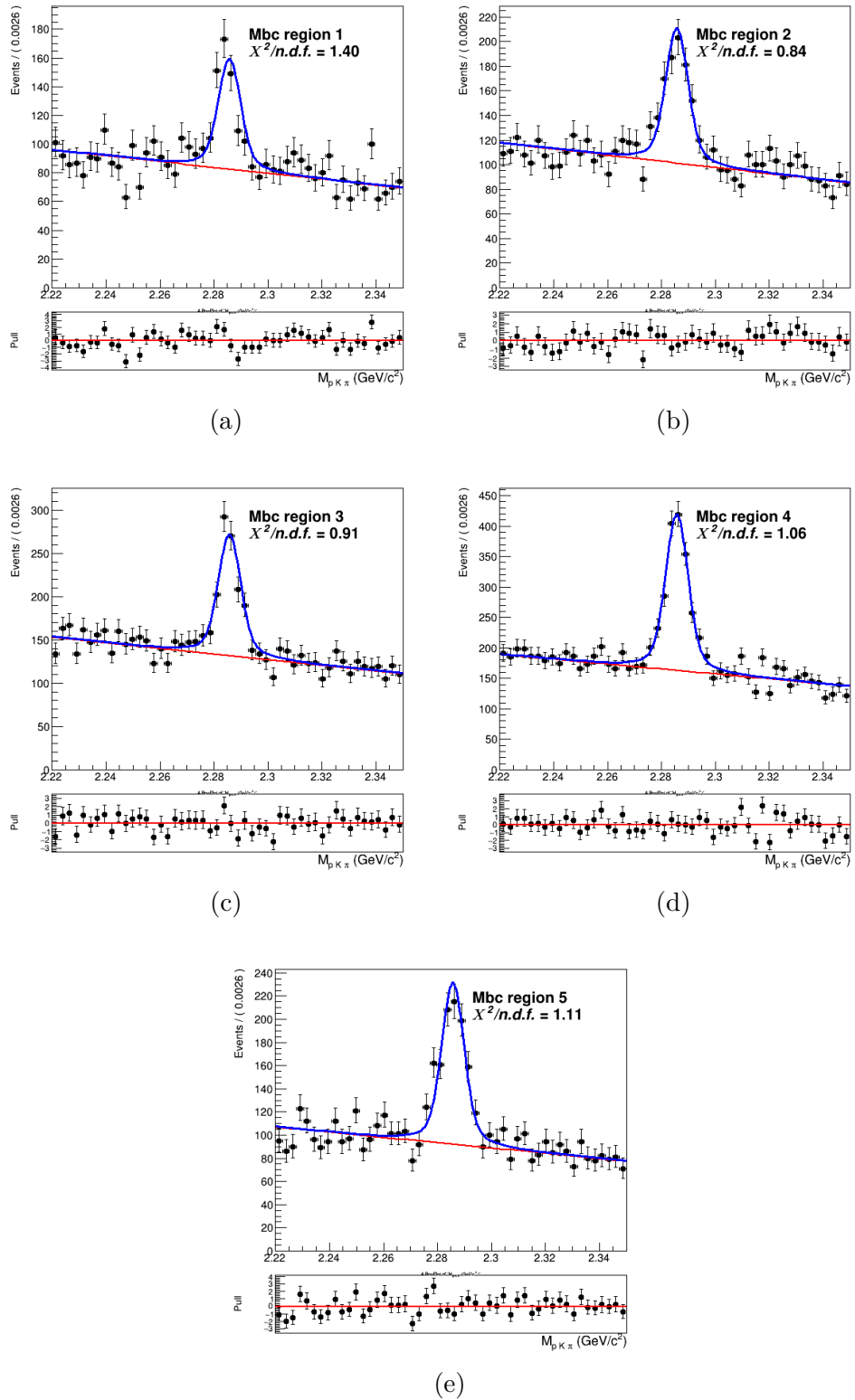


Figure (21) Fits of $M(pK\pi)$ in 5 different regions of M_{bc} : $5.25 < M_{bc} < 5.258 \text{ GeV}/c^2$, $5.258 < M_{bc} < 5.266 \text{ GeV}/c^2$, $5.266 < M_{bc} < 5.274 \text{ GeV}/c^2$, $5.274 < M_{bc} < 5.282 \text{ GeV}/c^2$, $5.282 < M_{bc} < 5.29 \text{ GeV}/c^2$.

209 The 2D PDF describing the crossfeed background is consequently modified:

$$P_{B,\Lambda_c}^{CrossBkg}(M_{bc}, M(pK\pi)) = [\Gamma_{Nov}(M_{bc}) + \Gamma_{ARG}(M_{bc})] \times [F(M(pK\pi)|M_{bc})] \quad (6)$$

210 where the conditional PDF $F(M(pK\pi)|M_{bc})$ describing the invariant mass is still a sum of
 211 $\rho_{Cheb1}(M(pK\pi))$ and $\rho_G(M(pK\pi))$, but their fraction is now parametrized as a function
 212 of M_{bc} .

213 In Figures 22- 23 one can appreciate the improvement obtained with this correction.

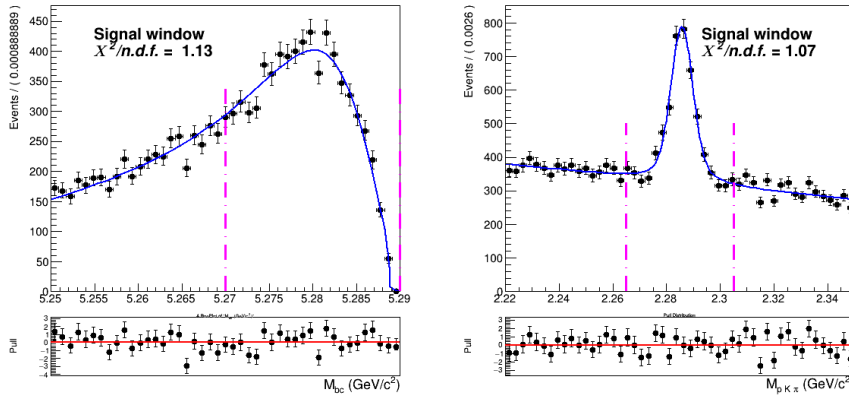


Figure (22) Signal region projections in M_{bc} and $M(pK\pi)$ after the parametrization.

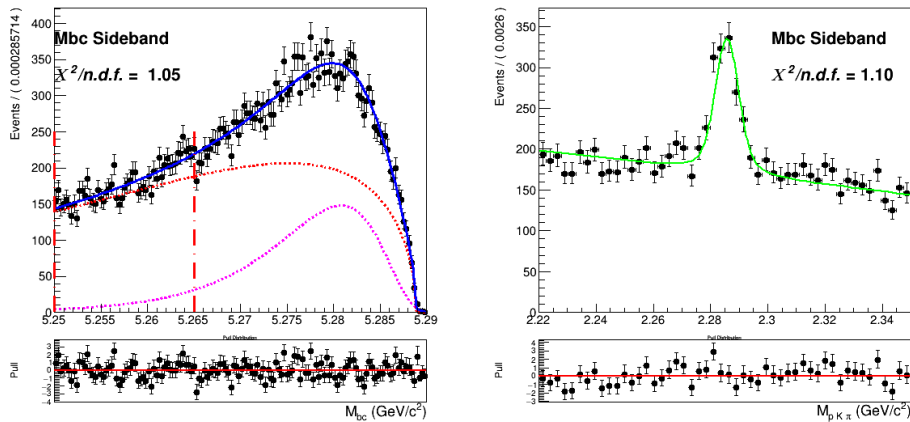


Figure (23) M_{bc} sideband region projection after the parametrization.

215 Continuum background

216 Besides the dataset recorded at the energy of the $\Upsilon(4S)$ resonance ($E_{CMS}^{on-res} = 10.58$ GeV),
 217 the *Belle* experiment recorded a sample of $89.4 fb^{-1}$ at an energy 60 MeV below the
 218 nominal $\Upsilon(4S)$ resonance ($E_{CMS}^{off-res} = 10.52$ GeV). The dataset allows to check for an
 219 appropriate modeling of the continuum MC simulation. Using the official tables
 220 (<https://belle.kek.jp/secured/nbb/nbb.html>) the off-resonance sample is scaled by

$$\frac{\mathcal{L}^{on-res}}{\mathcal{L}^{off-res}} \left(\frac{E_{CMS}^{off-res}}{E_{CMS}^{on-res}} \right)^2 \quad (7)$$

taking into account the difference in luminosity and in E_{CMS} (Energy in center of mass system).

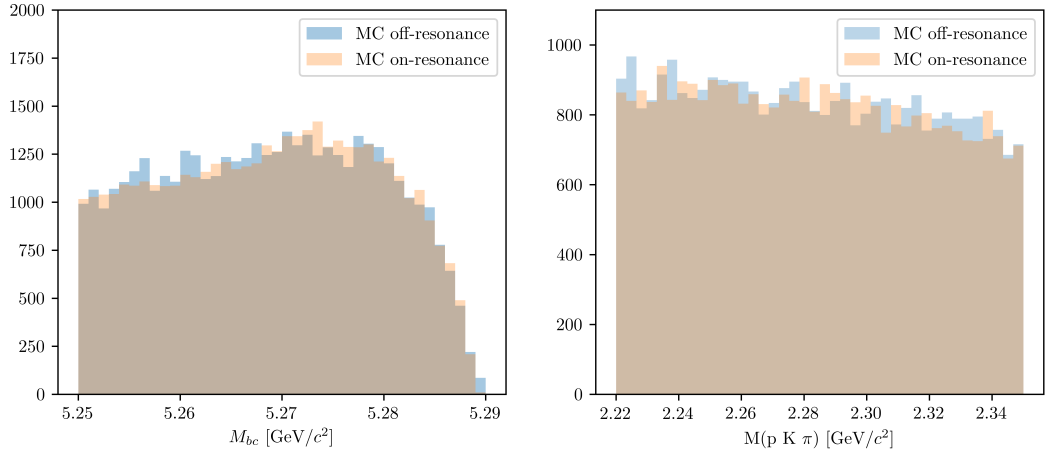


Figure (24) M_{bc} and $M(pK\pi)$ comparison between on-/off-resonance (scaled) Monte Carlo simulated continuum. The scaling is applied according to Eq. (7) and shifting the M_{bc} distribution by $E_{CMS}^{on-res} - E_{CMS}^{off-res}$.

The plot in Fig.24 shows the M_{bc} and $M(pK\pi)$ distributions in the MC on-/off-resonance continuum after the scaling¹.

Ideally, provided that there's a good agreement between MC and data for the off-resonance sample and also between the MC on-/off-resonance continuum after the scaling, one could directly use the scaled off-resonance data to describe the continuum background in the fit on data. There are two reasons that prevent this very straightforward approach:

- First, since the off-resonance MC (and data) present very low statistics (Fig. 26a shows the Λ_c invariant mass in off-resonance data), scaling them with all the applied selection cuts would cause the PDF describing the continuum to be very much affected by statistical fluctuations.
- Secondly, the B meson candidates are reconstructed in both on-resonance and off-resonance events for values of $M_{bc} \geq 5.22 \text{ GeV}/c^2$, but the E_{CMS} differs: there can be effects of correlations between the applied *SignalProbability* cut and the M_{bc} variable that one needs to take into account.

¹it is obtained with the MC off-resonance sample being composed of 6 streams: the total amount is normalized

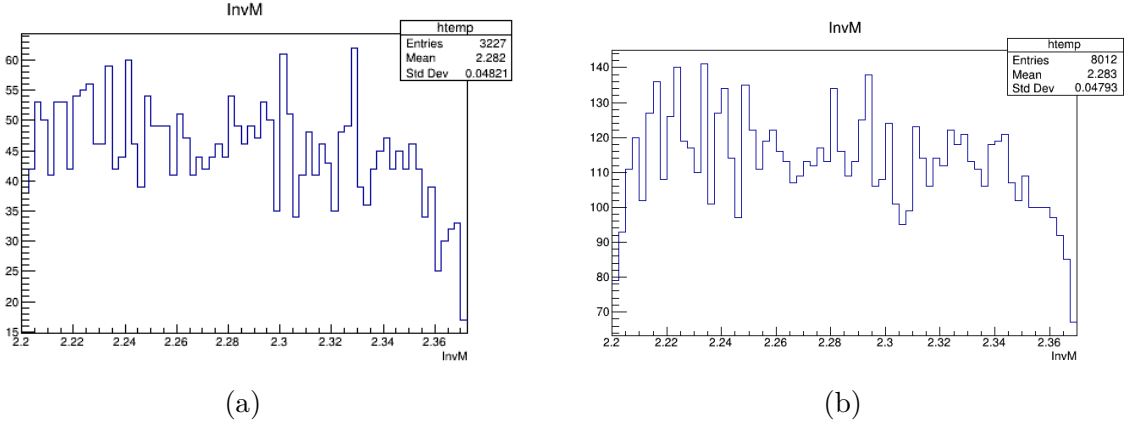


Figure (26) On the left: Λ_c invariant mass in off-resonance data (all nominal cuts applied). On the right: Λ_c invariant mass in off-resonance data after the continuum suppression cut removal.

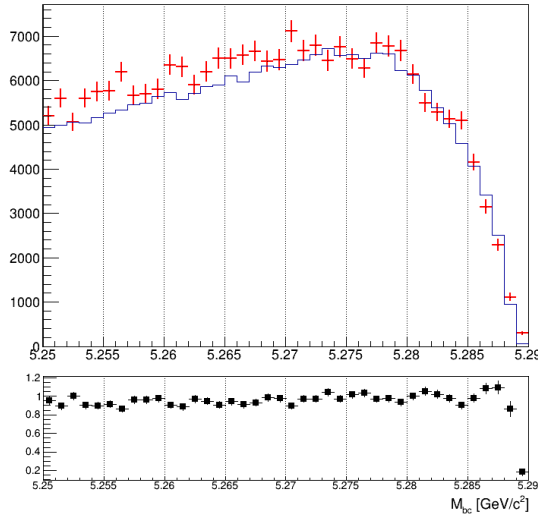


Figure (25) M_{bc} distributions of the MC (scaled) off-resonance sample (in red) and on-resonance (in blue) using 5 streams statistics and all nominal selection cuts applied.

237 In Fig. 25 one can notice some discrepancy in the shapes, apart from the not negligible
 238 statistical fluctuations in the (scaled) off-resonance distribution. In the Λ_c invariant mass
 239 one doesn't expect correlation effects, but nevertheless there can be differences due to
 240 the limited statistics of the off-resonance sample. In fact, in the case of on-resonance MC
 241 some events in which Λ_c candidates survive nominal selection cuts are visible and can
 242 be described with a small Gaussian on the top of the flat background (Fig.31a). On the
 243 contrary the off-resonance sample doesn't show anything else beside the flat background
 244 (the Fig.31b shows a 5 streams statistics).

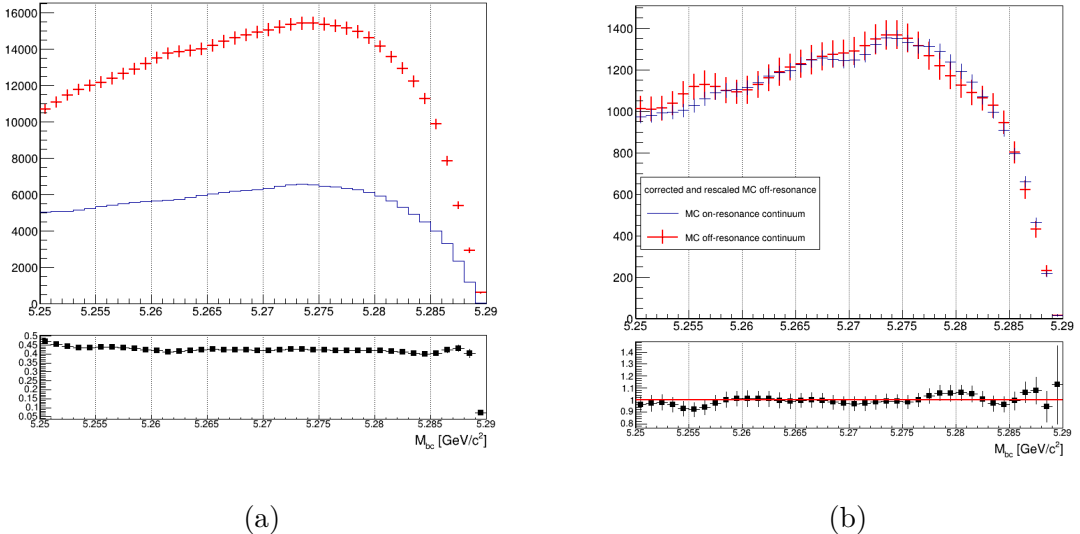


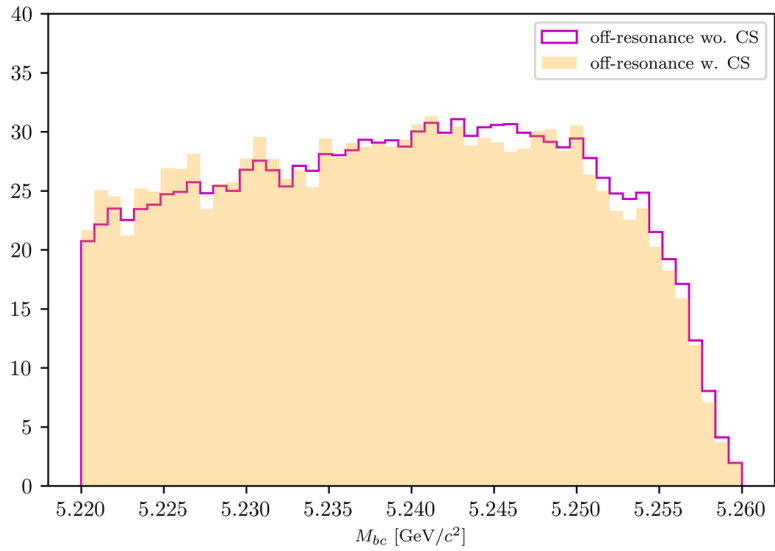
Figure (27) On the left: M_{bc} distributions of the MC off-resonance sample without continuum suppression and the MC continuum sample with applied continuum suppression. On the right: M_{bc} distributions of the corrected scaled MC off-resonance and on-resonance MC continuum.

245 The procedure adopted to obtain the PDF describing the continuum background M_{bc}
246 distribution is the following:

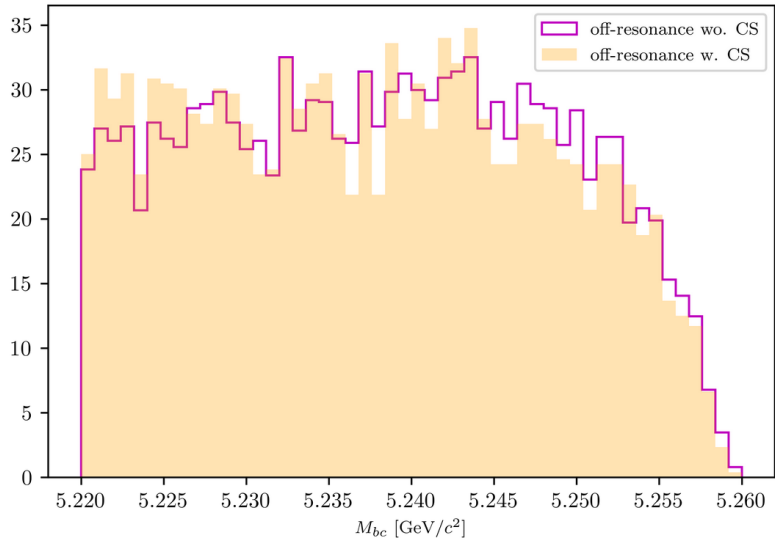
- 247
- 5 streams of off-resonance MC were scaled according to Eq. (7) without continuum
248 suppression being applied and compared to the distribution of 5 streams of on-
249 resonance continuum
 - From a ratio plot, like the one in Fig. 27a, the bin-correction is obtained to correct
250 the off-resonance data in the scaling procedure. To obtain the shape that can describe
251 the continuum background M_{bc} distribution on data the continuum suppression is not
252 applied on the off-resonance continuum sample, in order to acquire more statistics.
253

254 This procedure is first tested on an independent MC sample (see Fig. 27b) to check the
255 result on simulated data before applying it on data.

256 The validity of the method relies on the fact that on-/off-resonance continuum events are
257 well modeled in MC and that the shape of the M_{bc} distribution doesn't change significantly
258 when removing the continuum suppression cut both on MC and data (as one can see
259 from Figures 28a - 28b). Additionally, the continuum suppression cut efficiency should
260 be the same in data and MC in order to have the correct scaling on data with the above
261 mentioned method. Fig. 29 shows the distribution of the *foxWolframR2* variable in
262 off-resonance MC and data. The slight shift visible in data can cause a different impact on
263 data in terms of rejected continuum background when applying the *foxWolframR2* < 0.3
264 cut. It is found to reject about 60% of the continuum background in data, whereas it



(a)



(b)

Figure (28) Above: M_{bc} distributions of the MC off-resonance sample (5 streams) with and without continuum suppression. Below: M_{bc} distributions on data with and without continuum suppression.

rejects 55% of the continuum background in MC (56% in on-resonance MC). Therefore in data one can expect about 2.25% less continuum background events. This discrepancy is not statistical significant (the statistical uncertainty for the continuum background events is of the level of $\sim 1\%$), a simple correction to the number of events can be applied on data and its possible systematics can be then taken into account.

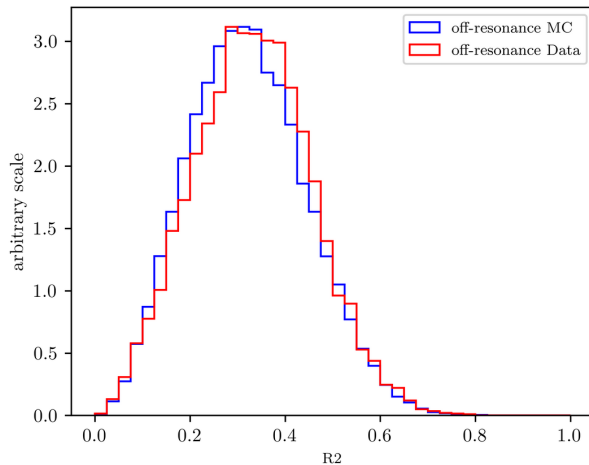


Figure (29) Distributions of variable *foxWolframR2* in off-resonance MC and data.

270 The obtained distribution can be then fitted (see Fig. 30), i.e. with a Novosibirsk function.
 271 This is the procedure which can be then applied on the off-resonance data to obtain the
 M_{bc} shape describing the continuum background in data.

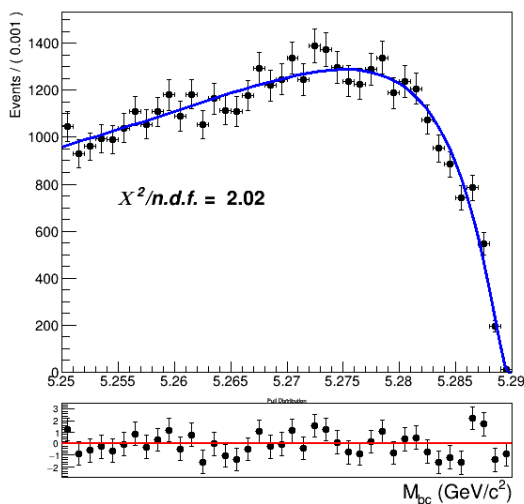


Figure (30) Fit of the M_{bc} distribution MC (scaled) off-resonance continuum (one stream).

272

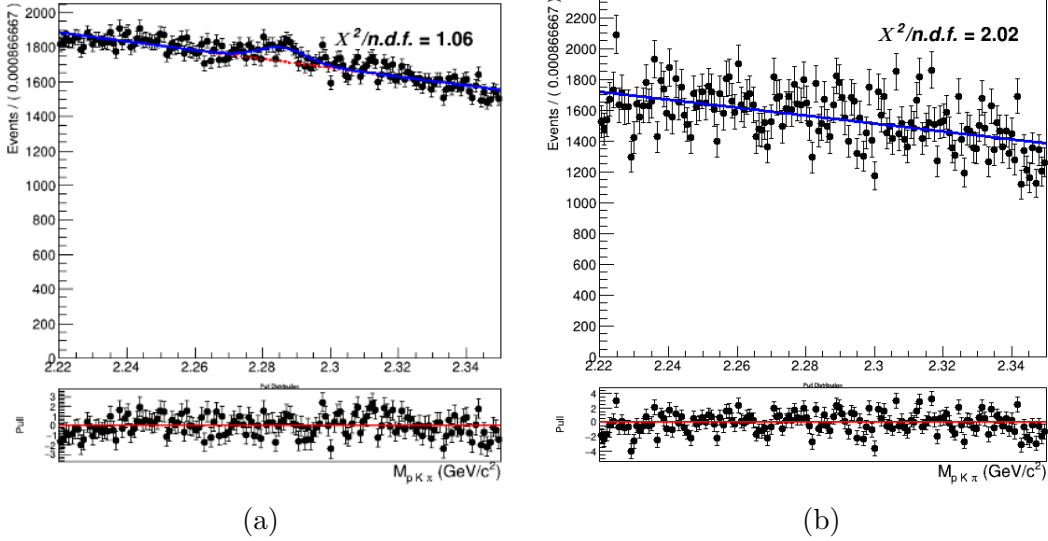


Figure (31) Comparison between 5 streams of MC on-resonance continuum 31a) and off-resonance (scaled) continuum in $M(pK\pi)$ (31b).

The shape describing the Λ_c invariant mass is obtained from the simulated on-resonance continuum, again using 5 streams statistics (see Fig. ??).

Finally, it is possible to examine the validity of the whole procedure on the independent stream. Fig. 33 shows the M_{bc} , $M(pK\pi)$ projections of the two dimensional fit with the one-dimesional PDFs obtained with the above described procedure. The 2D PDF used can be written as:

$$P_{B,\Lambda_c}^{Continuum}(M_{bc}, M(pK\pi)) = \Gamma_{Nov}(M_{bc}) \times [\rho_{Cheb1}(M(pK\pi)) + \rho_{G1}(M(pK\pi))]$$

where, as already anticipated, the invariant mass is described by a sum of a first order Chebychev polynomial and the peak by a single Gaussian function.

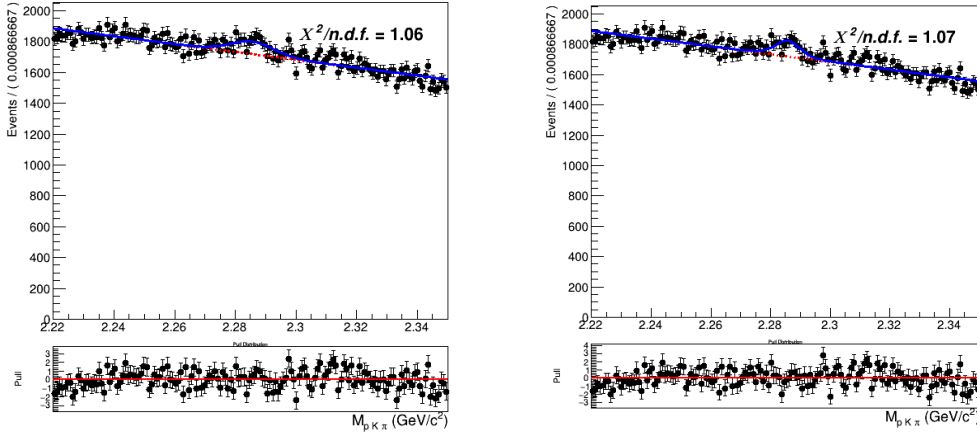


Figure (32) Λ_c invariant mass fits using five streams. On the left: fit of the Λ_c invariant mass of on-resonance continuum using the one Gaussian description (all nominal cuts applied). On the right: fit of the Λ_c invariant mass of on-resonance continuum using the same three gaussian PDF to describe the peak in the signal invariant mass (all nominal cuts applied).

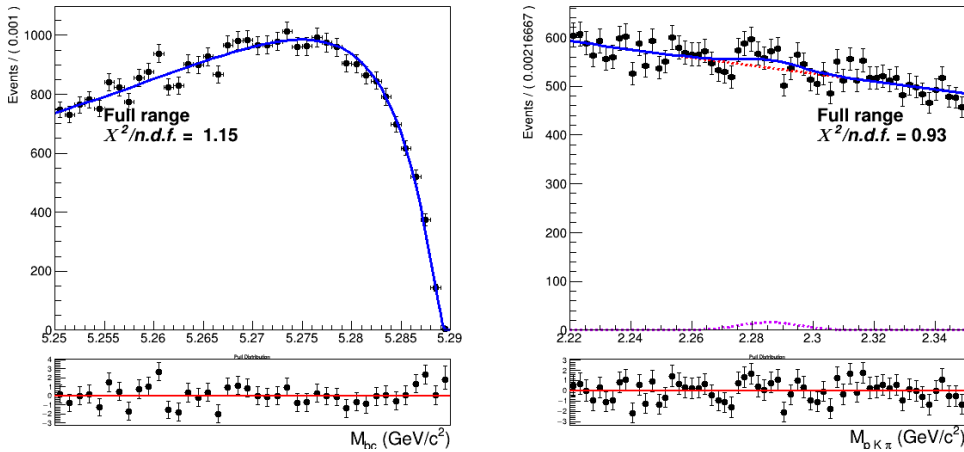


Figure (33) Two dimensional fit of continuum events (one stream).

284 It was then also investigated to alternatively use the same triple Gaussian PDF (used
 285 in Eq. 2 for the signal peak) to describe the peak, as it is shown in Fig. 32 . The two
 286 descriptions seem to be equivalent. The final fits described in Sec. 4.2 were performed
 287 with the one Gaussian description (keeping all parameters fixed), but it was also tried
 288 with the alternative three Gaussian description (with main Gaussian having the width as
 289 free parameter): no significant difference was noticed and the signal yields differ by only
 290 about 10% of the statistical uncertainties. Though, for consistency reasons, on data the
 291 second description will be applied.

292 **4.2 Two dimensional fit**

293 All the already discussed PDFs describing the various categories of events were constructed
 294 using five streams. Then an independent stream is used to test if the total PDF enables
 295 to extract the signal yield in an unbiased way. In order to test this a total of six fits are
 296 performed on six different streams of generic MC. Exemplary, the distributions of stream
 297 0 overlaid by the fitted PDF are depicted in Fig. 34 (see Appendix .1 for the projections
 298 in signal and sideband regions). In all six fits all the shaping parameters are kept fixed,
 299 except:

- 300 • σ_{G1} : the width of the wider of the three Gaussian functions in $\rho_G(M(pK\pi))$
 301 • σ_{CB} parameter for the Crystal Ball describing the signal peak in M_{bc}

302 In the M_{bc} distribution the σ_{CB} parameter for the Crystal Ball describing the generic
 303 background is expressed as function of the signal σ_{CB} with a ratio fixed from the MC. As
 304 for the normalizations, mis-/reconstructed signal events and generic background events
 305 are floated in the two dimensional unbinned maximum likelihood fits. The continuum
 306 background normalization is kept fixed to the value obtained by the off-resonance scaling
 307 procedure. Instead the normalization of crossfeed background events deserves a special
 308 treatment, At possible choice would be to express it as a function of the ratio of crossfeed
 309 events with respect to the misreconstructed signal events and keep it fixed o the MC value
 310 (this is done then in the fit on all tagged B mesons, i.e. in Sec. 4.4). This would make
 311 sense according to the fact that the two categories of events are similar: in both cases the
 312 B mesons were not correctly reconstructed, either because of missing or wrongly added
 313 particles (misreconstructed signal events) or, in the case of crossfeed events because it was
 314 a different one (B^0 meson instead of charged one). Since the amount of misreconstructed
 315 signal depends on the branching ratio itself, this method is not viable. Therefore, as for the
 316 crossfeed background the normalization of the PDF described in Eq. (6) is parametrized
 317 in the form:

$$N_{CrossBkg} P^{CrossBkg}(M_{bc}, M(pK\pi)) = k \cdot N_{B^0} \cdot N_{misRecSig}/N_{sig} \cdot P^{CrossBkg}(M_{bc}, M(pK\pi)) \quad (8)$$

- 318 • defining a sort of "probability ratio": $k = \frac{N_{crossfeed}/N_{B^0}}{N_{misRecSig}/N_{sig}}$, where the numerator
 319 represents the probability of misreconstructing B^0 as B^+ events and the denominator
 320 the probability of misreconstructing signal events. This ratio is calculated from MC
 321 and will be kept fixed also while fitting data.

- 322
- 323 • N_{B^0} is the total number of B^0 events in the dataset (MC or data).
- 324 • $N_{misRecSig}$ is the floated normalization of misreconstructed signal events
- 325 • $N_{sig} = N_{recSig}/\epsilon$ is the total number of signal events expressed as function of the
 326 floated normalization of reconstructed signal events and the signal reconstruction
 327 efficiency.

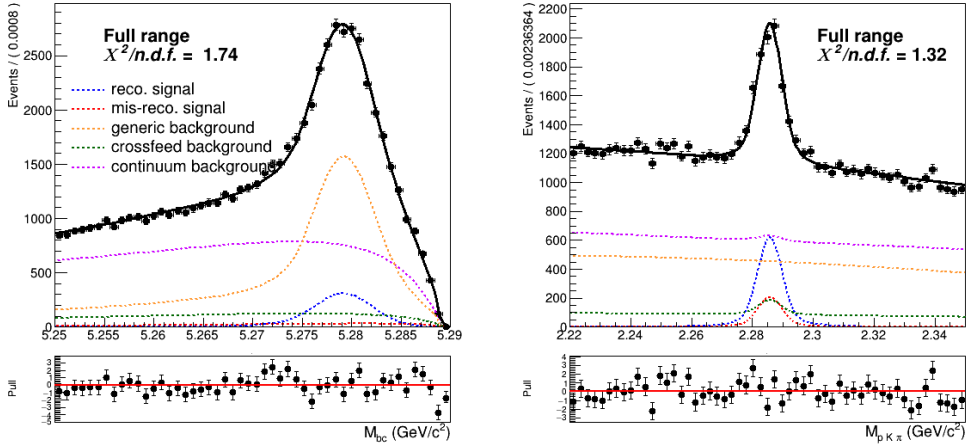


Figure (34) Two dimensional fit on stream 0 Monte Carlo simulated data.

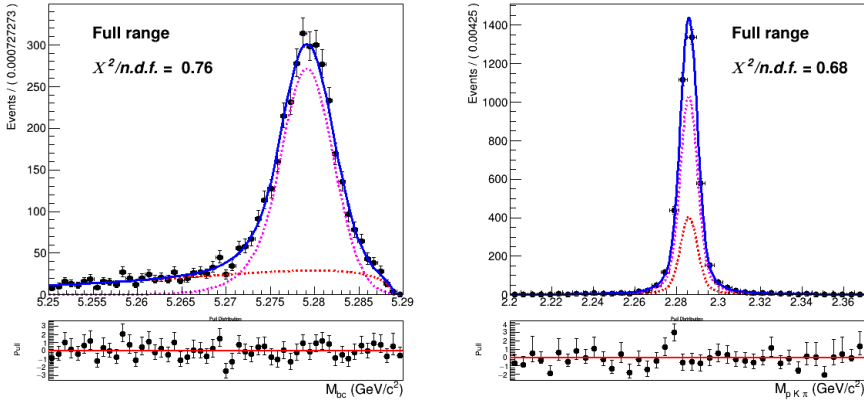


Figure (35) Two dimensional fit of Total Signal of stream 0 used to extract the expected reconstructed (corresponding to the PDF colored in magenta) and expected misreconstructed yields (corresponding to the PDF colored in red).

328 In Table 1 the signal yields of the fits (**Reconstructed Signal**) to the two dimensional
 329 distributions for the six streams of $B^- \rightarrow \Lambda_c^+$ flavor-correlated decays are listed and
 330 compared to the yields obtained from fits of signal distributions of each individual stream.
 331 The latter are the "expected" yields of reconstructed signal from a fit to the total signal
 332 events in the individual stream as the one plotted on Fig. 35 where all the parameters of
 333 the PDFs described in Eq. (2) are kept fixed and the corresponding yields are extracted
 334 from the fit.

	Reconstructed Signal		Total Signal			
	fit	expected	fit	MC truth	fit - MC truth	
stream 0	3072 ± 113	2928 ± 66	4037 ± 121	4061	-24	-0.6%
stream 1	2919 ± 115	2956 ± 66	4098 ± 126	4084	14	0.3%
stream 2	2627 ± 119	2940 ± 66	4031 ± 126	4138	-107	-2.6%
stream 3	2865 ± 111	2850 ± 66	4140 ± 123	4105	35	0.9%
stream 4	3328 ± 119	3046 ± 67	4076 ± 126	4176	-100	-2.2%
stream 5	2959 ± 114	2816 ± 65	4080 ± 129	4001	79	2.0%
sum	17770	17538	24462	24565	-103	-0.4%

Table (1) Comparison of fitted and expected signal yields, fitted and truth-matched total signal for six streams of Belle generic MC when fitting the two dimensional distributions of M_{bc} and $M(pK\pi)$.

The table also reports the fitted and truth-matched number of total signal (sum of reconstructed and misreconstructed signal) events. One can notice that, despite the deviations of total signal events being within statistical uncertainties, the results for reconstructed signal (first column) show fluctuations which exceed the statistical uncertainties, especially in case of stream 2 and 4 (see also Fig. 36 and Fig. 37). One can notice also an overall tendency towards higher values for the signal yields (the sum is about $2\sigma^{stat.}$ away from the sum computed for the expected yields).

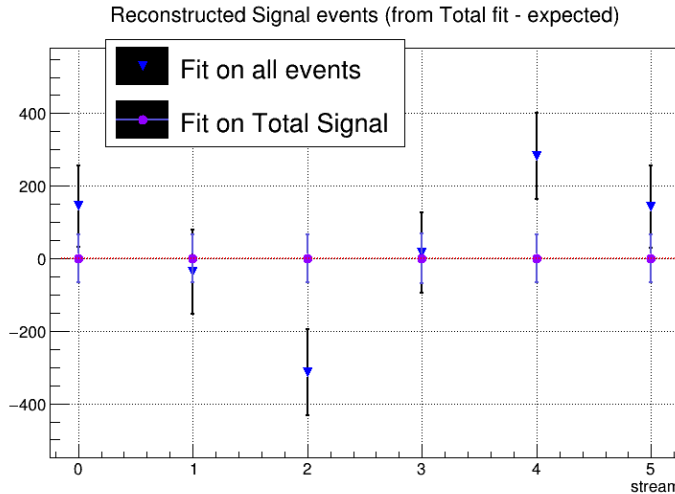


Figure (36) Differences between results from the fits and "expected" values for signal yields as reported in the first columns on Table1 .

Additionally, one can investigate the behaviour for different signal-to-background ratio. Thus, a second test of the fit model is performed. Using the six independent streams the amount of total signal is varied between 25% and 150% of the nominal values. The plot in Fig. 38 shows the values of reconstructed signal obtained in the total fits versus those expected by the fits on total signal events. One can see that the values distribute

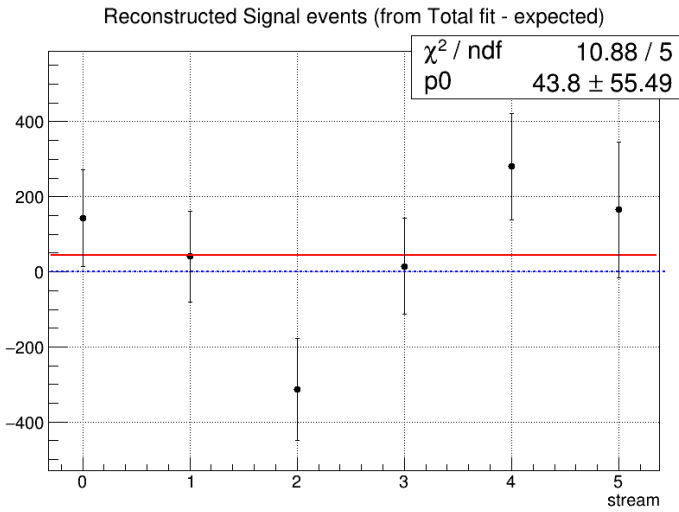


Figure (37) Fitted-expected subtracted values for reconstructed signal yields with associated uncertainties summed in quadrature.

³⁴⁷ according to a linear dependence. In Fig. 39 the linearity test is expressed in terms of
³⁴⁸ $\mathcal{B}(B^+ \rightarrow \bar{\Lambda}_c^- X)$ instead.

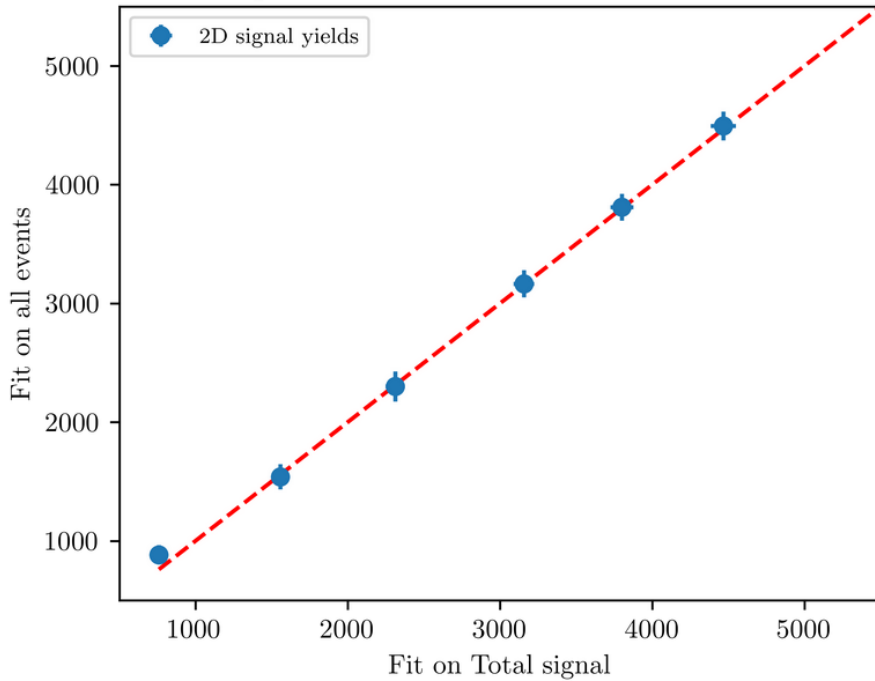


Figure (38) Linearity test: on the x-axis the obtained reconstructed signal yields from fits on different amounts of total signal; on y-axis the yields of reconstructed signal obtained fitting all events (as in Fig. 34). The dashed red line represents the 1:1 linear dependence.

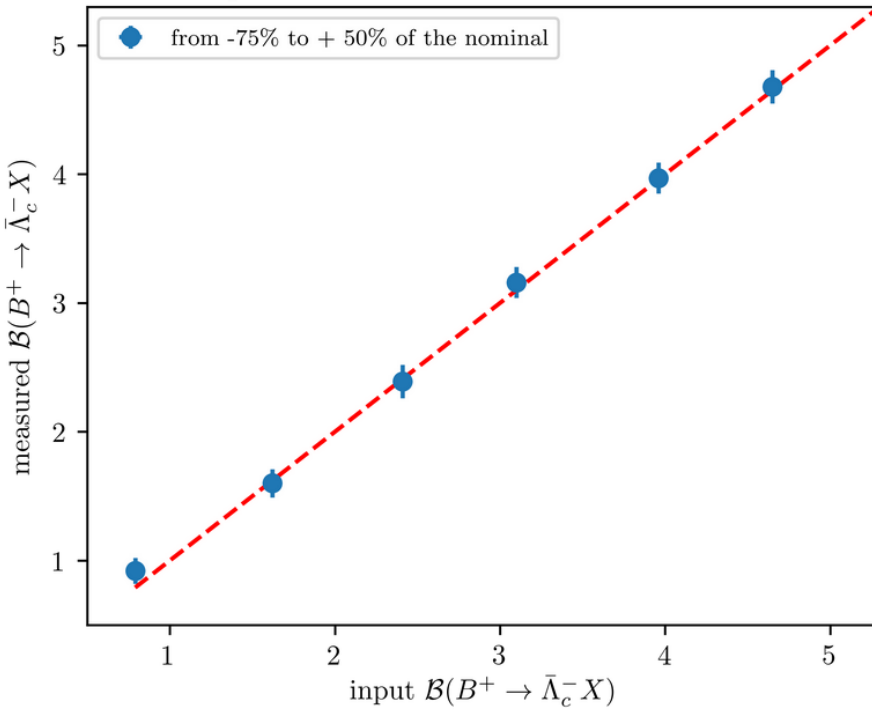


Figure (39) Linearity test: on the x-axis the input branching ratio value corresponding to the signal yields displayed on the x-axis in Fig. 38; on y-axis the measured branching fraction values corresponding to the signal yields of reconstructed signal displayed on the y-axis in Fig. 38.

349 For the fit model also toy MC pseudo-experiments were performed in order to confirm the
 350 behavior of the fit setup. With toy MC experiments the yields, errors and the pulls of the
 351 fit are studied by generating our own pseudo-datasets, according to the MC (see plots in
 352 the next page). 3×10^3 pseudo-datasets are constructed, where each dataset was generated
 353 with the expected amount of events, distributed according to the Poisson distribution.
 354 Then the composition of each toy pseudo-experiment is fitted as if they were data, and
 355 the pull-value distributions of the fit results are calculated. The pulls distributions are
 356 centered at zero, indicating there's no significant bias in the fitted yields/parameters.

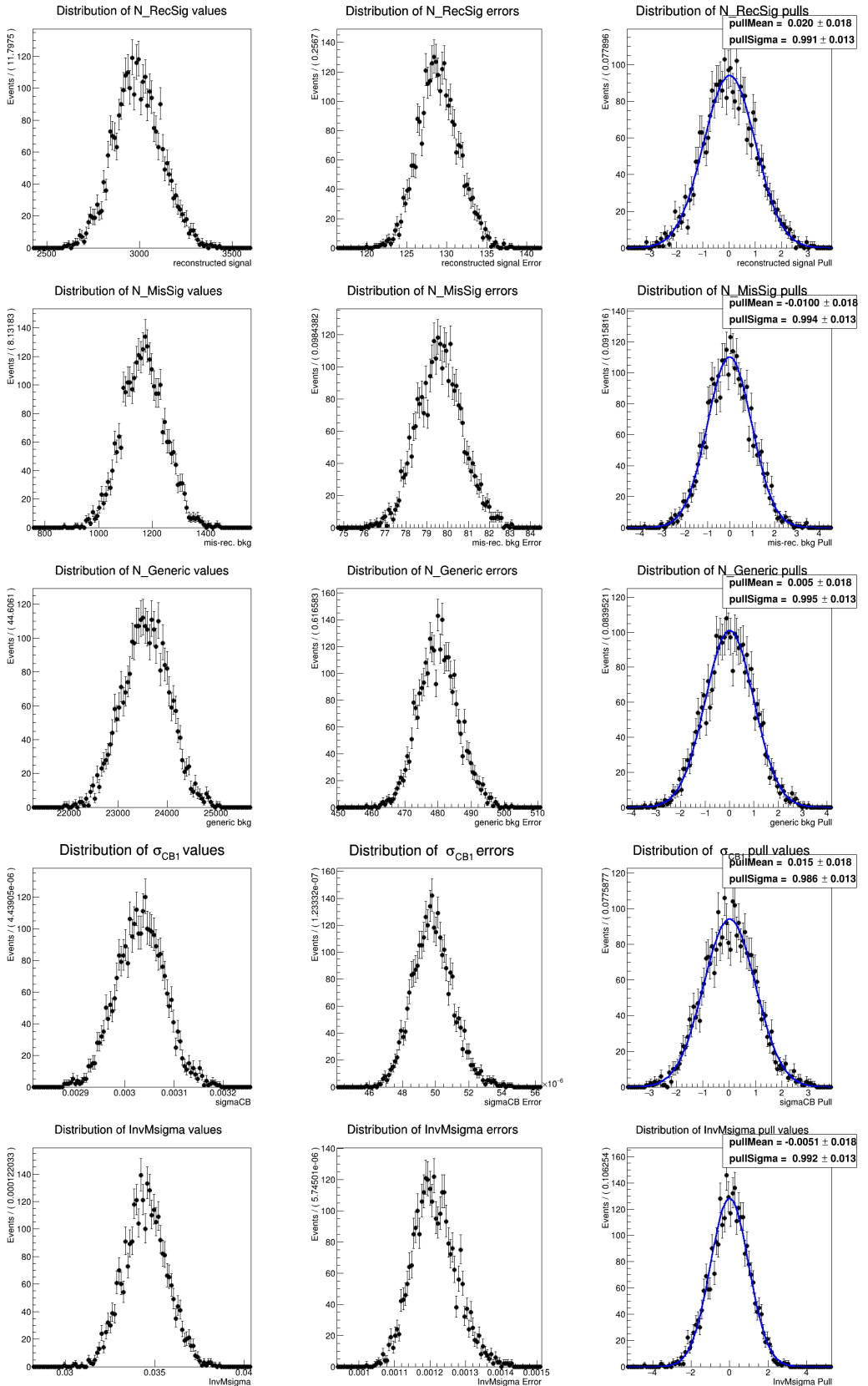


Figure (40) Toy MC study plots for the two dimensional fit model

357 4.3 Probability Density Functions (PDFs) for the B_{tag}

358 The M_{bc} distribution of the tagged B mesons is fitted with a Crystal Ball as for the
 359 "peaking" component and the "flat" component is fitted with a Novosibirsk function (Fig.
 360 41). The crossfeed background, consisting of neutral B mesons tagged as charged B , is
 361 fitted instead with a sum of a Novosibirsk and an asymmetric Gaussian PDF (Fig. 42).
 362 Both fits shows a $\chi^2/n.d.f.$ considerably higher than one and pulls exceeding 3σ deviation
 363 in some regions, but the systematics represented by this is negligible compared to other
 364 sources of systematic uncertainties and statistical uncertainties in the two dimensional fit.

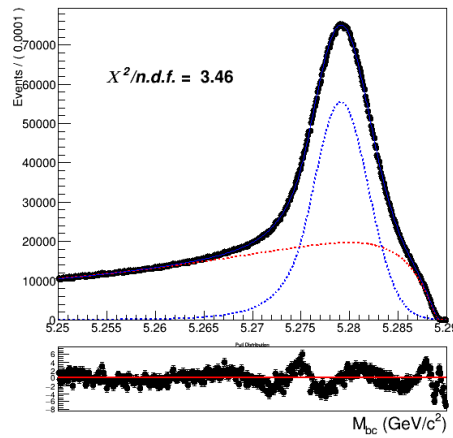


Figure (41) Fitted distribution of tagged charged B mesons: reconstructed signal events are described by the blue dotted PDF, the misreconstructed with a Novosibirsk function (red dotted).

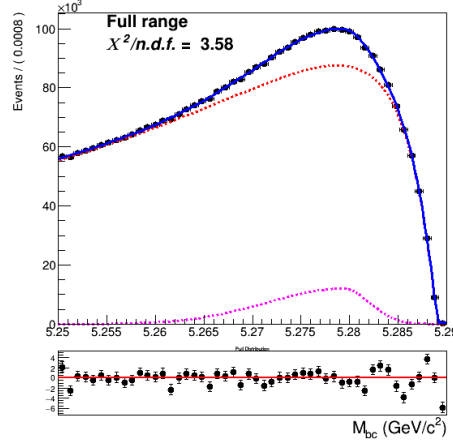


Figure (42) Crossfeed distribution fitted with a sum of Novosibirsk (red) and asymmetric Gaussian PDF (magenta)

365 As for the continuum background, a similar procedure as the one described already for the
 366 two dimensional fit was adopted:

- 367 • first the off-resonance sample is scaled accordingly
 368 • the ratio between the scaled off-resonance and the on-resonance in MC is calculated
 369 in each bin (see Fig.43a)
 370 • the bin-correction is applied on an independent stream and the scaled and bin-
 371 corrected M_{bc} distribution is compared with the on-resonance distribution as shown
 372 in Fig.43b

373 As for the B_{tag} continuum background the statistics is much larger than in the 2D sample,
 374 there's no need to remove the continuum suppression cut on the off-resonance sample.

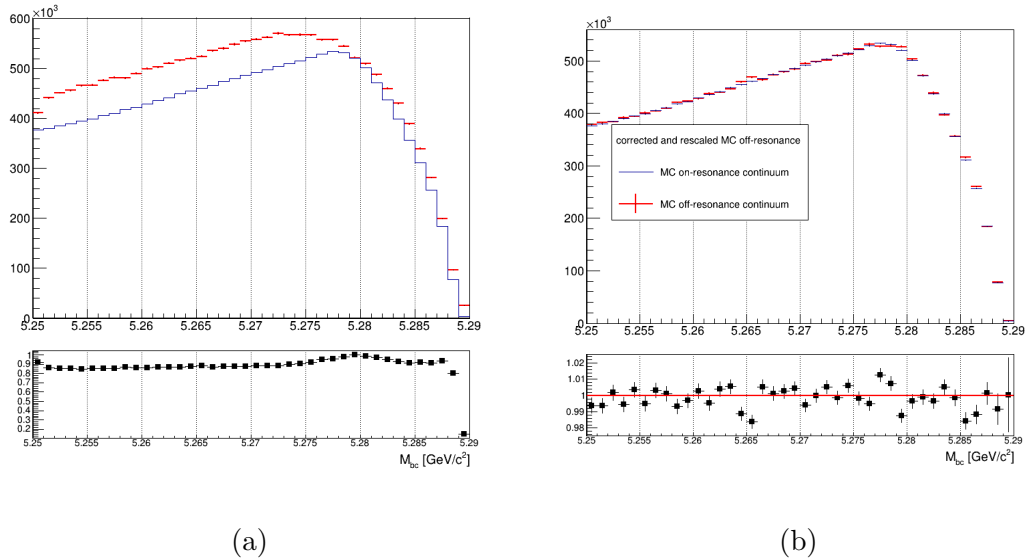


Figure (43) On the left: M_{bc} distributions of the MC off-resonance sample and the MC continuum sample with applied continuum suppression. On the right: M_{bc} distributions of the corrected scaled MC off-resonance and on-resonance MC continuum.

375 **4.4 B_{tag} fit**

376 An independent Monte Carlo stream was used to test the total fit model on tagged B meson
 377 candidates. As in the 2D fit, the parameter for the width, σ_{CB} , of the Crystal Ball is floated
 378 and the ratio between expected crossfeed background events and misreconstructed signal
 379 events is fixed from the MC. The Novosibirsk function describing the misreconstructed
 380 signal is also not fully constrained: the parameter describing the tail is free. To avoid
 381 introducing significant systematic uncertainties in the fit deriving from the M_{bc} endpoint
 382 region, where one has a smearing effect due to variations of the beam energy at the MeV
 383 level, the range for the fit is restricted to values between 5.250 and 5.287 GeV/c². Yields
 384 for the reconstructed and misreconstructed signal are obtained from the fit:

385

386

NrecSig	$4.2681 \cdot 10^6 \pm 5871$
NmisSig	$5.8787 \cdot 10^6 \pm 5128$

387 The Total Signal (the sum NrecSig+NmisSig) is 10146748 ± 4380 (to be compared with
 388 10158571 from the Monte Carlo). This reflects a $\sim 2.5\sigma$ discrepancy between the true MC
 389 value and the result from the fit. This can produce some systematic effect, but the relative
 390 error is at the $\sim \%$ level. This is still negligible compared to the systematic uncertainty
 391 corresponding to the the N_{tag} determination, and furthermore in the branching fraction
 392 calculation it is also negligible compared to the statistical uncertainty on the extracted
 393 yields from the two dimensional fit.

394 To check the stability of the fit model a toy MC study was performed with 3×10^3
 395 pseudo-datasets (as it was done for the two-dimensional fit model). No evidence for
 396 possible biases in the reconstructed signal yields was found (see Fig. 45).

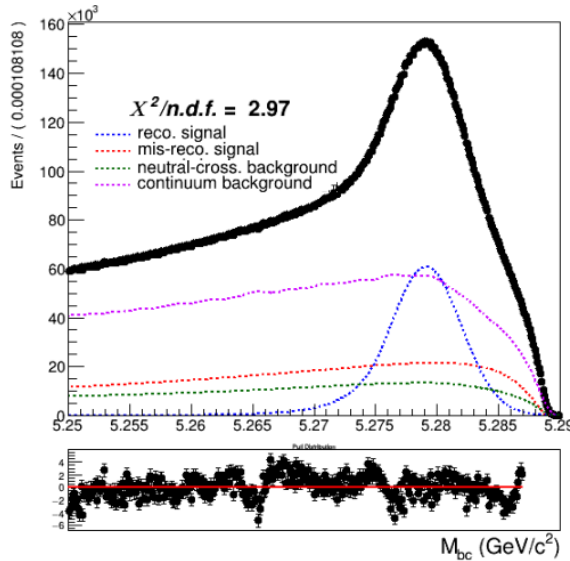


Figure (44) Total fit of tagged B mesons on Monte Carlo simulated data.

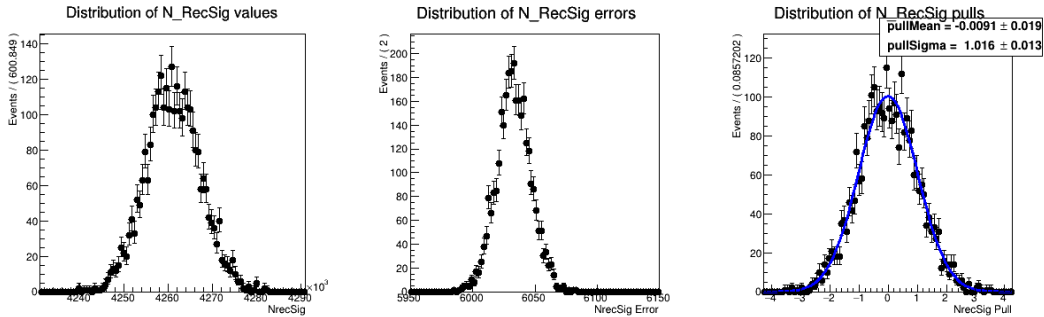


Figure (45) Plots showing distributions of the fitted signal yields, errors and the pull distribution of all pseudo-fits. (see Appendix .1 for the other free parameters' results)

397 4.5 Λ_c and FEI efficiency

398 The efficiency in reconstructing the Λ_c baryon after correctly tagging the charged B
 399 meson, can be estimated from Monte Carlo simulated data as the fraction of correctly
 400 reconstructed signal events that have a correctly reconstructed B_{tag} companion, i.e.:

$$\frac{N_{recSig}(B_{tag}, \Lambda_c)}{N_{recSig}(B_{tag}^{sig})} \quad (9)$$

401 where $N_{recSig}(B_{tag}, \Lambda_c)$ are the yields of reconstructed signal from the two dimensional
 402 fits (reported in Table 1) and $N_{recSig}(B_{tag}^{sig})$ are the yields of correctly reconstructed signal
 403 in a fit of B mesons tagged in events where one of the two mesons decayed hadronically
 404 and inclusively into a Λ_c baryon (see Fig 46). To minimize statistical uncertainties, in
 405 the efficiency calculation the results from all the two dimensional fits were used and six
 406 streams of B_{tag} candidates reconstructed in signal events were used for the M_{bc} shown
 407 below.

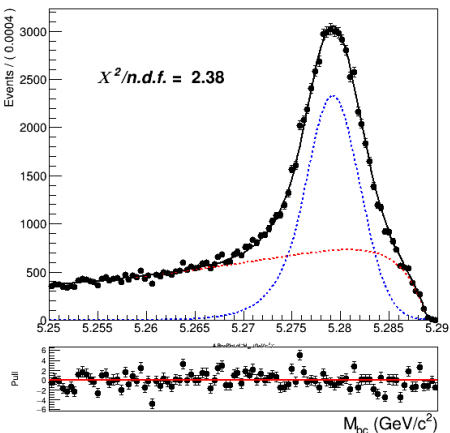


Figure (46) Fit of tagged B mesons in the "signal events" sample

408 From this and the results listed in sec. 4.2 the efficiency to reconstruct Λ_c is obtained :

409

$$410 \quad \epsilon_{\Lambda_c} = \frac{N_{recSig}(B_{tag}, \Lambda_c)}{N_{recSig}(B_{tag})} = 44.83 \pm 0.32\%$$

411 The yields from the fit shown in (Fig. 46) can be used also to calculate the FEI tag-side
412 efficiency for signal events, i.e. the efficiency to tag the B meson accompanying a B_{sig}
413 decaying into a Λ_c on the signal side. Whereas results from the fit of charged B_{tag} shown
414 in Fig. 41 can be used to calculate the hadronic tag-side efficiency in the generic B^+B^-
415 events case.

416 The ratio between the two efficiencies is calculated: $\frac{\epsilon_{FEI,sig}^+}{\epsilon_{FEI}^+} = 0.908 \pm 0.017$
417

418 4.6 Studies of Systematic Effects

419 In Table 2 the systematic uncertainties of the various considered sources are summarized.
 420 The full estimate of the systematic uncertainty is summed up in quadrature and applied
 421 to the result in Section 4.17 Their individual calculation is outlined in the subsequent
 422 subsections.

source	%
Continuum modeling	0.07
Crossfeed PDFs	0.07
Crossfeed fraction	0.06
2DFit crossfeed normalization	0.02
2DFit crossfeed peaking fraction	0.09*
$\epsilon_{FEI,sig}^+/\epsilon_{FEI}^+$	0.06
ϵ_{Λ_c}	0.02
Fit bias	0.06
PID	0.05
Total	0.17

Table (2) Systematic uncertainties in the determination of the $B^+ \rightarrow \bar{\Lambda}_c^- X$ branching fraction in %.

423 * this represents the dominant uncertainty, but in Sec. 4.11 it will be explained how it
 424 can be possibly reduced.

425 4.7 Continuum background modeling

426 Regarding this source of systematics, one has to take into account two different types.
 427 First of all the statistical uncertainties, which are reflected in the uncertainties on the
 428 PDF parameters. To estimate this type of uncertainty two-dimensional fits with varied
 429 parameters' values by their uncertainties (a fit with $+\sigma$ and $-\sigma$) were performed.
 430 Whereas, the estimation of statistical uncertainty in the case of the B_{tag} should be
 431 estimated in principle varying each bin content of its error. On first approximation this is
 432 equivalent to vary the nominal number of events described with the histogram PDF by
 433 Poissonian variation. Exemplary, fits used to estimate the impact of these uncertainties
 434 are shown here in Figures 47 - 48. The yields obtained from those fits for benchmark
 435 stream5 results are then compared with the ones already reported previously and a mean
 436 deviation value is obtained for both the two-dimensional fit and the B_{tag} fit.

Fit	$-\sigma$	$+\sigma$	$\pm\bar{\sigma}$
2D	87	53	70
B_{tag}	10218	10620	10419

Table (3) Offsets on the signal yields obtained in the two dimensional and B_{tag} fit and mean deviations reported in the last column.

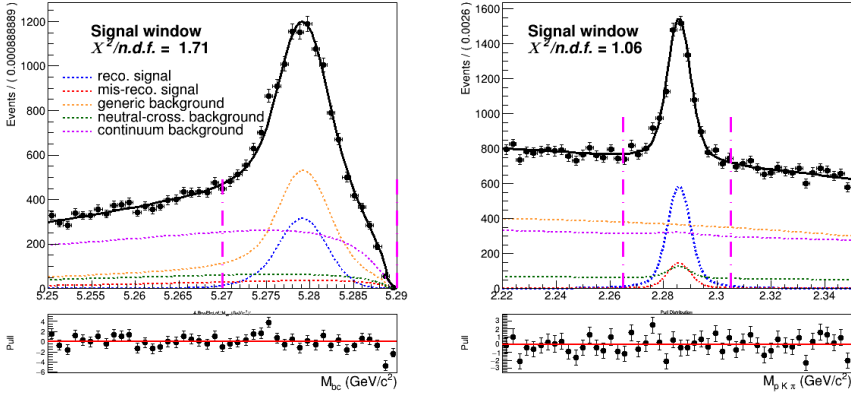


Figure (47) Signal window projections of a two dimensional fit on Monte Carlo simulated data where the shaping parameters were varied of their uncertainties.

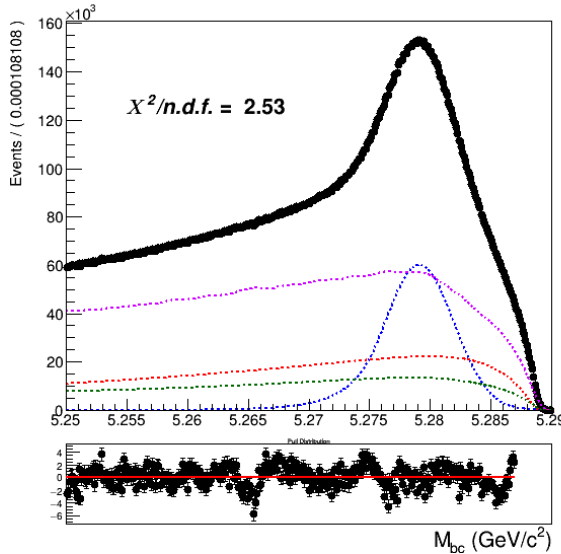


Figure (48) Fit of tagged B meson candidates on Monte Carlo simulated data where the amount of continuum was varied according to poissonian fluctuations.

437 The estimated systematic uncertainty on Br value from this source is 0.07%.

438 The other type of systematic uncertainty in modeling the continuum is originated by the
 439 continuum suppression cut having a slightly different efficiency on data (as a consequence
 440 of the shift in off-resonance MC and data visible in the the *foxWolframR2* distribution
 441 in Fig. 29). As already discussed, it originates a possible discrepancy of about 2.25% in
 442 continuum background events in the two dimensional fit (and only 1.25% in the B_{tag} fit).
 443 The statistical uncertainty on this fraction of events can also be taken into account as
 444 systematics. Being the number of events in the off-resonance data sample without the
 445 continuum suppression applied is very small (less than 10^4 in the two dimensional fit and

446 about 18500 in the B_{tag} fit), the uncertainty in the mentioned fraction of events is negligible
 447 compared to the statistical uncertainty on the on-resonance continuum background events
 448 in MC: it would account for 0.002% on the BR value. Therefore, this second source of
 449 uncertainty is not taken into account. There would be also a third of systematic uncertainty
 450 given by potential difference in the on-/off-resonance correction between data and MC,
 451 but there's no way one can estimate it properly.

452 **4.8 Crossfeed background modeling**

453 Since also the shapes of the PDFs describing the crossfeed background are fully fixed to the
 454 ones determined with the limited Monte Carlo statistics, also their statistical uncertainties
 455 need to be taken into account as possible source of systematics. The procedure to estimate
 456 this source of systematic uncertainty is the same described in the previous section regarding
 457 the continuum background. In the table below the signal yields' offsets are listed changing
 458 the parameters within their uncertainties, and the mean offsets value used to calculate the
 459 expected uncertainty on the BR value. The resulting absolute systematic uncertainty is
 460 about 0.07% on the BR value.

Fit	$-\sigma$	$+\sigma$	$\pm\bar{\sigma}$
2D	51	90	71
B_{tag}	5400	5700	5550

Table (4) Offsets on the signal yields obtained varying the parameters of crossfeed background PDFs within their uncertainties in the two dimensional and B_{tag} fit and mean deviations reported in the last column.

461 **4.9 Crossfeed ratio**

462 The crossfeed/misreconstructed signal "probability ratio" ($k = \frac{N_{crossfeed}/N_{B^0}}{N_{misRecSig}/N_{sig}}$) defined in
 463 Eq. (8) is kept fixed in the two-dimensional fit and the ratio bewteen crossfeed and
 464 misreconstructed events is also kept fixed in the B_{tag} fit to the values found in MC. This
 465 choice was made according to the fact that the two categories of events are similar: in both
 466 cases the B mesons were not correctly reconstructed, either because of missing or wrongly
 467 added partilces (misreconstructed signal events) or, in the case of crossfeed events because
 468 the tagged B meson was not the required one (B^0 meson instead of a $B^{+/-}$ meson). The
 469 ratio between these two categories of events is therefore expected to be very similar in
 470 MC and data, though there's no guarantee that the efficiency to reconstruct them is the
 471 same in data and consequently the above mentioned ratios could be differ on data.
 472 Unfortunately there's no direct way to have an estimate of the possible discrepancy for
 473 them.

474 In [3] (and previously in [4]) it was found that there's a substantial difference in terms of

475 tagging efficiency for FEI applied on Monte Carlo and on Belle data, being the discrepancy
 476 around $\sim 20\%$. We can assume that the efficiency for the two categories of events on data
 477 will both differ of that value and the ratio of the events being the same MC value, but in
 478 absence of any other method to estimate the uncertainty on it one can consider a maximal
 479 discrepancy of to 20% between Monte Carlo and data to study the impact on the yields².

480 Therefore, for the two-dimensional fit the ratio k was artificially varied of $\pm 20\%$,
 481 whereas in the case of the B_{tag} fit the number of crossfeed events were varied artificially in
 482 order to have $\pm 20\%$ different ratio, keeping the previously determined Monte Carlo ratio
 483 fixed.

Fit	$-\sigma$	$+\sigma$	$\pm\bar{\sigma}$
2D	54	69	61
B_{tag}	2807	3940	3374

Table (5) Offsets on the signal yields obtained varying of $\pm 20\%$ the k ratio in the two dimensional and the ratio of crossfeed/misreconstructed events in the B_{tag} fit and mean deviations reported in the last column.

484 The estimated systematic uncertainty on Br value from this source is 0.06%.

485 4.10 Parametrization of crossfeed normalization in the 2D fit

486 In the previous section, regarding the two-dimensional fit, the uncertainties arising from
 487 the fixed "probability ratio" k were investigated. Besides those, one can consider also
 488 systematic uncertainties of statistical nature deriving from Eq. (8), were only the number
 489 of mis-/reconstructed signal events ($N_{recSig}/N_{misrecSig}$) are floated and fitted by the 2D fit.
 490 As already done in the case of continuum and crossfeed PDFs, this type of systematics is
 491 estimated repeating the 2D fit varying the parameters by their uncertainties. This source
 492 of systematics originates an uncertainty of 0.02% on the Br value.

493 4.11 Crossfeed peaking fraction in the 2D fit

494 When discussing the crossfed background modeling (see Fig. 17), it was said that among
 495 the crossfeed background events there are also those that belong to $B^0 \rightarrow \Lambda_c$ decays, which
 496 peak in the Λ_c mass. The branching ratio of those decays is also still measured with poor
 497 accuracy (e.g. $\mathcal{B}(\bar{B}^0 \rightarrow \bar{\Lambda}_c^+ X) = (5.0^{+2.1}_{-1.5})\%$), therefore the amount of crossfeed events
 498 peaking in $M(pK\pi)$ on data can differ significantly from MC. To estimate this source of
 499 systematics the amount of peaking events was varied in order to cover the uncertainties in
 500 the branching fraction mentioned above and repeating the two-dimensional fit.

²This method was also validated with the control decay sample and the originated uncertainty is well within the PDG reported ones.

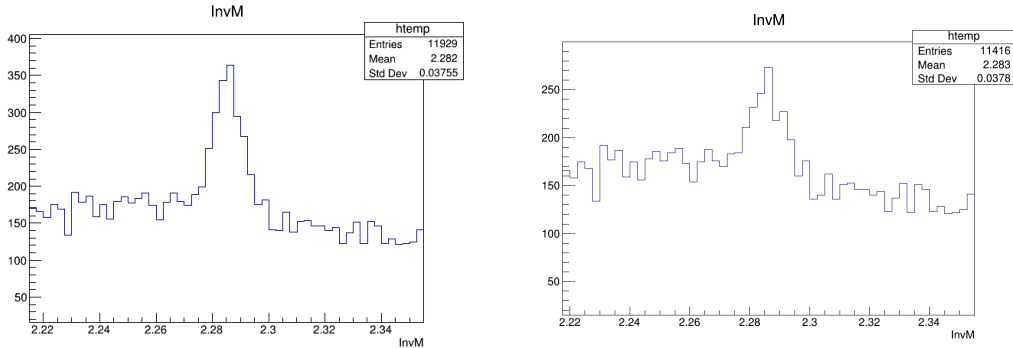


Figure (49) Λ_c invariant mass of crossfeed background with different amount of peaking events. On the left: Λ_c invariant mass corresponding to $\mathcal{B}(\bar{B}^0 \rightarrow \bar{\Lambda}_c^+ X) = 5.0 + 2.1\%$. On the right: Λ_c invariant mass corresponding to $\mathcal{B}(\bar{B}^0 \rightarrow \bar{\Lambda}_c^+ X) = (5.0 - 1.5)\%$

Fit	$-\sigma$	$+\sigma$	$\pm\bar{\sigma}$
2D	89	90	90

Table (6) Offsets on the signal yields obtained varying the amount of peaking crossfeed in the Λ_c invariant mass and mean deviation.

501 The uncertainty originated is estimated to be of 0.09% on the Br value. But once
 502 results from a new and more accurate measurement of $\mathcal{B}(\bar{B}^0 \rightarrow \bar{\Lambda}_c^+ X)$ (and the one
 503 corresponding to the flavor-anticorrelated decays) are available (once I obtained them)
 504 one can recompute this estimation with the updated uncertainties on the branching ratio
 505 of neutral decays, which should reduce the impact of this systematic uncertainty on the
 506 measurement.

507 4.12 Efficiencies

508 The ratio between the two FEI efficiencies is: $\frac{\epsilon_{FEI,sig}^+}{\epsilon_{FEI}^+} = 0.908 \pm 0.017$

509 The uncertainty on this value originates a systematic uncertainty of 0.06% on the Br
 510 value. The Λ_c reconstruction efficiency is determined to be $\epsilon_{\Lambda_c} = 44.83 \pm 0.32\%$. The
 511 systematic uncertainty originated by its uncertainty is 0.02% on the Br value.

512 4.13 Fit biases

513 The small bias on the reconstructed signal seen in the two-dimensional fit model has to
 514 be corrected when fitting data, but the uncertainty on it has to be taken into account in
 515 the systematics. Also the discrepancy in the total signal fit result observed in the B_{tag}
 516 (Sec. 4.4) needs to be included in the systematic effects. Propagating the two sources of

517 systematics in the branching fraction calculation results in an additional 0.06% uncertainty
518 on the branching fraction value.

519 4.14 PID efficiency correction

520 The PID selection efficiency for the three charged particles in the signal decay needs to
521 be corrected on MC due to various differences, when comparing to data. The Belle PID
522 group has prepared a set of correction factors and tables of systematic uncertainties for
523 PID efficiencies for all charged particles. The proton identification efficiency was studied
524 in [5]. The inclusive Λ^0 decay $\Lambda^0 \rightarrow p\pi^-$ was used to examine the proton identification
525 efficiency difference between data and MC in *Belle*. The datasets for the SVD1 and SVD2
526 periods are treated separately, and the efficiency ratio dependence on proton charge,
527 momentum and polar angle is considered. The study is done for the proton ID cut values
528 0.6, 0.7, 0.8 and 0.9³. The binning on the momentum starts at 0.2 GeV. The proton ID
529 efficiency is defined as

530

$$531 \epsilon_{PID} = \frac{\text{number of } p\text{ tracks identified as } p}{\text{number of } p\text{ tracks}}$$

532

533 and the comparison between MC efficiency and data efficiency by a double ratio
534 defined as

535

$$536 R_p = \epsilon^{data}/\epsilon^{MC}$$

537

538 The average proton ID correction is estimated to be: $R_p = 0.969 \pm 0.003$.

539 The kaon identification efficiency was studied in detail in Belle Note 779 [6] (http://belle.kek.jp/secured/belle_note/gn779/bn779.ps.gz). The decay $D^{*+} \rightarrow D^0\pi^+$
540 followed by $D^0 \rightarrow K^-\pi^+$, was used to examine it. As for the proton identification efficiency
541 it considers the dependence on Kaon charge, momentum and polar angle and same ID cut
542 values⁴.

544 For Kaons and Pions the average ID correction is estimated to be $R_K = 0.853 \pm 0.010$
545 and $R_\pi = 0.983 \pm 0.008$ respectivley.

546 The final PID efficiency systematic error is determined to be 0.01% on the branching
547 fraction value.

548 4.15 crossfeed peak fraction

549 This source of systematics arises from the fact that thereâŽs (still) a significant uncertainty
550 on B_0 decays , i.e.: $(5.0^{+2.1}_{-1.5})\%$

³Here, proton ID cut value X means $\mathcal{L}_{p/K} > X$ and $\mathcal{L}_{p/\pi} > X$

⁴Here, Kaon ID cut value X means $\mathcal{L}_{K/\pi} > X$, so for values below X the tracks are identified as pions

551 **4.16 Sideband fit on data**

552 As a preliminary check of the quality of the shapes modeling, a fit of the sideband
 553 region $2.225 < M(pK\pi) < 2.245 \text{ GeV}/c^2$ projection in M_{bc} was performed. The only
 554 events present in this sideband region are: the generic, the crossfeed and the continuum
 555 backgrounds. Therefore the only free parameters in the fit are:

- 556 • the width of the generic background Crystal Ball σ_{CB2}
 557 • the normalization of the generic background
 558 • the normalization of the crossfeed background

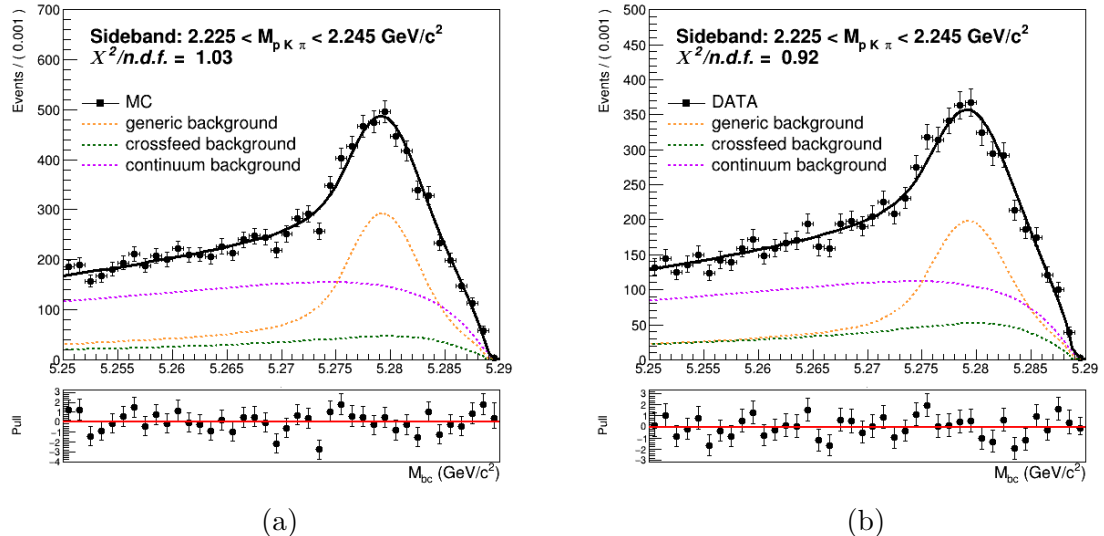


Figure (50) Fitted M_{bc} distributions corresponding to the projection in the sideband region of Λ_c invariant mass distribution in Monte Carlo and in data.

559 The fit shows a really good agreement with data points, from which one can assume that
 560 the shapes of the three main background contributions are describing at a good level the
 561 data. Moreover the fitted fractions of the background components present a quite good
 562 MC-data agreement:

Background	MC truth	Fit on MC	Fit on Data
Crossfeed	10.66 %	$12.22 \pm 2.69 \text{ \%}$	$17.76 \pm 3.21 \text{ \%}$
Generic	38.49 %	$37.11 \pm 2.55 \text{ \%}$	$34.64 \pm 3.04 \text{ \%}$

566 **4.17 Measured $B^+ \rightarrow \bar{\Lambda}_c^- X$ inclusive Branching Fraction**

567 Now that all ingredients are available, it's possible by mean of the formula in Eq. 4 (at
 568 the beginning of this Chapter) , to calculate the branching ratio for the charged correlated
 569 decays into Λ_c baryons.

570 As the measurement is performed considering only the $\Lambda_c \rightarrow pK\pi$ decays, to evaluate the
 571 inclusive $B^+ \rightarrow \bar{\Lambda}_c^- X$ Branching Ratio on Monte Carlo simulated data one needs to take
 572 into account the value set for that particular final state: the total $Br(\Lambda_c^+ \rightarrow pK^-\pi^+) =$
 573 5.53% in Belle Generic MC (including resonant decays). Using the results from the
 574 two dimensional fits, the B_{tag} fit (with/without background included) and with all the
 575 needed factors known, one can calculate $\mathcal{B}(B^+ \rightarrow \bar{\Lambda}_c^- X)$ on the six independent streams
 576 as displayed in ???. From the reported values one can notice first of all the effect of the
 577 bias encountered in Sec. 4.2, pushing the branching fraction to higher values (first column)
 578 compared to the expected ones and the branching ratio set in Belle MC. The discrepancy
 579 is of the order of 1σ statistical uncertainty.

	total fit	signal fit	BELLE MC VALUE
stream 0	$(3.20 \pm 0.12)\%$	$(2.96 \pm 0.07)\%$	$(2.95 \pm 0.03)\%$
stream 1	$(3.04 \pm 0.12)\%$	$(2.99 \pm 0.07)\%$	$(2.91 \pm 0.03)\%$
stream 2	$(2.73 \pm 0.12)\%$	$(2.99 \pm 0.07)\%$	$(2.90 \pm 0.03)\%$
stream 3	$(2.98 \pm 0.12)\%$	$(2.90 \pm 0.07)\%$	$(2.91 \pm 0.03)\%$
stream 4	$(3.26 \pm 0.13)\%$	$(3.07 \pm 0.07)\%$	$(2.90 \pm 0.03)\%$
stream 5	$(3.08 \pm 0.12)\%$	$(2.85 \pm 0.07)\%$	$(2.92 \pm 0.03)\%$
average	$(3.05 \pm 0.05)\%$	$(2.96 \pm 0.03)\%$	$(2.93 \pm 0.01)\%$

580 Comparing the obtained values with the branching fraction measured by BaBar experiment
 581 (see results reported by *BaBar* [1]), the uncertainties appear substantially reduced
 582 (statistical uncertainties almost by factor four).

583

584 **5 $B^- \rightarrow D^0$ control decay**

585 To monitor the analysis steps, which are applied to both measured and simulated data, a
586 control decay of the form

587

588
$$B^+ \rightarrow D^0 X, D^0 \rightarrow K^+ \pi^-$$

589 is used. The statistics is much more abundant for this channel.

590 **5.1 Dataset used**

591 For this analysis the amount of data and Monte Carlo simulated data used was restricted
592 to the SVD2 period: experiments ranging from 31 to 65. This choice was made to save
593 processing time, anyway most of the $B\bar{B}$ meson pairs were produced in this range of
594 experiments (620×10^6 out of almost 800×10^6).

595 **5.2 Event selection and reconstruction**

596 The approach used for the inclusive decays reconstruction is the same as for the $B \rightarrow \Lambda_c$
597 analysis. The same FEI training was used, though excluding the signal decay $D^0 \rightarrow K^+ \pi^-$
598 from the decay chains used by the FEI to reconstruct the B_{tag} . Same preliminary selection
599 criteria were applied to the tag-side B meson candidates as well.

600 In the *rest of event* (ROE) of the reconstructed B_{tag} meson, to select $D^0 \rightarrow K^+ \pi^-$ signal
601 candidates, the following event selection criteria are applied:

- 602 • $dr < 2$ cm and $|dz| < 4$ cm
603 • $\frac{\mathcal{L}_K}{\mathcal{L}_K + \mathcal{L}_\pi} > 0.6$

604 For the D^0 candidates a vertex fit is performed with `TreeFitter`, requiring it to converge.
605 If there are more than one D^0 combination, then the best candidate based on the χ^2
606 probability is chosen. The D^0 signal region is defined to be $|M_{D^0} - m_{D^0}| < 30$ MeV/ c^2
607 ($\sim 3\sigma$), where m_{D^0} is the nominal mass of D^0 .

608

609 **5.3 Signal selection optimization**

610 Following the same procedure as for the $B \rightarrow \Lambda_c$ analysis, the optimized selection cuts
611 obtained for the event based ratio of the 2-nd to the 0-th order Fox-Wolfram moments,
612 the B_{tag} signal probability and the momentum of the D^0 candidates in the center of mass
613 system are:

- 614 • $foxWolframR2 < 0.3$
615 • $SignalProbability > 0.004$

- 616 • $p_{CMS}^{D^0} > 1 \text{ GeV}/c^2$

617 Figure 51 shows the distributions of M_{bc} and invariant mass in the signal region⁵ for the
 618 $B^- \rightarrow D^0 X$ reconstructed events after the selection cuts were applied.

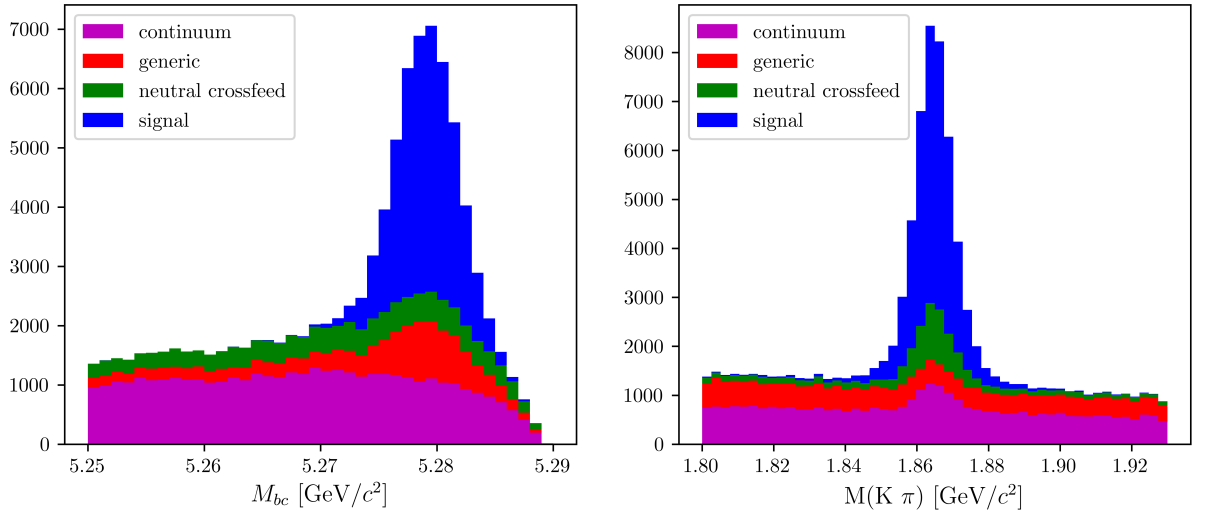


Figure (51) Distribution of M_{bc} (left) and invariant mass of charged correlated D^0 candidates (right), in the signal region after the above mentioned selection cuts.

619 **5.4 Probability Density Functions (PDFs) for two dimensional
 620 fit**

621 As already said the main goal of the control sample analysis is to ensure that the method
 622 used to extract the signal yields discriminating the correctly reconstructed from the
 623 misreconstructed signal events by fitting is valid. The reconstructed events in M_{bc} are
 624 fitted with a Crystal Ball, the misreconstructed signal with a Novosibirsk function. As in
 625 the $B \rightarrow \Lambda_c$ analysis both components have a correspondent peak in the D^0 mass which is
 626 fitted with a sum of three gaussians with a common mean. The fitted distribution of M_{bc}
 627 and $M(\pi K)$ are shown in Fig. 52 with signal MC sample.

⁵signal region: $M_{bc} > 5.27 \text{ GeV}/c^2$ and $|M_{D^0} - m_{D^0}| < 30 \text{ MeV}/c^2$

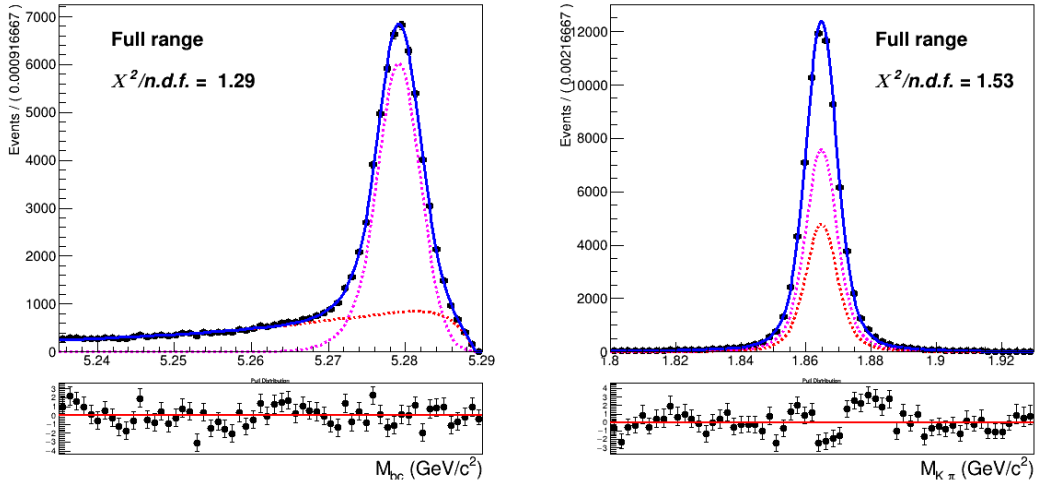


Figure (52) Two dimensional fit of total signal events in M_{bc} and $M(pK\pi)$ (in magenta reconstructed signal PDF, misreconstructed signal PDF in red)

628 As already seen in the $B \rightarrow \Lambda_c$ analysis besides the misreconstructed signal the other
629 background components are:

- 630 • **generic** (charged B) background
631 • **crossfeed** (neutral B) background
632 • **continuum** background

633 **Generic background**

634 The generic background deriving from other B^+B^- events presents a similar shape in
635 M_{bc} : it is fitted again with a sum of Crystal Ball and Novosibirsk function. Instead the
636 distribution in the D^0 mass is fitted with a sum of first order Polynomial function and a
637 small gaussian peak, which is due to the small amount of flavor anti-correlated $B^+ \rightarrow D^0$
638 reconstructed events (see Fig. 53). The total two-dimensional PDF is a product of the
639 one-dimensional PDFs in M_{bc} and D^0 mass:

$$P_{B,D^0}^{GenBkg}(M_{bc}, M(K\pi)) = [\Gamma_{CB}(M_{bc}) + \Gamma_{Nov}(M_{bc})] \times [\rho_{pol1}(M(K\pi)) + \rho_G(M(K\pi))] \quad (10)$$

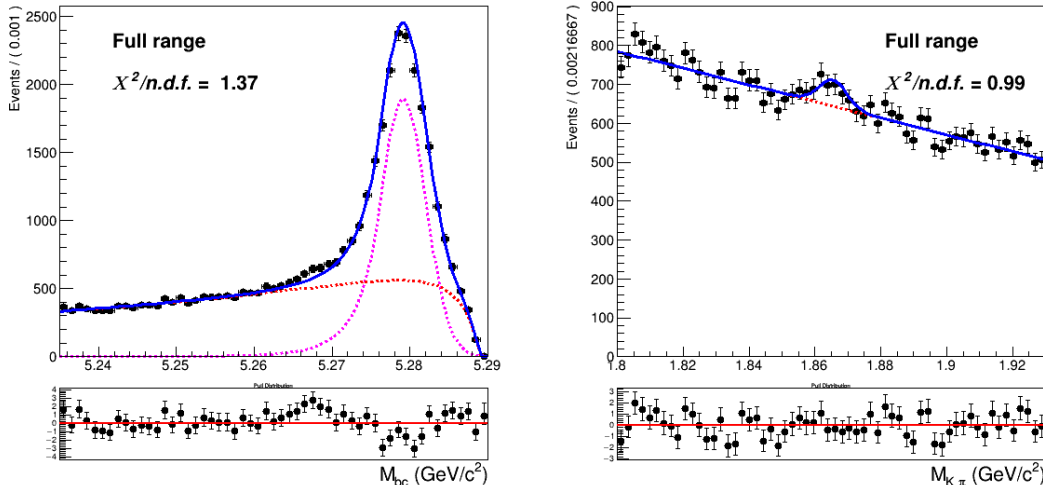


Figure (53) Two dimensional fit of generic ($B^+ B^-$) background events in M_{bc} and $M(K\pi)$.

640 **Crossfeed background** The crossfeed background deriving from $B^0 \bar{B}^0$ events is shown
 641 in Fig. 54. The M_{bc} distribution is fitted with a sum of Novosibirsk and Argus functions.
 642 The distribution in the D^0 mass is fitted with a first order Chebyshev polynomial and the
 643 D^0 mass peak is fitted with the same sum of three gaussians used to describe the signal
 644 peak (same parametrization used already in $B \rightarrow \Lambda_c$ analysis).

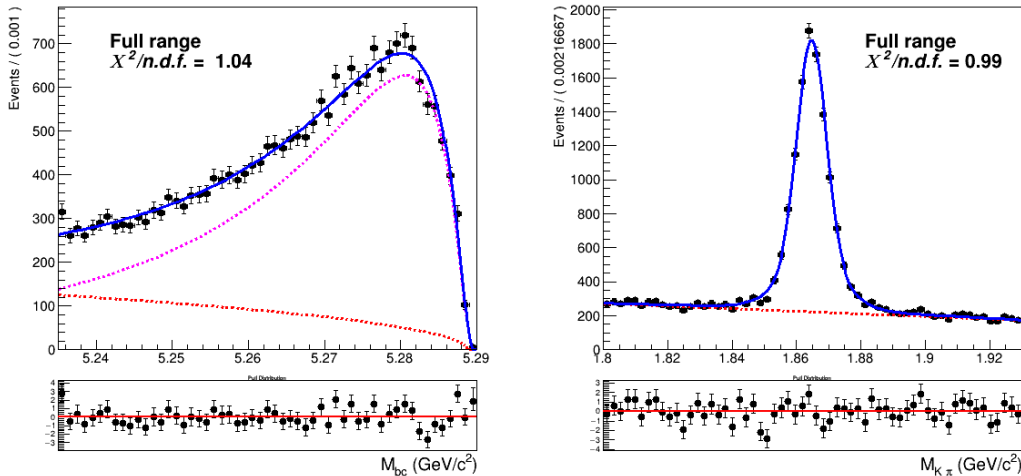


Figure (54) Two dimensional fit of crossfeed ($B^0 \bar{B}^0$) events in M_{bc} and $M(K\pi)$.

645 Continuum background

646 The procedure adopted to model the continuum background is the same used for the
 647 $B \rightarrow \Lambda_c$ decays, but in this case the available statistics is enough to perform the scaling
 648 with all the selection cuts also in the case of the two-dimensional fit (not removing the
 649 continuum suppression).

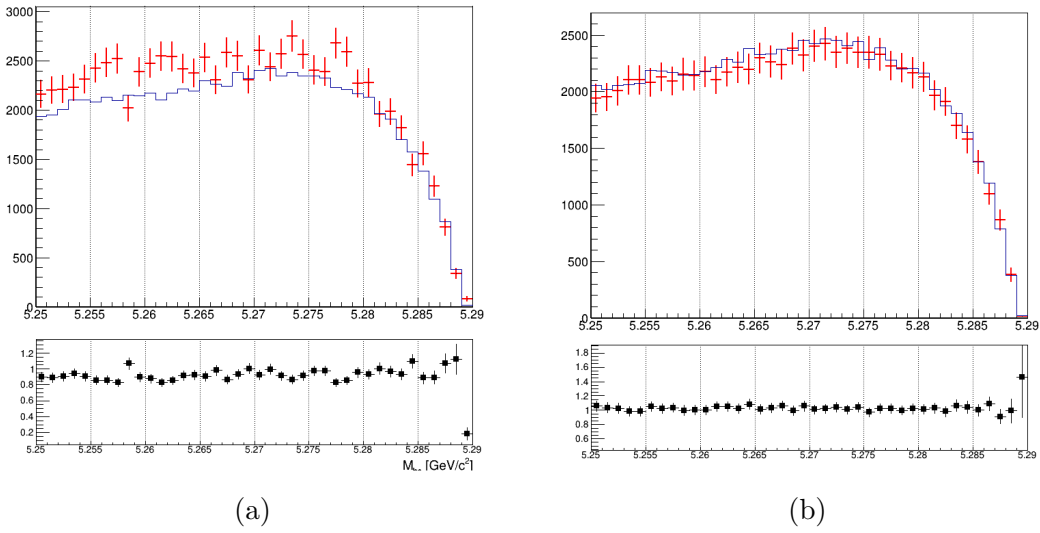


Figure (55) In Fig. 55a M_{bc} distributions of the MC (scaled) off-resonance sample (in red) and on-resonance (in blue). In Fig. 55b M_{bc} distributions of the corrected scaled off-resonance and on-resonance MC continuum.

For each bin a correction factor is calculated, in order to have a reasonable match with the expected continuum background. Fig. 55b shows the applied correction on an independent MC sample. As in the case of $B \rightarrow \Lambda_c$ analysis, then the resulting M_{bc} distribution is fitted with a Novosibirsk function , whereas the D^0 mass distribution is fitted with a sum of first order Chebyshev polynomial and the sum of three gaussians used to describe the signal peak (as shown in Fig. 56). The fraction of events in the peak is the same in on- and off-resonance MC. This method is applied also to scale the off-resonance data.

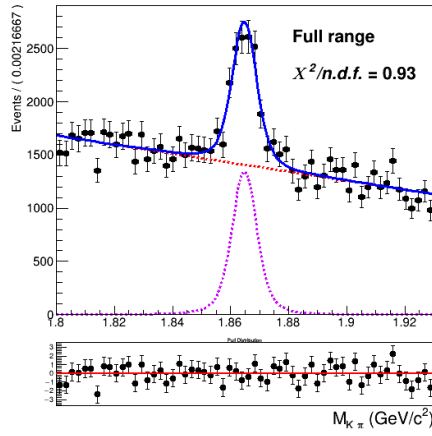


Figure (56) D^0 mass fit of scaled off-resonance Monte Carlo

657 **5.5 2D Fit on Monte Carlo simulated data**

658 As in the $B \rightarrow \Lambda_c$ study, five streams of Monte Carlo simulated data have been used to
 659 get values for the shaping parameters for the individual components described in the
 660 previous section and the fit model is tested on an independent stream.

661 For the six fits, the exact same conditions (floated parameters and fixed width ratios)
 662 were applied as to the two dimensional fit in the case of the $B \rightarrow \Lambda_c$ study. Exemplary, the
 663 distributions of stream 0 overlaid by the fitted PDF are depicted in Fig. 57 (see Appendix
 664 .2 for the projections of signal regions and sidebands).

665 In Table 7 the yields for reconstructed and misreconstructed signal are listed for each
 666 stream.

667

stream	0	1	2	3	4	5
NrecSig	56986 ± 400	57766 ± 437	55607 ± 426	57068 ± 372	58385 ± 369	57501 ± 437
NmisSig	31453 ± 321	30513 ± 350	32580 ± 350	33340 ± 399	29966 ± 390	32012 ± 355

Table (7) reconstructed and misreconstructed signal yields obtained fitting 6 independent streams

668 To be sure that the PDFs enables us to extract the signal yield in an unbiased way, the
 669 sum of reconstructed and misreconstructed signal yields, i.e. total signal, from the fits are
 670 compared to the true values of each stream (Table 8). There are quite some differences
 671 between the fitted signal yield and the true values in individual streams. However, all
 672 these deviations are within statistical expectations.

673

streams	fit	MC truth	fit - MC truth	
stream 0	88439 ± 340	88144	+ 295	(+0.33%)
stream 1	88279 ± 361	88551	-272	(- 0.31%)
stream 2	88187 ± 360	88487	-300	(- 0.34%)
stream 3	90408 ± 372	90149	+ 259	(+ 0.29%)
stream 4	88351 ± 383	87981	+ 370	(+ 0.42%)
stream 5	89513 ± 366	89710	-197	(- 0.22%)
sum	533177	533022	+155	(+0.03%)

Table (8) Comparison of fitted and truth-matched total signal events in each stream.

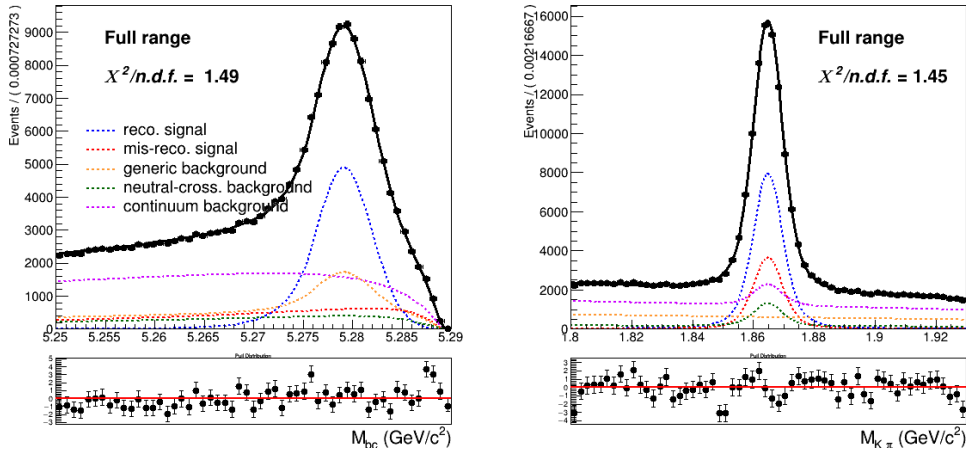


Figure (57) Two dimensional fit on stream 0 Monte Carlo simulated data.

674 5.6 2D Fit on data

675 After obtaining the model for the continuum background scaling and correcting the M_{bc}
 676 distribution of the off-resonance data, the model tested on Monte Carlo simulated data is
 677 applied on data with same free parameters and yields. Fig. 58 shows the projections of the
 two dimensional fit (see Appendix .2 for the projections of signal regions and sidebands).

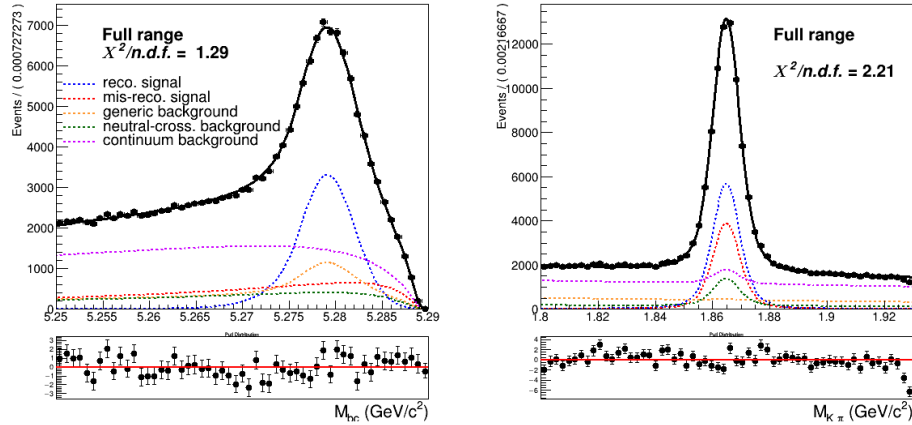


Figure (58) Two dimensional fit on Data (same conditions applied as in Fig. 57)

678
 679 Yields for the reconstructed and misreconstructed signal and for generic background are
 680 obtained from the fit:
 681

NrecSig	35629 ± 368
NmisSig	24425 ± 311
Generic	24596 ± 407

ratio	MC	DATA
NmisSig/NrecSig	0.56 ± 0.01	0.68 ± 0.01
NmisSig/Generic	0.90 ± 0.02	0.99 ± 0.02
Generic/NrecSig	0.62 ± 0.01	0.69 ± 0.02

Table (9) Comparison of ratios of yields from the two dimensional fits on Monte Carlo simulated data and on Data.

684 The total normalization from the fit is 174230 ± 407 (to be compared with the total
 685 data events: 173964).

686

687 Since in the case of the two dimensional fit for the measurement of $B^- \rightarrow \Lambda_c^+ X$ decays
 688 the crossfeed normalization was parametrized in the form described by Eq. (8), the 2D fit
 689 shown above is repeated with the parametrized normalization for the crossfeed background
 690 and the scaled signal reconstruction efficiency for data. Fig. 59 shows this second fit.
 691 In the following table yields for the reconstructed and misreconstructed signal and for
 692 generic background obtained from this second fit are reported:

693

NrecSig	36553 ± 360
NmisSig	24115 ± 283
Generic	25900 ± 409

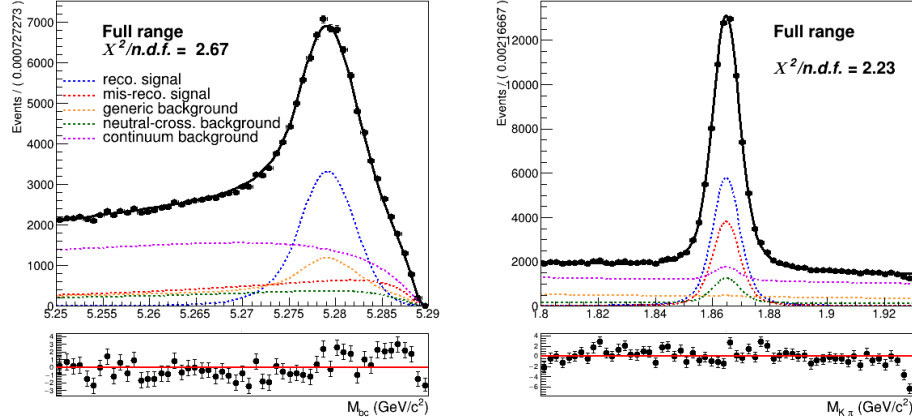


Figure (59) Two dimensional fit on Data with parametrized normalization of crossfeed background

695 5.7 Probability Density Functions (PDFs) for the B_{tag}

696 Like for the signal model in the 2D fit the M_{bc} distribution of the tagged charged B
 697 mesons is fitted with a Crystal Ball as for the reconstructed signal component, whereas
 698 the misreconstructed signal component is fitted with a Novosibirsk function (Fig. 60a).

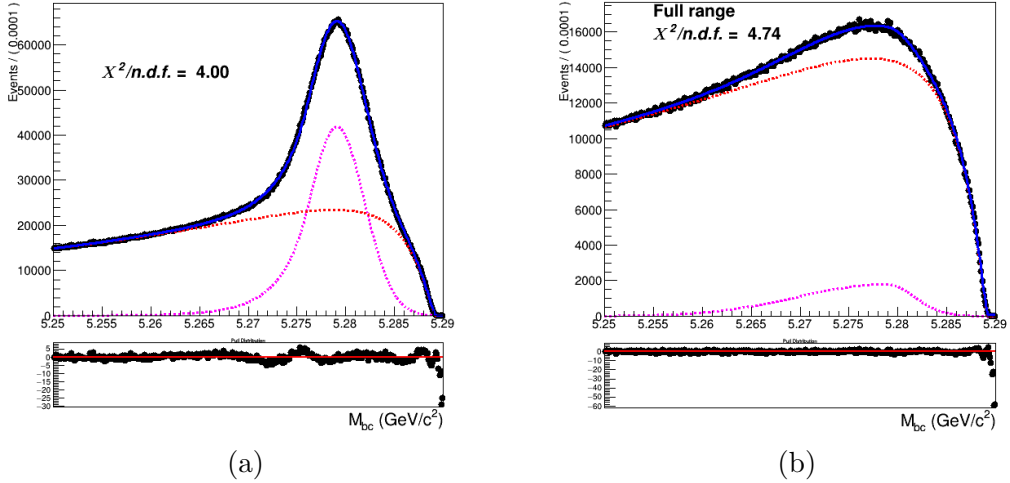


Figure (60) On the left: fitted distribution of tagged charged B mesons, reconstructed signal events (magenta) are described by a Crystal Ball whereas the misreconstructed signal events (red) are described by a Novosibirsk function. On the right: Crossfeed distribution fitted with a sum of Novosibirsk (red) and asymmetric Gaussian PDF (magenta)

699 The crossfeed background is fitted instead with a sum of a Novosibirsk and an asymmetric
 700 Gaussian PDF (Fig. 60b).

701
 702 Regarding the continuum background component, same procedure used for the 2D fit was
 703 applied to the M_{bc} distribution of the continuum background in this case (see Fig. ?? for
 704 the result).

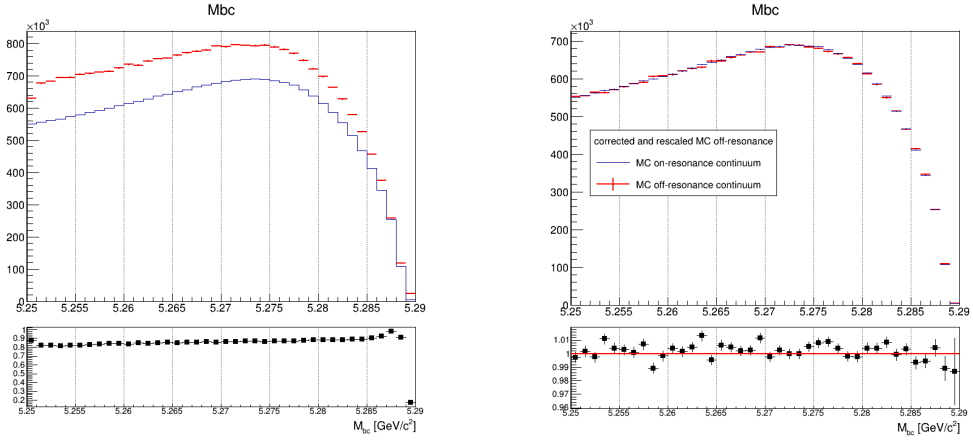


Figure (61) On the left: M_{bc} distributions of the MC off-resonance sample and the MC continuum sample. On the right: M_{bc} distributions of the corrected scaled MC off-resonance and on-resonance MC continuum.

705 5.8 B_{tag} Fit on Monte Carlo simulated data

706 An independent Monte Carlo stream was used to test the total fit model on tagged B
 707 mesons candidates. The usual condition is applied to the crossfeed background events:
 708 the ratio between its contribution and misreconstructed signal events is fixed from the
 709 other Monte Carlo stream.
 710 In this fit the shaping parameters that are not kept fixed are the Crystal Ball width (σ_{CB})
 711 and the width of the Novosibirsk function describing the misreconstructed signal events.
 712 As in the case of B_{tag} fit in Sec. 4.4 the range for the fit is restricted to values between
 713 5.250 and 5.287 GeV/c^2 .

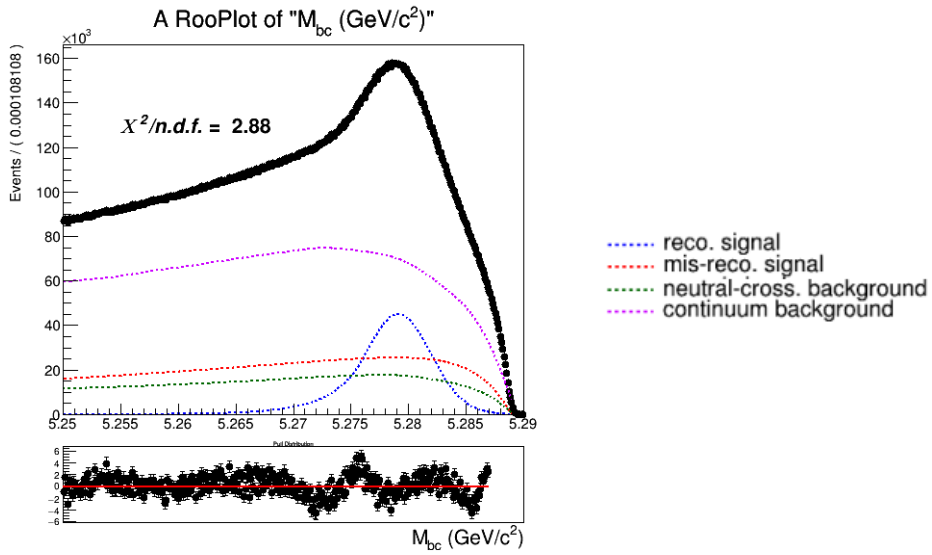


Figure (62) Total fit of tagged B mesons

714 Yields for the reconstructed and misreconstructed signal are obtained from the fit:

NrecSig	$3.25110 \cdot 10^6 \pm 6759$
NmisSig	$7.41107 \cdot 10^6 \pm 5341$

716 One can then compare the sum NrecSig+NmisSig (the so called total signal) with the true
 717 value known from the Monte Carlo and the same for the total number of events in this
 718 particular stream:

	fit	MC value
Total Signal	$10.662 \cdot 10^6 \pm 5249$	$10.671 \cdot 10^6$
Total events	$38.601 \cdot 10^6 \pm 6886$	$38.610 \cdot 10^6$

721 The discrepancy in the total signal events from the fit and the MC here is about 1.7σ , but
 722 the relative error is an order of magnitude smaller than the one found in B_{tag} fit in 4.4
 723 (below the %level), therefore it's negligible.

724 5.9 B_{tag} Fit on data

725 The fit model tested on Monte Carlo simulated data is then applied with the same method
 726 on data Fig. 63.

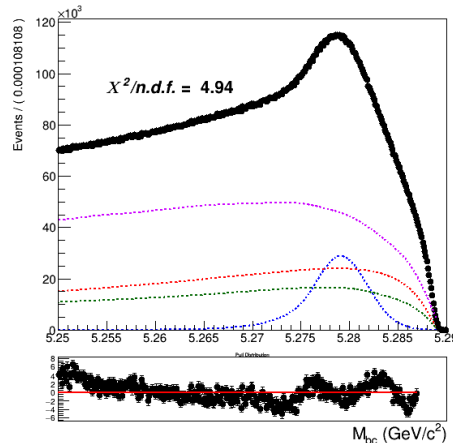


Figure (63) Total fit of tagged B^+ mesons candidates on data

727 Yields for the reconstructed and misreconstructed signal are obtained from the fit:

NrecSig	$2.011 \cdot 10^6 \pm 5858$
NmisSig	$6.975 \cdot 10^6 \pm 4667$
Total Signal	$8.982 \cdot 10^6 \pm 4587$

ratio	MC	DATA
NmisSig/NrecSig	2.28 ± 0.01	3.47 ± 0.01

Table (10) Comparison of ratios of yields from the tagged B mesons fits on Monte Carlo simulated data and on Data.

729 5.10 PID efficiency correction

730 The PID selection is applied only to Kaons: $\frac{\mathcal{L}_K}{\mathcal{L}_K + \mathcal{L}_\pi} > 0.6$

731 Using the values provided in the global tag **BellePID** (as done in the $B \rightarrow \Lambda_c$ study),
732 the average Kaon ID correction for this analysis is estimated to be $R = 0.976 \pm 0.008$.

733 5.11 D^0 and FEI efficiency

734 The efficiency in reconstructing the D^0 after correctly tagging the charged B meson, can
735 be estimated from the 2D fit on Monte Carlo simulated data, using the reconstructed
736 signal yield and from a sample of B_{tag} candidates reconstructed in signal events in the
737 Monte Carlo: where from B^+B^- at least a D^0 decaying into πK is produced.

738 For the latter a fit is performed to extract the yield of correctly tagged B mesons (Fig.
739 64)

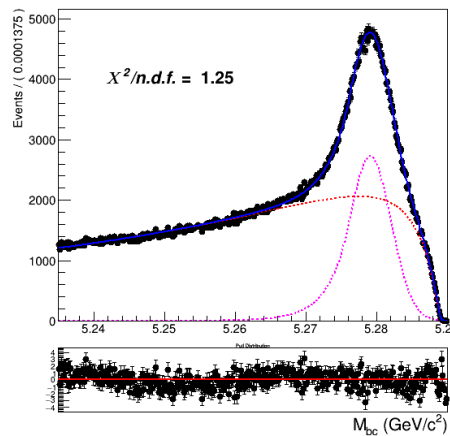


Figure (64) Fit of tagged B mesons in the "signal events" sample

740 Yields for the reconstructed and misreconstructed signal :

NrecSig	$1.46779 \cdot 10^{-5} \pm 767$
NmisSig	$6.16717 \cdot 10^{-5} \pm 1028$

742 From this and the results listed in Sec. 5.5 the efficiency to reconstruct D^0 is obtained :

$$743 \quad \epsilon_{D^0} = \frac{NrecSig(2D)}{NrecSig((B_{tag}^{sig})} = 39.1 \pm 0.4\%^6 \quad (\text{KID efficiency corrected value for data: } 38.2 \%)$$

746 The results from the fit shown in (Fig. 64) can be used also to calculate the FEI tag-side
747 efficiency for signal events, i.e. the efficiency to tag the B meson accompanying a B_{sig}
748 decaying into a D^0 on the signal side. Whereas results from the fit of charged B_{tag} shown

⁶the error reflects the limited Monte Carlo statistics

749 in Fig. 60a can be used to calculate the hadronic tag-side efficiency in the generic B^+B^-
 750 events case.

751 The ratio of the two efficiencies is found to be: $\frac{\epsilon_{FEI,sig}^+}{\epsilon_{FEI}^+} = 1.50 \pm 0.01$
 752

753 5.12 Studies of Systematic Effects

754 The systematic uncertainties are studied the same way as in the case of the $B^+ \rightarrow \bar{\Lambda}_c^- X$
 755 branching fraction. The values are reported in the next section. Again, the dominant
 756 systematic uncertainty is the one originated by the continuum background modeling and
 757 its incidence in terms of relative error on the branching fraction value is same as for the
 758 $B^+ \rightarrow \bar{\Lambda}_c^- X$ study.

759 5.13 Measured $B^+ \rightarrow \bar{D}^0 X$ inclusive Branching Fraction

760 The inclusive branching fraction of $B^+ \rightarrow \bar{D}^0 X$ can be determined by:

$$Br(B^+ \rightarrow \bar{D}^0) = \frac{r}{Br(D^0 \rightarrow K^+\pi^-)\epsilon_{D^0}} \cdot \frac{\epsilon_{FEI}^+}{\epsilon_{FEI,sig}^+} \quad (11)$$

761 Where

- 762 • $r = \frac{N_{tag,D^0}}{N_{tag}}$ is the ratio of reconstructed signal yield in the two dimensional fit and in
 763 the M_{bc} fit of the tagged B mesons.
- 764 • ϵ_{D^0} is the D^0 reconstruction efficiency calculated as fraction of reconstructed signal
 765 events with correct tag of which then also a correctly reconstructed D^0 is recon-
 766 structed in the signal side.
- 767 • $\frac{\epsilon_{FEI}^+}{\epsilon_{FEI,sig}^+}$ is the ratio of the FEI efficiencies: the hadronic tag-side efficiency for generic
 768 B^+B^- events (ϵ_{FEI}^+) and signal-side dependent one ($\epsilon_{FEI,sig}^+$) where one of the two B
 769 mesons decays inclusively into the signal channel ($D^0 \rightarrow K^+\pi^-$)
- 770 • $Br(D^0 \rightarrow K^+\pi^-) = 3.8\%$ in Belle DECAY.DEC table, $Br(D^0 \rightarrow K^+\pi^-) = 3.95\%$
 771 in PDG.

772 In Monte Carlo: $Br(B^+ \rightarrow \bar{D}^0) = 79.4 \pm 0.6^{(stat.)}\%$ (true MC value: 79.1%)
 773

774 As for the Data, the value obtained using a fixed ratio of crossfeed events with respect to
 775 misreconstructed signal events is: $Br(B^+ \rightarrow \bar{D}^0) = 78.3 \pm 0.8^{(stat.)}\%$
 776

777 While, introducing the parametrization of the crossfeed normalization in the two dimen-
 778 sional fit gives a larger value: $Br(B^+ \rightarrow \bar{D}^0) = 80.3 \pm 0.8^{(stat.)}\%$

779 Nevertheless, the latter is in agreement with the value reported by the PDG: $(79 \pm 4)\%$
780 One can conclude that the obtained results have proven the validity of the method chosen
781 for the measurements.
782 The systematic uncertainties are dominating as one can see from the Table below, listing
783 the contribution of the various sources of systematics in terms of Branching Fraction in
784 percentage.

785

continuum modelling	1.8 %
Crossfeed PFDs	0.4 %
Crossfeed fraction	0.8 %
FEI efficiency	0.5 %
ϵ_{D^0}	0.8 %
PID	0.6 %
Total	2.3 %

Table (11) Sources of systematic uncertainties and their contributions.

786 **6 $B^- \rightarrow \bar{\Lambda}_c^-$ decays**

787 Applying the same procedure already illustrated in Sec. 4, the optimized selection cuts for
 788 the charged flavor-anticorrelated decays are:

- 789 • $\text{foxWolframR2} < 0.3$
 790 • $\text{SignalProbability} > 0.1$
 791 • $p_{CM\text{S}}^{\Lambda_c} < 1.5 \text{ GeV}/c$

792 **6.1 Probability Density Functions (PDFs) for the two dimensional fit**
 793

794 The PDFs used to describe the signal distributions are the same already used in Sec. 4.1
 795 (only the shaping parameters differ) and an example of the 2D fit is shown in Fig. 65.
 796 Also the generic background deriving from other B^+B^- events presents similar shapes of
 797 the distributions as shown already in Sec. 4.1, therefore the probability density functions
 798 used are the same (fit is shown in Fig. 66).

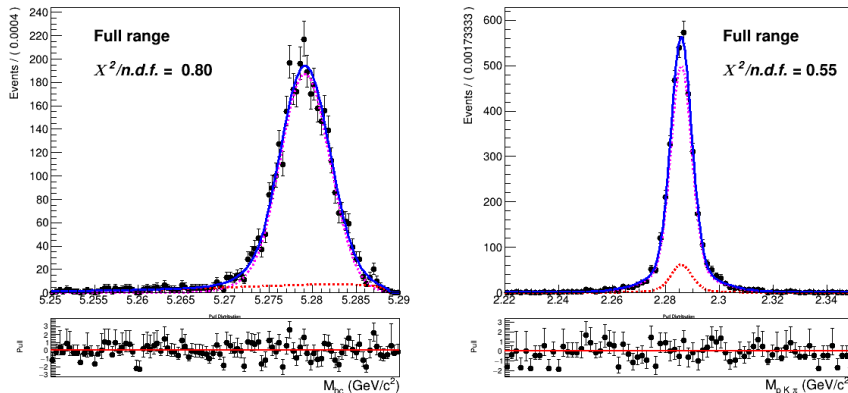


Figure (65) Two dimensional fit of total signal events in M_{bc} and $M(pK\pi)$.

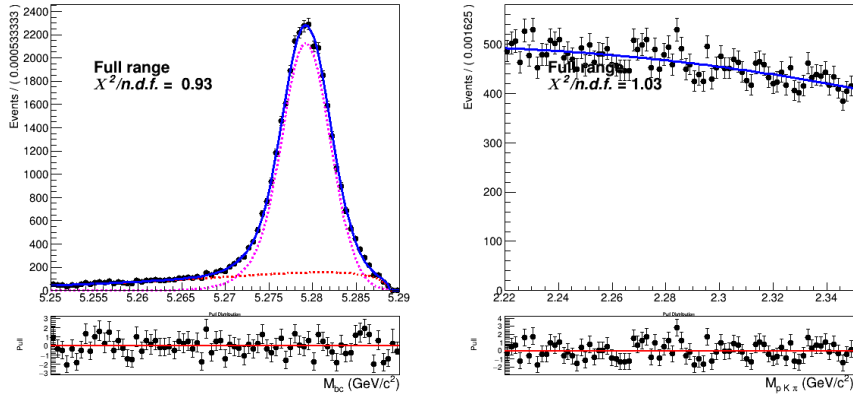


Figure (66) Two dimensional fit of generic (B^+B^-) events in M_{bc} and $M(pK\pi)$.

799 The same can be said about the misreconstructed B^0 events (Fig. 67)

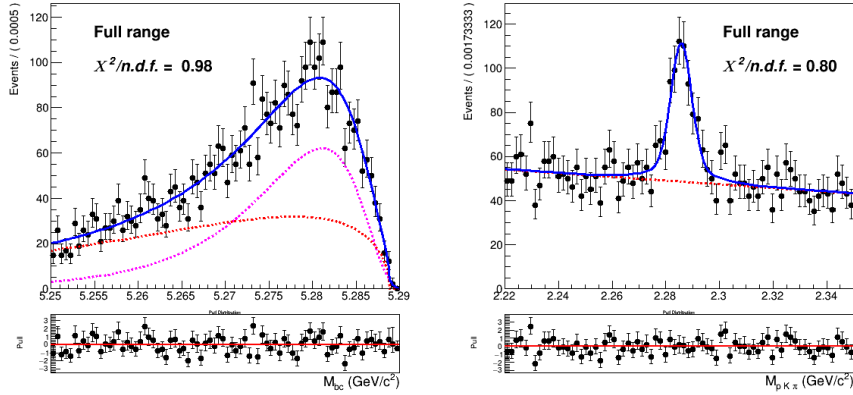


Figure (67) Two dimensional fit of crossfeed ($B^0\bar{B}^0$) events in M_{bc} and $M(pK\pi)$.

800 To check that the shapes determined using 5 streams of Monte Carlo are describing with
 801 reasonable accuracy the 2D distribution, the projections of the fit of the two-dimensional
 802 distributions in the signal and sideband regions are plotted (Fig. 69 - Fig. 71). One can see
 803 the same tendencies of undershooting/overshooting the Λ_c invariant mass peak, as in the
 804 case of charged correlated decays (Figures 18 - 19). But when examining the independent
 805 Monte Carlo stream distribution overlaid by the determined PDF in the very same regions
 806 (see Figures 72 - 74) those effects are so much diminished, according to the statistics, that
 807 the effects are within statistical fluctuations and therefore negligible, contrary to the case
 808 of charged flavor-correlated decays.

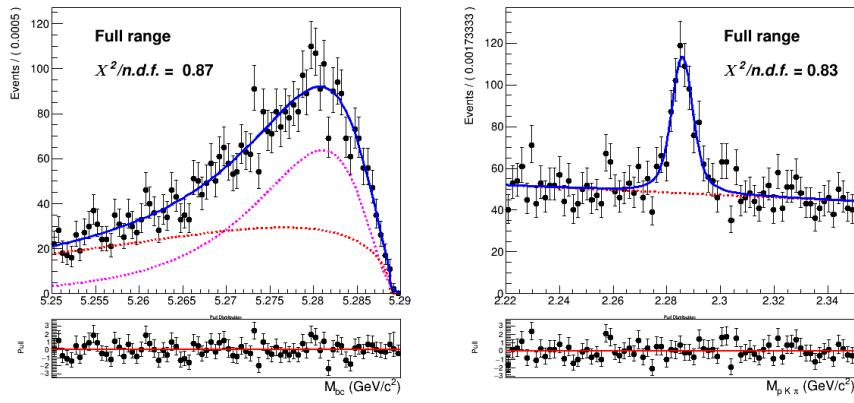


Figure (68) Two dimensional fit of crossfeed ($B^0 \bar{B}^0$) events in M_{bc} and $M(pK\pi)$.

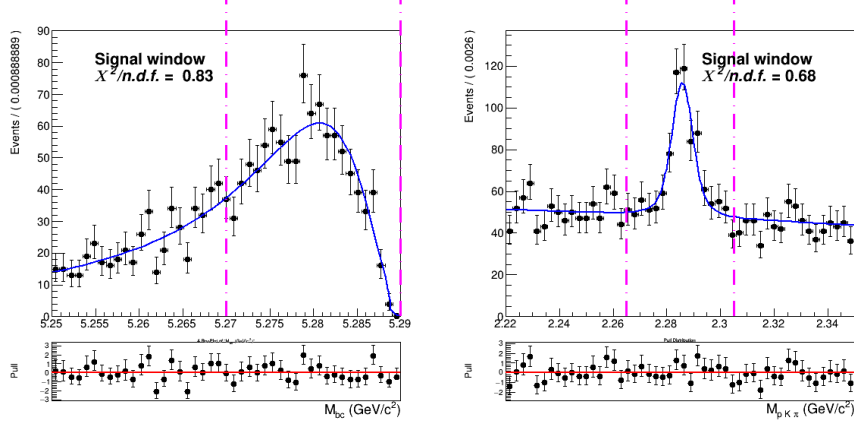


Figure (69) Signal region projections in M_{bc} and $M(pK\pi)$ of the fit of crossfeed events.

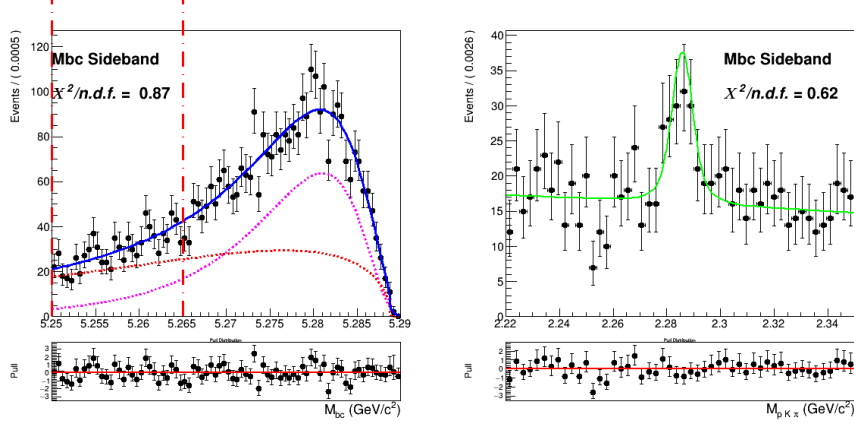


Figure (70) M_{bc} sideband region projection of the fit of crossfeed events in $M(pK\pi)$.

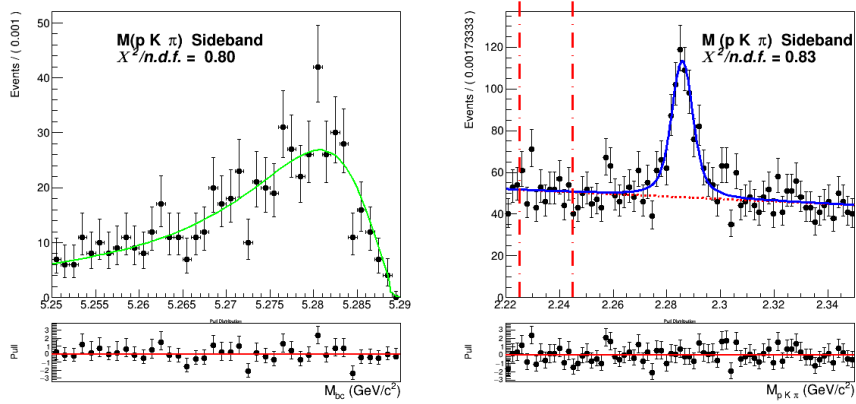


Figure (71) $M(pK\pi)$ sideband region projection of the fit of crossfeed events in M_{bc} .

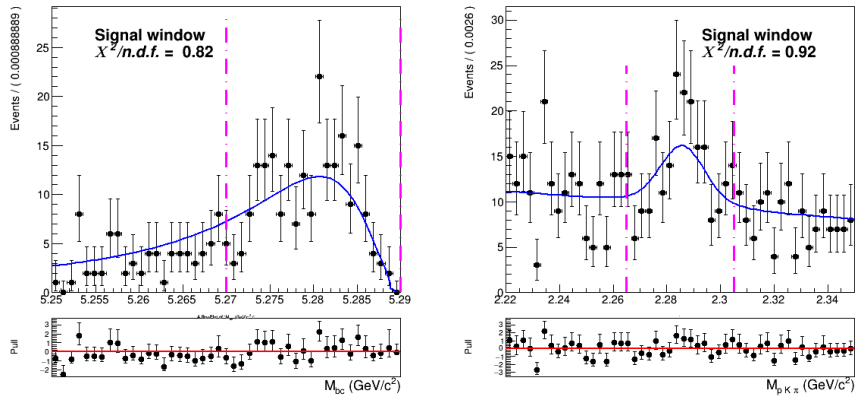


Figure (72) Signal region projections in M_{bc} and $M(pK\pi)$ of the fit of crossfeed events.

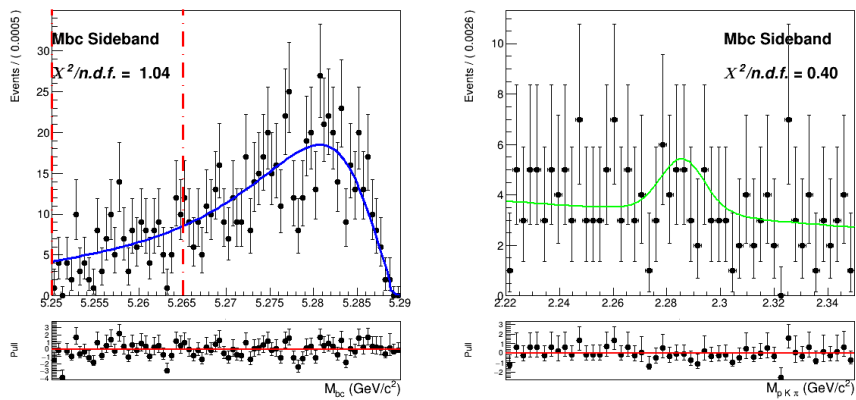


Figure (73) Two dimensional fit of crossfeed ($B^0\bar{B}^0$) events in M_{bc} and $M(pK\pi)$.

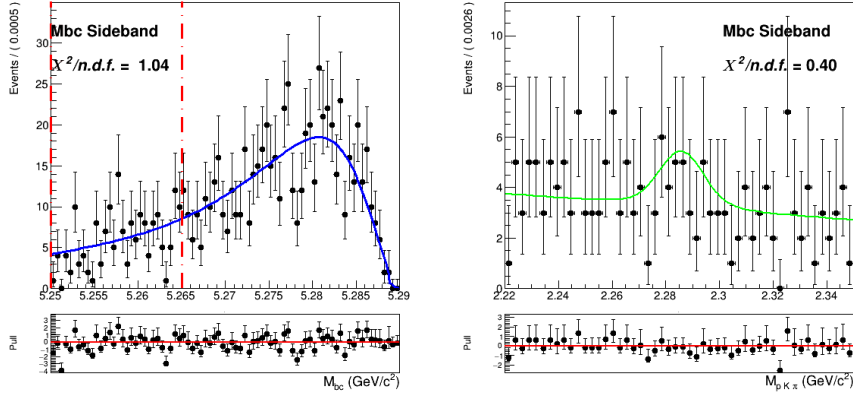


Figure (74) Two dimensional fit of crossfeed ($B^0\bar{B}^0$) events in M_{bc} and $M(pK\pi)$.

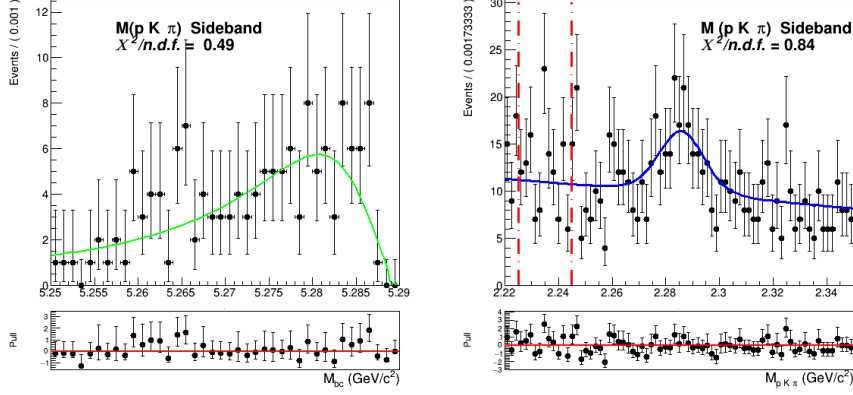


Figure (75) Two dimensional fit of crossfeed ($B^0\bar{B}^0$) events in M_{bc} and $M(pK\pi)$.

809 The procedure adopted to model the continuum background is the same used for the
 810 charged correlated $B \rightarrow \Lambda_c$ decays. To obtain the shape that can describe the continuum
 811 background M_{bc} distribution, the continuum suppression is not applied on the off-resonance
 812 continuum sample in order to acquire more statistics. It is then scaled and corrected for
 813 the *SignalProbability* correlated effects. The scaling and bin-correction procedure was
 814 carried out on a sample of five streams of on- and off-resonance MC. From a ratio plot,
 815 like the one in Fig. 76a, showing the continuum on-resonance distribution in M_{bc} and the
 816 scaled continuum off-resonance distribution without the continuum suppression applied,
 817 the bin-correction is obtained to correct the off-resonance data in the scaling procedure.

818 The validity of this procedure is first tested on the sixth independent MC sample: Fig.
 819 76b shows the scaled and bin-corrected off-resonance continuum histogram compared with
 820 the continuum on-resonance distribution of the independent stream. Compared to the
 821 charged correlated decays one can notice larger statistical fluctuations but the overall
 822 result looks still fairly reasonable. In order to obtain the PDF describing the distribution
 823 the histogram is fitted (see Fig. 77a), i.e. with a Novosibirsk function.
 824 Since in the Λ_c invariant mass one doesn't expect correlation effects, one can fit directly the
 825 properly scaled distribution with a first order polynomial (see Fig. 77b) It is possible then
 826 to check the validity of the whole procedure on the on-resonance Monte Carlo independent
 827 stream (Fig. 78)

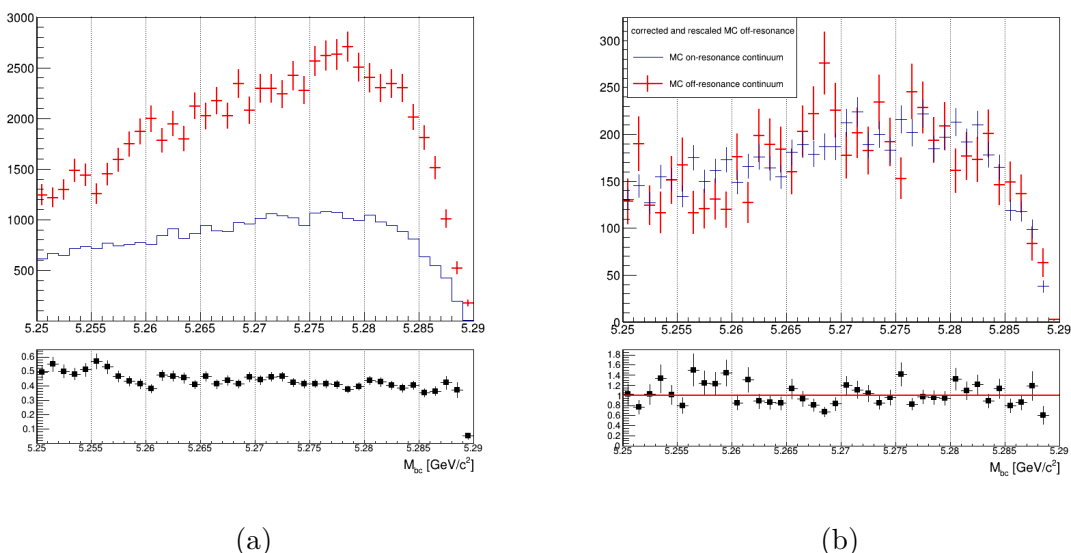


Figure (76) On the left: M_{bc} distributions of the MC off-resonance sample without continuum suppression and the MC continuum sample with applied continuum suppression (5 streams). On the right: M_{bc} distributions of the corrected scaled MC off-resonance and on-resonance MC continuum (independent stream).

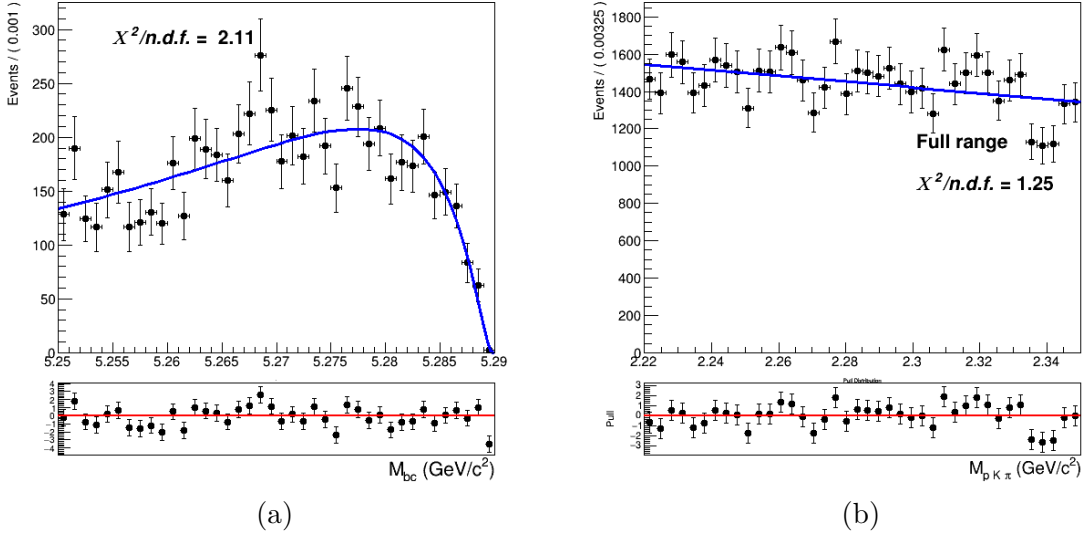


Figure (77) On the left: fit of the M_{bc} distribution MC (scaled and corrected) off-resonance continuum (one stream). On the right: fit of the Λ_c invariant mass distribution of five stream scaled off-resonance continuum.

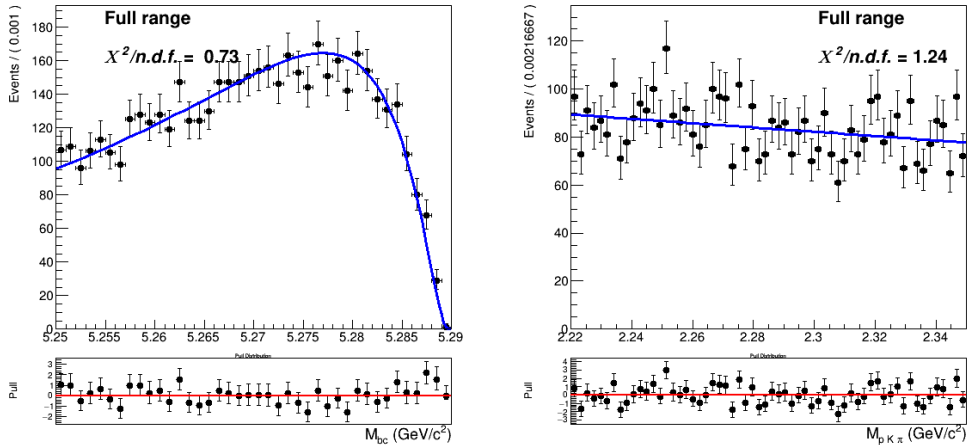


Figure (78) Continuum M_{bc} and $M(pK\pi)$ distributions overlaid by the PDFs obtained in fits shown in Figures 77a - 77b

828 6.2 Two dimensional fit

829 After obtaining the PDFs describing the various signal/background components using five
 830 streams statistics, the fit model is tested with six fits on the six independent Monte Carlo
 831 streams. The conditions for these six two dimensional fits are again the same used for the
 832 charged correlated decays (see Sec. 4.2). Exemplary, the distributions of stream 0 overlaid

833 by the fitted PDF are depicted in Fig. 79 (see Appendix .3 for the projections in signal
 834 and sideband regions). In Table 1 the signal yields of the fits (**Reconstructed Signal**)
 835 to the two dimensional distributions for the six streams of $B^- \rightarrow \bar{\Lambda}_c^-$ flavor-anticorrelated
 836 decays are listed and compared to the expected yields of reconstructed signal, and fitted
 837 and truth-matched total signal events are also compared, together with their deviations.

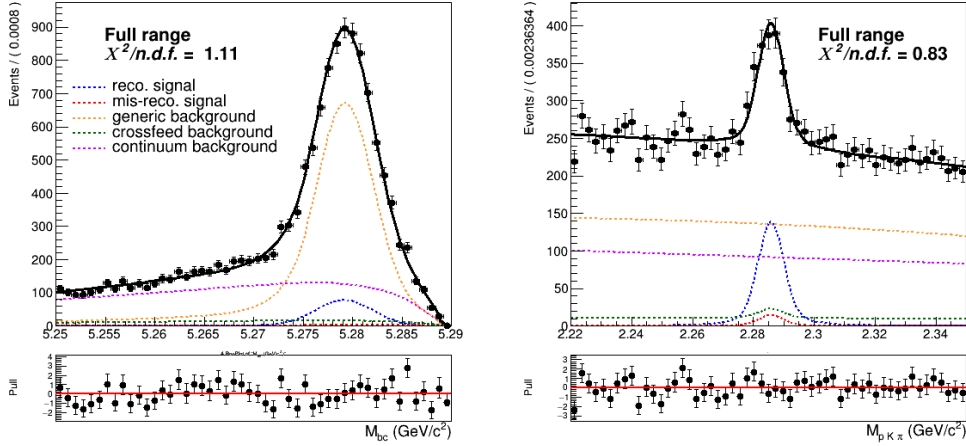


Figure (79) Two dimensional fit on stream 0 Monte Carlo simulated data.

	Reconstructed Signal		Total Signal			
	fit	expected	fit	MC truth	fit - MC truth	
stream 0	730 ± 60	660 ± 21	805 ± 65	765	40	5.2 %
stream 1	732 ± 60	698 ± 29	794 ± 63	785	9	1.1%
stream 2	759 ± 65	718 ± 29	800 ± 67	797	3	0.4%
stream 3	725 ± 58	702 ± 29	769 ± 60	802	-33	-4.1%
stream 4	829 ± 67	710 ± 29	944 ± 76	804	140	17.4%
stream 5	650 ± 61	675 ± 29	703 ± 62	760	-57	-8.1%
sum	4425	4163	4815	4718	102	+ 2.2%

Table (12) Comparison of fitted and expected signal yields, fitted and truth-matched total signal for six streams of Belle generic MC when fitting the two dimensional distributions of M_{bc} and $M(pK\pi)$.

838 Except for stream 4 all the fits show values of reconstructed signal within the 1σ uncer-
 839 tainties in agreement with the expected ones, but as already encountered in Sec. 4.2 a
 840 tendency of overestimation can be seen also in these fits, confirmed by the fit shown in Fig
 841 81. Again this small, but not negligible, bias has to be taken into account while fitting the
 842 data.

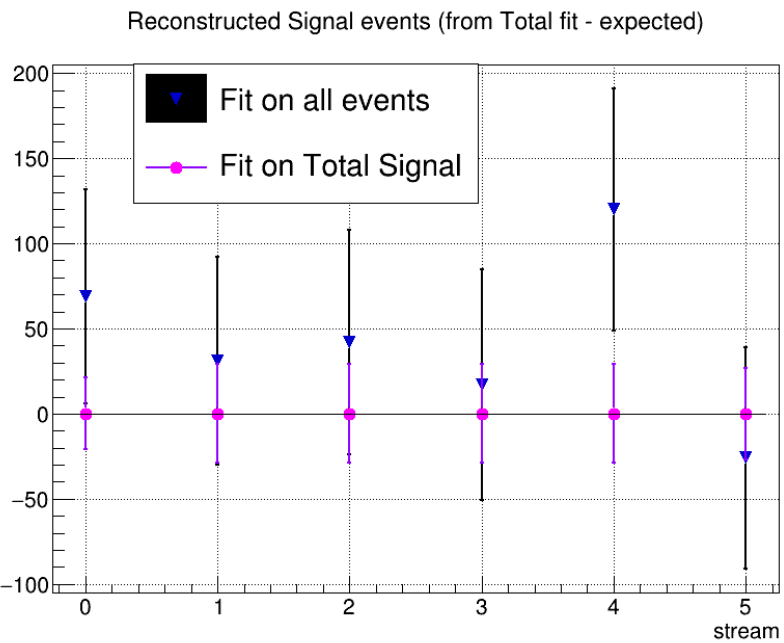


Figure (80) Differences between results from the fits and "expected" values for signal yields as reported in the first columns on Table 12 .

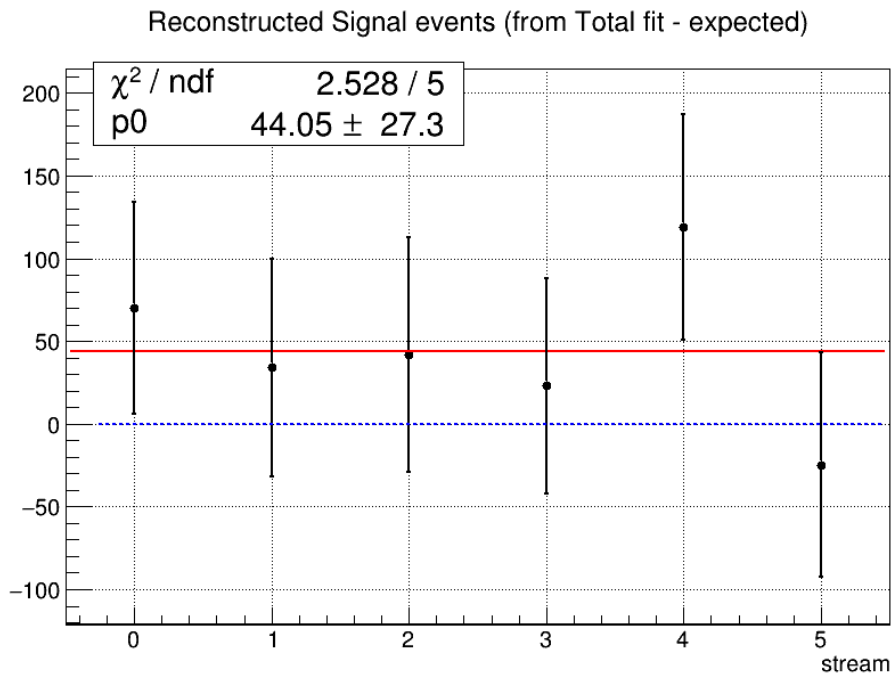


Figure (81)

⁸⁴³ Also the behaviour for different signal-to-background ratio was investigated using the six

844 independent streams of continuum and all the ten independent streams of $B\bar{B}$ events
 845 for the generic and crossfeed backgrounds and for the signal events. The amount of
 846 total signal is varied between 50% and 275% of the nominal (MC) values, in order to
 847 cover the values spanned by the uncertainties on the measurement performed by *BaBar*
 848 ($\mathcal{B}(B^+ \rightarrow \bar{\Lambda}_c^+ X) = 2.1^{+0.9}_{-0.6}$) and even the values covered by twice larger uncertainties as
 849 one can see in Fig. 83. The values seem to distribute according to a linear dependence,
 850 therefore also for this decay channel one doesn't expect any systematics due to different
 851 signal-to-background ratio.

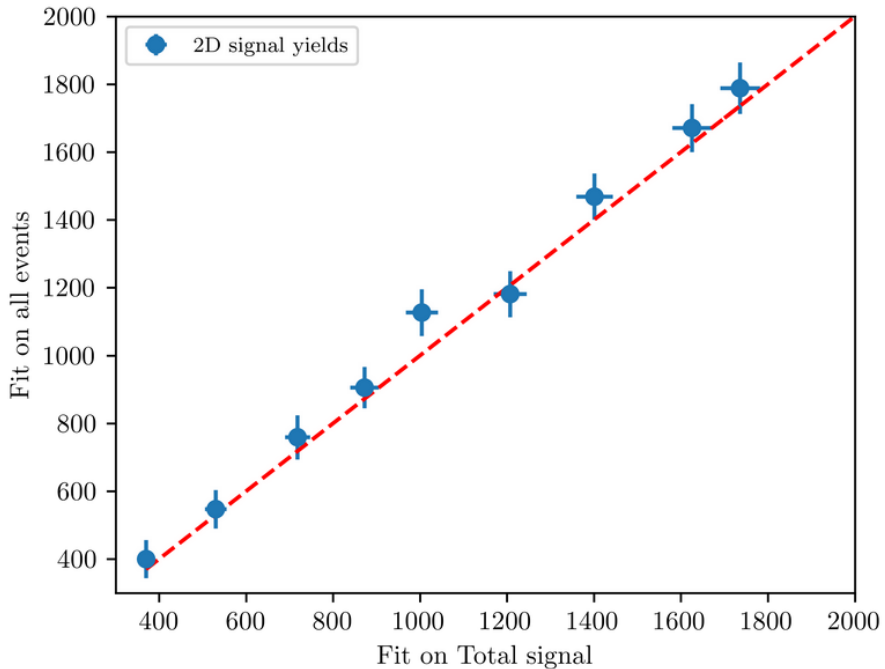


Figure (82) Linearity test: on the x-axis the obtained reconstructed signal yields from fits on different amounts of total signal; on y-axis the yields of reconstructed signal obtained fitting all events (as in Fig. 34). The dashed red line represents the 1:1 linear dependence.

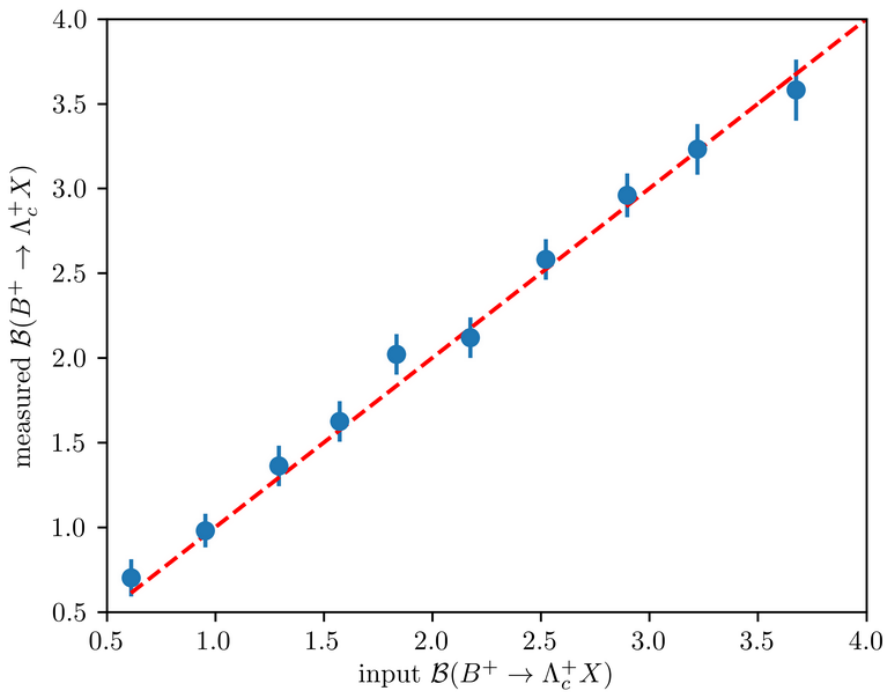


Figure (83) Linearity test: on the x-axis the input branching ratio value corresponding to the signal yields displayed on the x-axis in Fig. 82; on y-axis the measured branching fraction values corresponding to the signal yields of reconstructed signal displayed on the y-axis in Fig. 82.

⁸⁵² Toy MC pseudo-experiments were performed as well (see Appendix).

853 6.3 Probability Density Functions (PDFs) for the B_{tag}

854 The M_{bc} distribution of the tagged B mesons is fitted with a Crystal Ball as for the
 855 "peaking" component and the "flat" component is fitted with a Argus function (Fig. 84a).
 856 The crossfeed background, consisting of neutral B mesons tagged as charged B , is fitted
 857 instead with a sum of a Novosibirsk and an asymmetric Gaussian PDF (Fig. 84b).

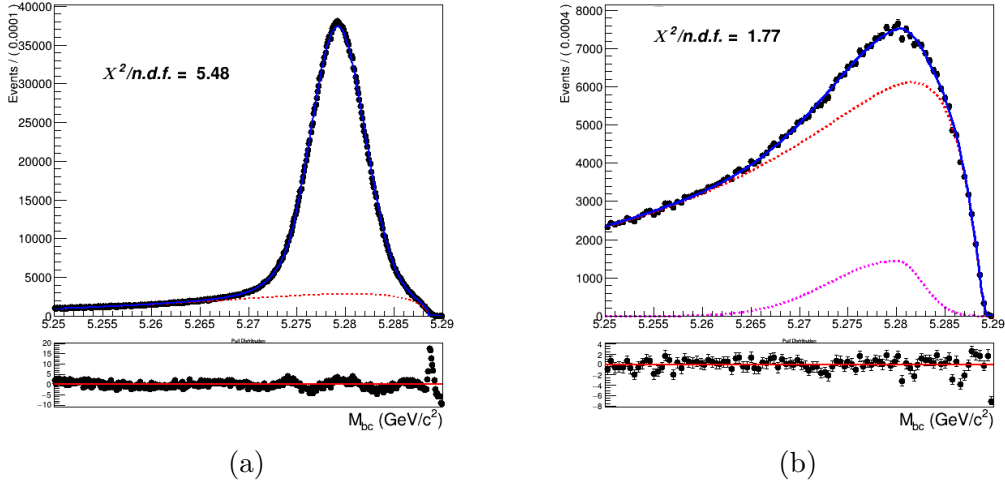


Figure (84) On the left: fitted distribution of tagged charged B mesons, reconstructed signal events (magenta) are described by a Crystal Ball whereas the misreconstructed signal events (red) are described by an Argus function. On the right: Crossfeed distribution fitted with a sum of Novosibirsk (red) and asymmetric Gaussian PDF (magenta)

858 As for the continuum background, same procedure as the one in the case of charged
 859 flavor-correlated decays is adopted:

- 860 • first the off-resonance sample is scaled accordingly with all the included cuts.
- 861 • the ratio between the scaled off-resonance and the on-resonance in MC is calculated
 862 in each bin (see Fig. 85a)
- 863 • the bin-correction is applied on an independent stream and the scaled and bin-
 864 corrected M_{bc} distribution is compared with the on-resonance distribution as shown
 865 in Fig. 85b

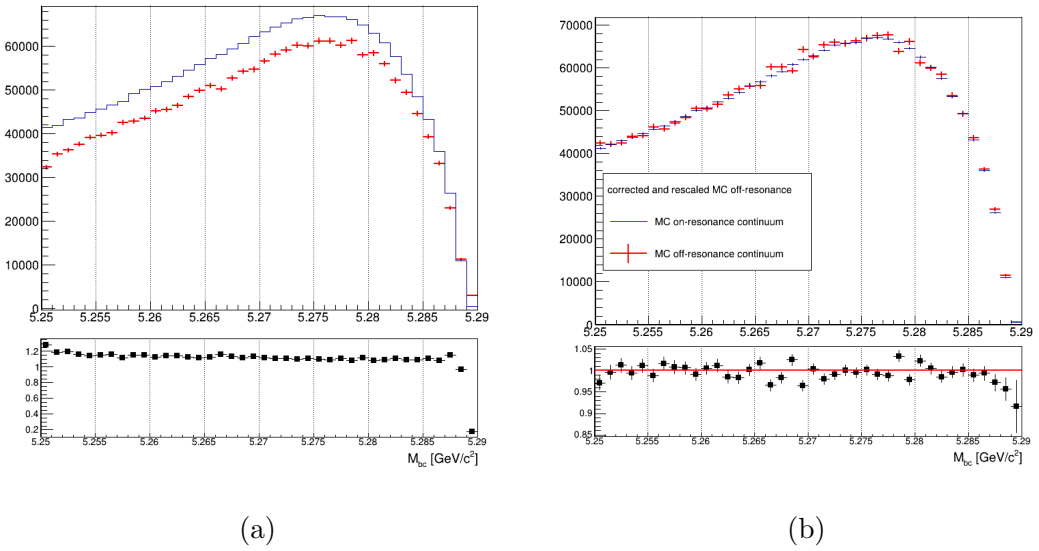


Figure (85) On the left: M_{bc} distributions of the MC off-resonance sample and the MC continuum sample with applied continuum suppression. On the right: M_{bc} distributions of the corrected scaled MC off-resonance and on-resonance MC continuum.

866 **6.4 B_{tag} fit**

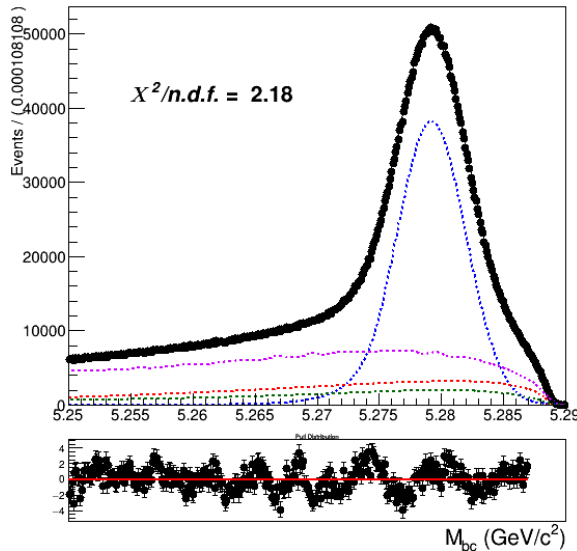


Figure (86) Total fit of tagged B mesons on Monte Carlo simulated data.

867 An independent Monte Carlo stream was used to test the total fit model on tagged B
 868 meson candidates. As in the 2D fit, the parameter for the width, σ_{CB} , of the Crystal Ball is
 869 floated and the ratio between expected crossfeed background events and misreconstructed
 870 signal events is fixed from the MC. The Argus function describing the misreconstructed
 871 signal is also not fully constrained: the parameter describing the tail is free. As in the
 872 previous B_{tag} fits, the range for the fit is restricted to values between 5.250 and 5.287
 873 GeV/c^2 . Yields for the reconstructed and misreconstructed signal are obtained from the
 874 fit:

875

NrecSig	$2.5099 \cdot 10^6 \pm 4408$
NmisSig	$7.82307 \cdot 10^5 \pm 2936$

877 The Total Signal (the sum NrecSig+NmisSig) is 3292168 ± 2423 (to be compared with
 878 3299629 from the Monte Carlo), which means a $\sim 3\sigma$ underestimation. As in the case of
 879 charged flavor-correlated decays, this can produce some systematic effect which needs to
 880 be taken into account. In fact, a slight underestimation of the Total Signal is found also
 881 in the result of the toy Monte Carlo study⁷: Fig. 87 shows the results for the Total Signal
 882 events and one can notice a mean value for the pulls consistently below zero.

⁷as usual performed with 3×10^3 pseudo-datasets

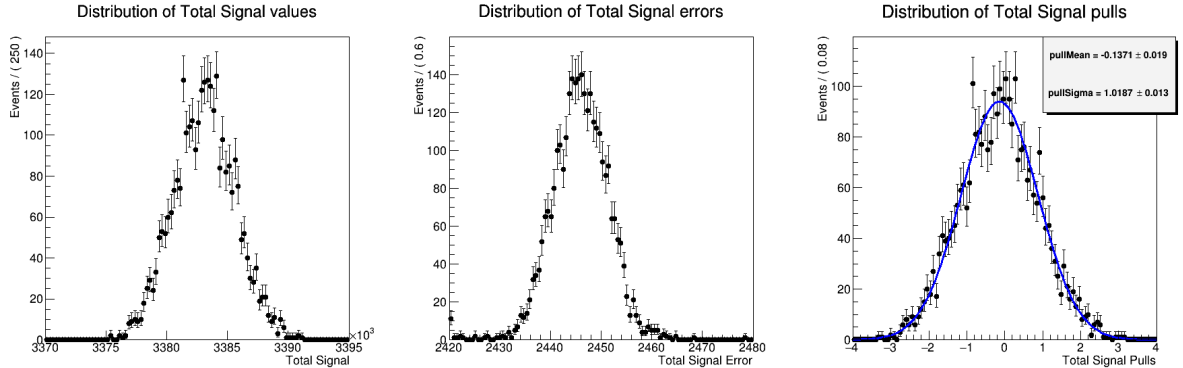


Figure (87) Toy MC fits of pseudo-data showing the Total Signal yield (left), Total Signal yield errors (center) and the pull distribution of the Total Signal (right).

883 6.5 Λ_c and FEI efficiency

884 The efficiency in reconstructing the Λ_c baryon after correctly tagging the charged B meson,
 885 is as usual estimated as the ratio:

$$\frac{N_{recSig}(B_{tag}, \Lambda_c)}{N_{recSig}(B_{tag}^{sig})} \quad (12)$$

886 where $N_{recSig}(B_{tag}, \Lambda_c)$ are the yields of reconstructed signal from the two dimensional fits
 887 (reported in Table 12) and $N_{recSig}(B_{tag}^{sig})$ are the yields of correctly reconstructed signal in
 888 a fit of B mesons tagged in events where one of the two mesons decayed hadronically and
 889 inclusively into a Λ_c baryon (see Fig 46). This ratio was calculated upon six streams of
 890 Monte Carlo simulated data.

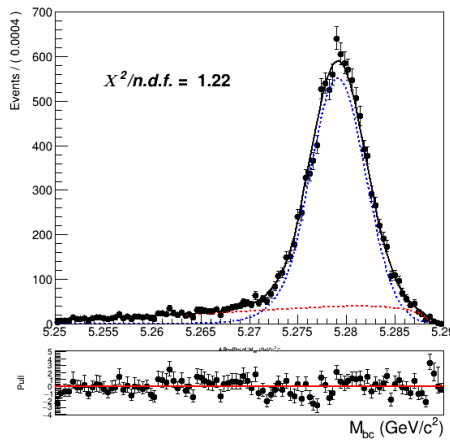


Figure (88) Fit of tagged B mesons in the "signal events" sample

891 From this and the results listed in Sec. 6.2 the efficiency to reconstruct Λ_c is obtained :

$$892 \quad \epsilon_{\Lambda_c} = \frac{N_{recSig}(B_{tag}, \Lambda_c)}{N_{recSig}(B_{tag})} = 40.95 \pm 1.77\%$$

894 The yields from the fit shown in Fig. 88) are then used to calculate the FEI tag-side
 895 efficiency for signal events. The yields from the fit of charged B_{tag} shown in Fig. 84a can
 896 be used to calculate the hadronic tag-side efficiency in the generic B^+B^- events case.

897 The ratio between the two efficiencies is calculated: $\frac{\epsilon_{FEI,sig}^+}{\epsilon_{FEI}^+} = 0.973 \pm 0.009$

899 6.6 Studies of Systematic Effects

900 The systematic uncertainties are estimated the same way as in the case of charged flavor-
 901 correlated decays (see Sec. 4.7 and the following Sections). In Table 13 the systematic
 902 uncertainties of the various considered sources are summarized. Their individual calculation
 903 is outlined in the subsequent subsections (the uncertainties on the PID efficiency corrections
 904 are the same already discussed in Sec. 4.14)

source	%
Continuum modeling	0.04
Crossfeed PDFs	0.01
Crossfeed fraction	0.01
2DFit crossfeed normalization	0.01
2DFit crossfeed peaking fraction	0.08*
$\epsilon_{FEI,sig}^+/\epsilon_{FEI}^+$	0.01
ϵ_{Λ_c}	0.05
Fit bias	0.05
PID	0.02
Total	0.12

Table (13) Systematic uncertainties in the determination of the $B^- \rightarrow \bar{\Lambda}_c^- X$ branching fractions in %.

905 * as in the case of charged flavor-correlated decays this uncertainty can be possibly
 906 reduced with a new measurement of $B^0 \rightarrow \Lambda_c$ decays.

907 6.7 Continuum background modeling

908 Exemplary, fits used to estimate the impact of these uncertainties deriving from statistical
 909 uncertainties are shown here in Figures 89 - 90. Mean deviation values are then obtained
 910 for both the two-dimensional fit and the B_{tag} fit.

911

Fit	$-\sigma$	$+\sigma$	$\pm\bar{\sigma}$
2D	21	22	22
B_{tag}	5800	5800	5800

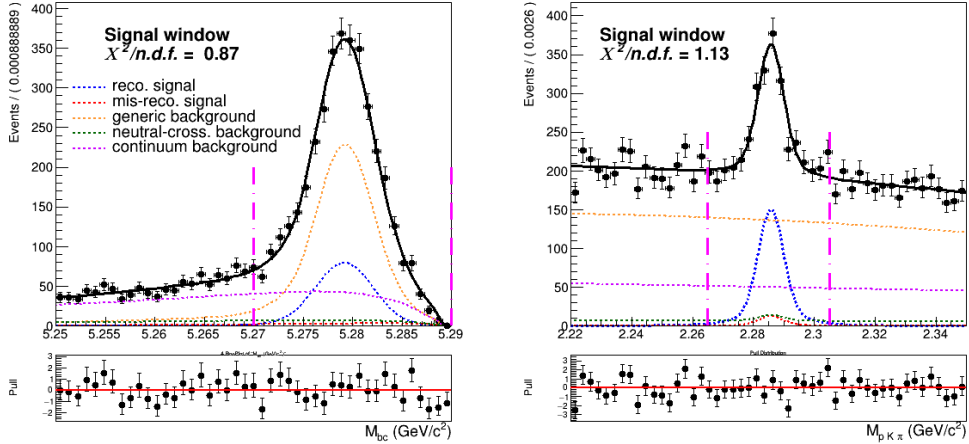


Figure (89) Signal window projections of a two dimensional fit on Monte Carlo simulated data where the shaping parameters were varied of their uncertainties.

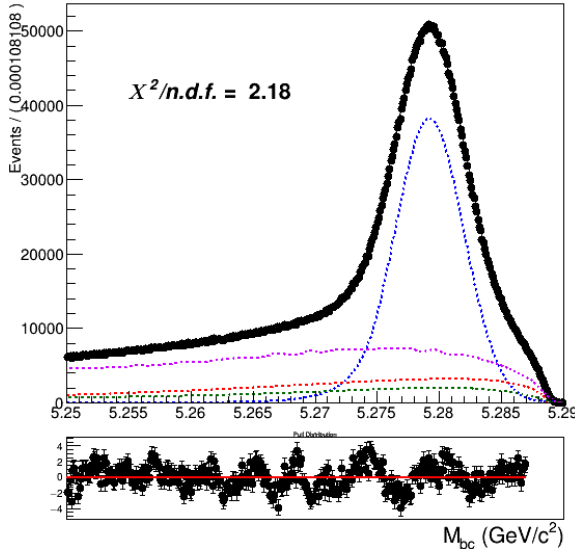


Figure (90) Fit of tagged B meson candidates on Monte Carlo simulated data where the shaping parameters were varied of their uncertainties.

912 The estimated systematic uncertainty on Br value from this source is 0.04%.

913 The continuum suppression cut is found to reject about 68% of the continuum back-
914 ground in data, whereas it rejects 64% of the continuum background in MC (66.5% in

915 on-resonance MC). This means that in data one can expect about 1.4% less continuum
 916 background events. The statistical uncertainty on this fraction of events can be also be
 917 taken into account as systematics. But again, as already seen in the case of charged flavor-
 918 correlated decays, the statistical uncertainty on the on-resonance continuum background
 919 events in MC originates a much larger systematic uncertainty: the relative systematic
 920 uncertainty deriving from the different impact on data of the continuum suppression would
 921 account for just 0.004% on the BR value (one order of magnitude smaller than systematics
 922 deriving from the statistical uncertainties). This second source is again consequently
 923 neglected.

924 6.8 Crossfeed background modeling

925 This source of systematic uncertainty is again estimated performing the fits varying the
 926 parameters of the Crossfeed PDFs by their uncertainties (see the table below for the
 927 deviations in terms of signal yields). The resulting absolute systematic uncertainty is
 928 about 0.006% on the BR value, which is rounded up to 0.01%.

Fit	$-\sigma$	$+\sigma$	$\pm\bar{\sigma}$
2D	3	3	3
B_{tag}	1500	1100	1300

Table (14) Offsets on the signal yields obtained varying the parameters of crossfeed background PDFs within their uncertainties in the two dimensional and B_{tag} fit and mean deviations reported in the last column.

929 6.9 Crossfeed ratio

930 As already done for the charged flavor-correlated decays, the systematic uncertainty
 931 on the crossfeed/misreconstructed signal "probability ratio" for the 2D fit and cross-
 932 feed/misreconstructed ratio is studied considering a maximal discrepancy up to 20%
 933 between Monte Carlo and data (the procedure adopted is the same as illustrated in
 934 Sec. 4.9).

Fit	$-\sigma$	$+\sigma$	$\pm\bar{\sigma}$
2D	4	8	6
B_{tag}	5800	800	3300

Table (15) Offsets on the signal yields obtained varying of $\pm 20\%$ the k ratio in the two dimensional and B_{tag} fit and mean deviations reported in the last column.

935 The estimated systematic uncertainty on Br value from this source is 0.01%.

936 **6.10 Parametrization of crossfeed normalization in the 2D fit**

937 The statistical uncertainties on the parameters used in the parametrization of crossfeed
938 normalization in the 2D fit are estimated to originate a systematic uncertainty of 0.01%
939 on the Br value.

940 **6.11 Crossfeed peaking fraction in the 2D fit**

941 As already done for the charged correlated decays, to estimate this systematic uncertainty
942 the amount of crossfeed events peaking in $M(pK\pi)$ was varied in order to cover the
943 uncertainties on the branching fraction for neutral decays and the two-dimensional fit
944 repeated with those values. The difference in signal yields obtained is reported in the
945 following table.

Fit	$-\sigma$	$+\sigma$	$\pm\bar{\sigma}$
2D	15	18	16

Table (16) Offsets on the signal yields obtained varying the amount of peaking crossfeed in the Λ_c invariant mass and mean deviation.

946 The uncertainty originated is estimated to be of 0.08% on the Br value.

947 **6.12 Efficiencies**

948 The ratio between the two FEI efficiencies is: $\frac{\epsilon_{FEI,sig}^+}{\epsilon_{FEI}^+} = 0.973 \pm 0.009$
949 The uncertainty on this value originates a systematic uncertainty of 0.01% on the Br
950 value. The Λ_c reconstruction efficiency is determined to be $\epsilon_{\Lambda_c} = 40.95 \pm 1.77\%$. When
951 propagating its uncertainty, a systematic error of 0.07% on the Br value is calculated.

952 **6.13 Fit biases**

953 The small bias on the reconstructed signal seen in the two-dimensional fit model produces
954 a not negligible systematic uncertainty on the branching fraction. The discrepancy in the
955 amount of the total signal estimated by the B_{tag} fit needs to be included as well in the
956 systematic effects. Propagating the two sources of systematics in the branching fraction
957 calculation results in an additional 0.05% uncertainty on the branching fraction value.

958 **6.14 Measured $B^+ \rightarrow \Lambda_c^+$ inclusive Branching Fraction**

959 Using the results from the two dimensional fit reported in Table 12 with all the needed
960 factors known, it's possible to examine the agreement between the the branching ratio
961 value used in MC generation and the measured ones. As in the charged flavor-correlated
962 decays the average of measured values are about 1σ statistical uncertainty away from

⁹⁶³ the average value of the branching ratio set in MC (actually already the average value
⁹⁶⁴ obtained with the total signal fits shows this tendency).

	total fit	signal fit	BELLE MC VALUE
stream 0	(1.32 ± 0.11)%	(1.19 ± 0.04)%	(1.233 ± 0.007)%
stream 1	(1.32 ± 0.11)%	(1.26 ± 0.05)%	(1.218 ± 0.007)%
stream 2	(1.37 ± 0.12)%	(1.29 ± 0.05)%	(1.218 ± 0.007)%
stream 3	(1.31 ± 0.11)%	(1.26 ± 0.05)%	(1.215 ± 0.007)%
stream 4	(1.50 ± 0.12)%	(1.26 ± 0.05)%	(1.218 ± 0.007)%
stream 5	(1.12 ± 0.12)%	(1.22 ± 0.05)%	(1.217 ± 0.007)%
average	(1.32 ± 0.05)%	(1.25 ± 0.02)%	(1.220 ± 0.003)%

Table (17) Measured branching fraction values obtained using the results listed in Table 12 for the six different streams (only statistical uncertainties are displayed) and its average.

⁹⁶⁵ As in the charged flavor-correlated decays the precision obtained on Monte Carlo simulated
⁹⁶⁶ data is improved by factors compared to the branching fraction measured by BaBar
⁹⁶⁷ experiment (see [?]).

968 Appendices

969 .1 $B^- \rightarrow \Lambda_c^+$ decays: additional plots

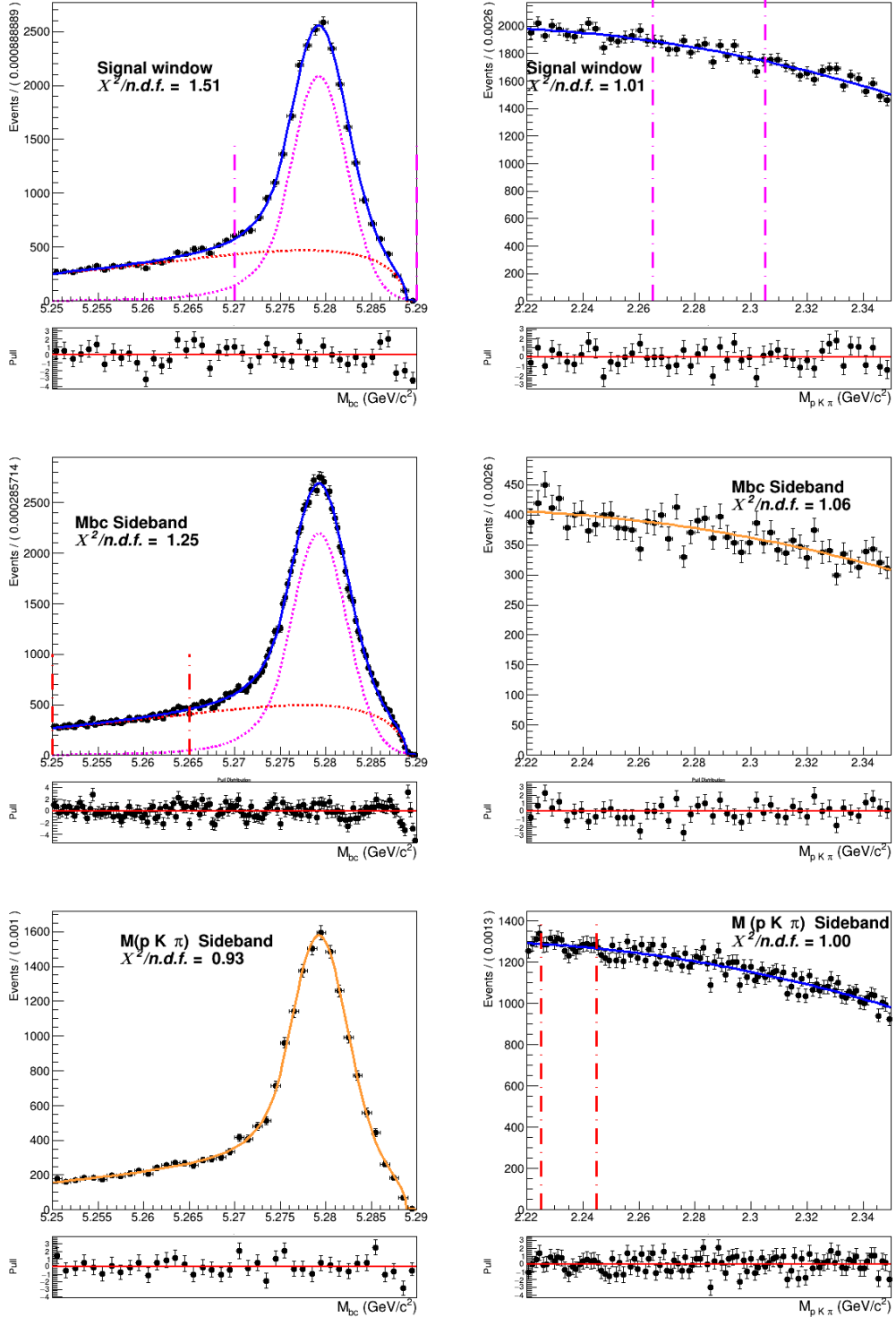


Figure (91) Signal region and sidebands of the two dimensional fit of generic background shown in Fig. 13

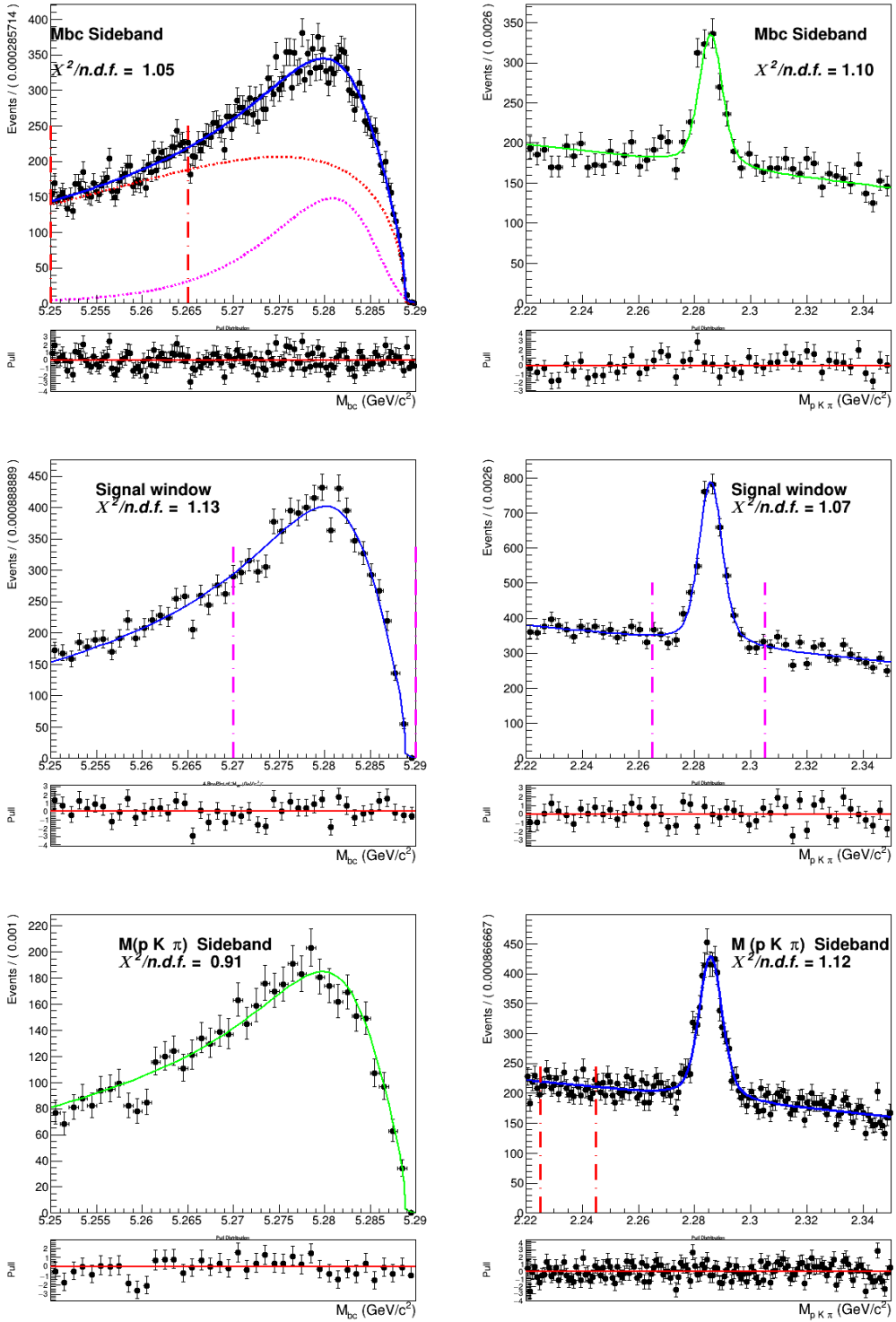


Figure (92) Signal region and sidebands of the two dimensional fit of crossfeed background after parametrization

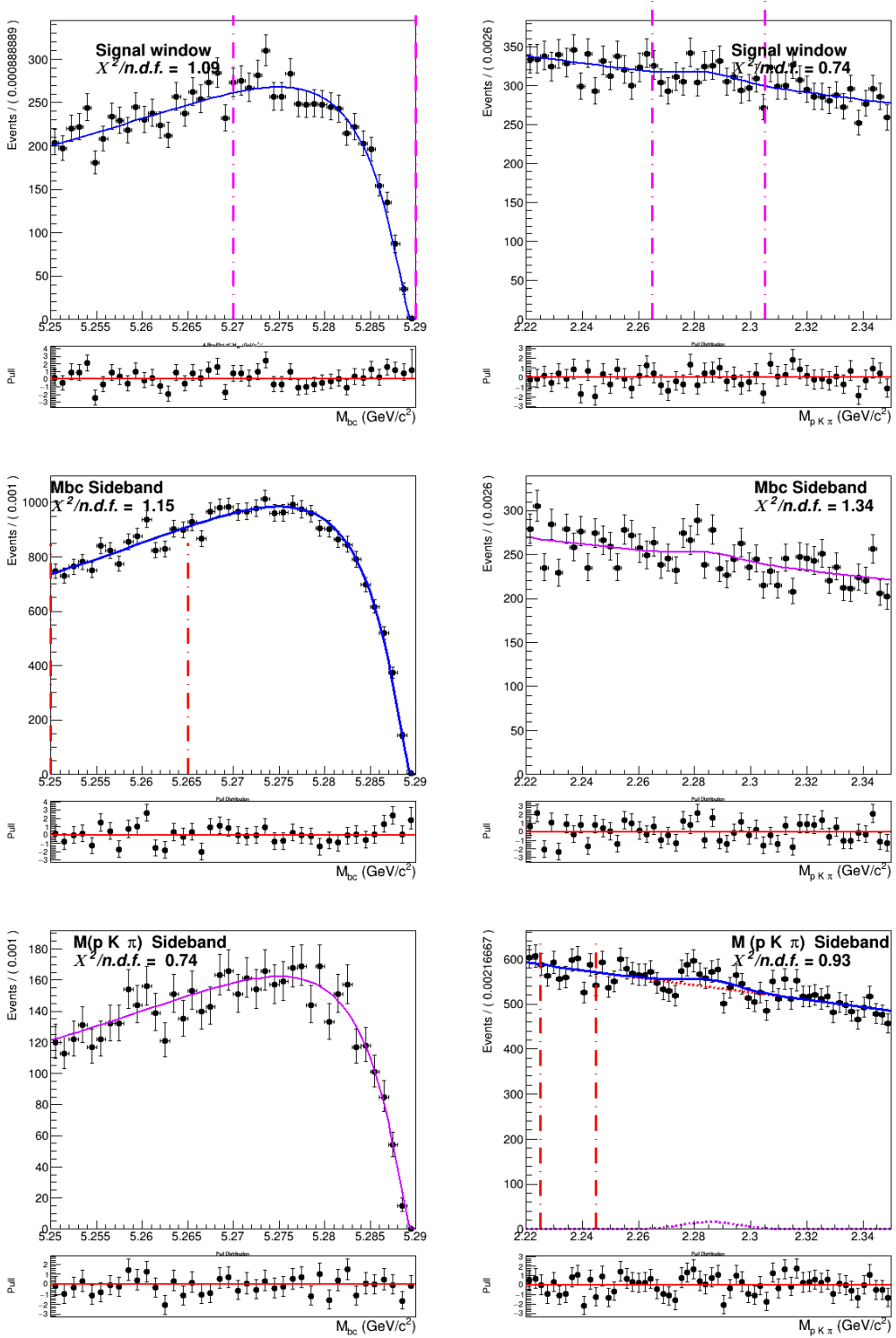


Figure (93) Signal region and sidebands of the two dimensional fit of continuum background shown in Fig. 33

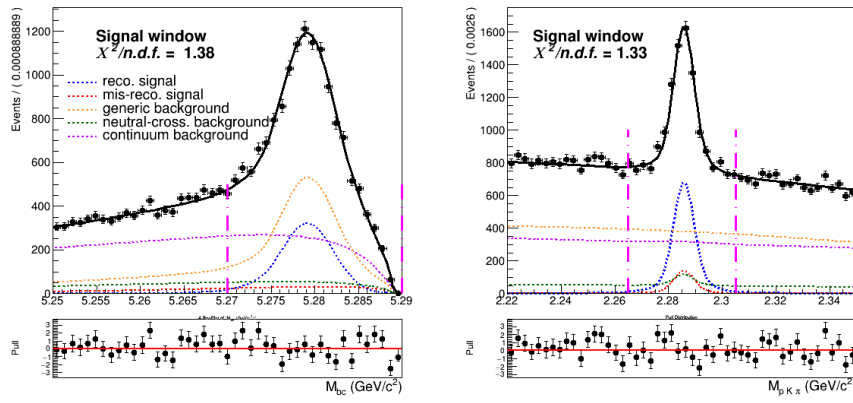


Figure (94) Signal region ($2.22 < M(pK\pi) < 2.35 \text{ GeV}/c^2$ and $5.27 < M_{bc} < 5.29 \text{ GeV}/c^2$) projections pf the dimensional fit on stream 0 Monte Carlo simulated data.

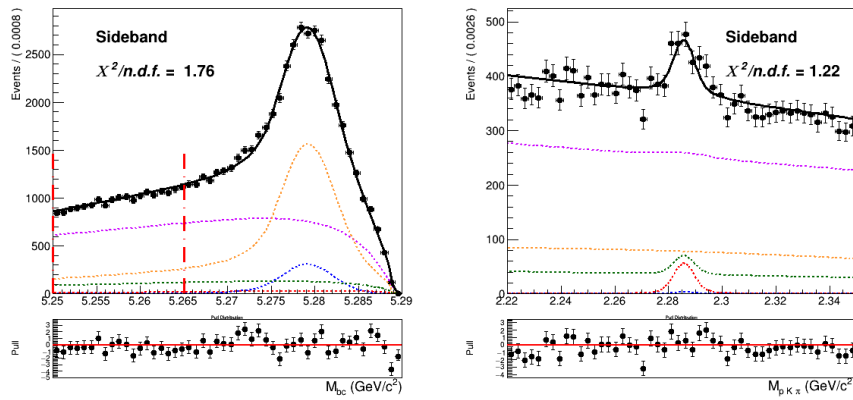


Figure (95) Sideband region of $5.25 < M_{bc} < 5.265 \text{ GeV}/c^2$ projection of the two dimensional fit on stream 0 Monte Carlo simulated data.

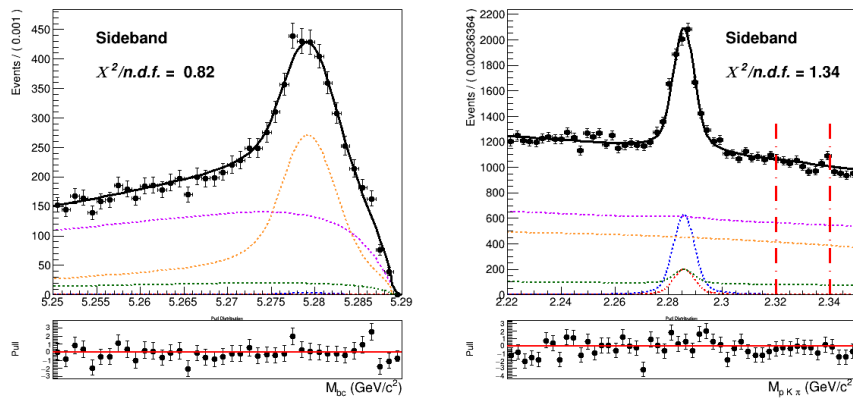


Figure (96) Sideband region of $2.22 < M(pK\pi) < 2.35 \text{ GeV}/c^2$ projection of the two dimensional fit on stream 0 Monte Carlo simulated data.

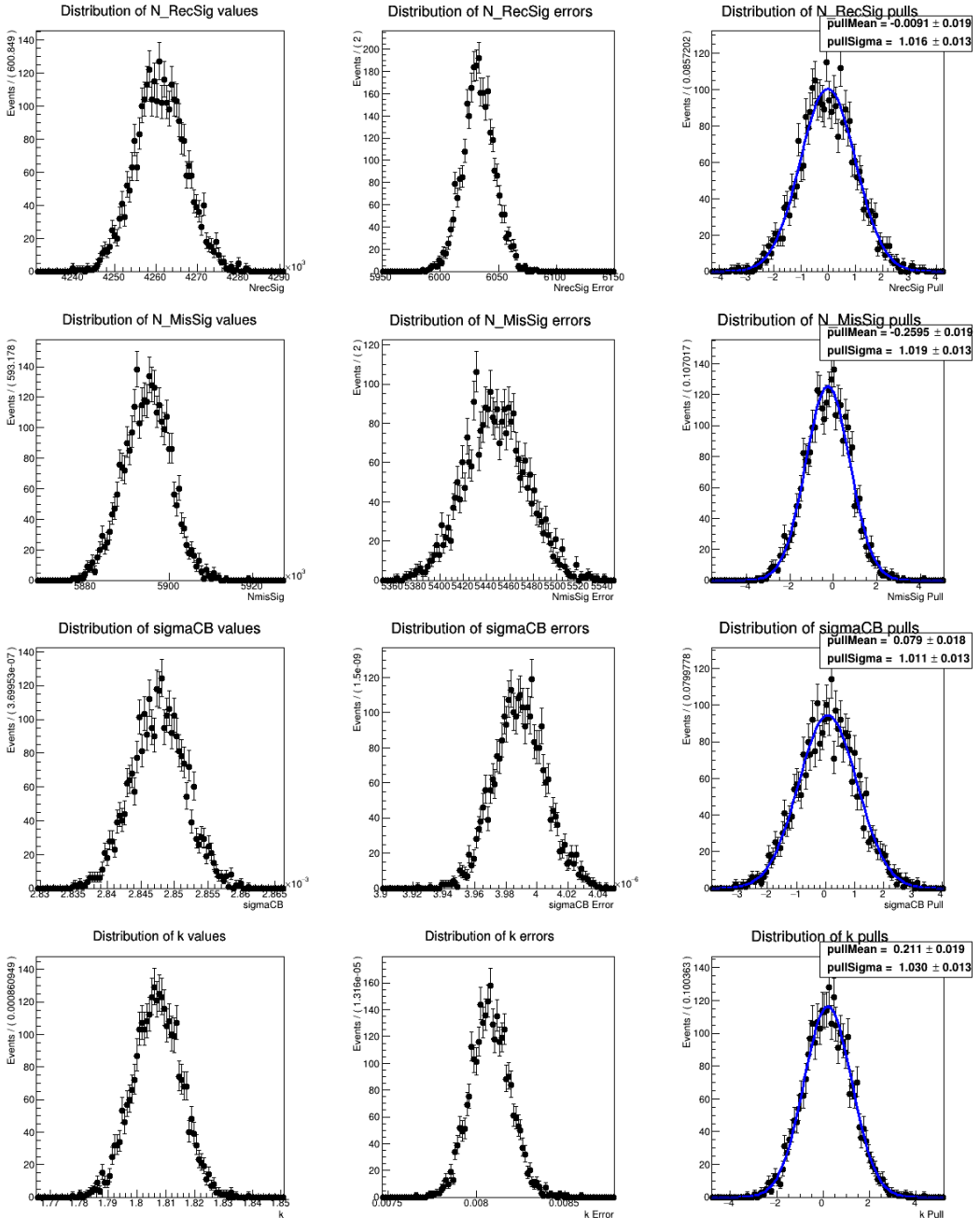


Figure (97) Toy MC study for the B_{tag} fit model described in Sec. 4.4

970 .2 $B^- \rightarrow D^0$ decays: additional plots

971 Figures 98-100 show the projections of signal regions and sidebands in M_{bc} and in the D^0
 972 invariant mass of the two dimensional fit on stream 0.

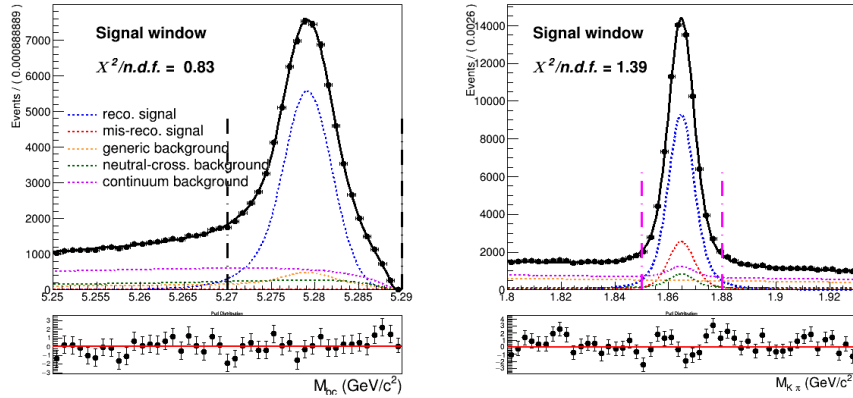


Figure (98) Signal region ($1.85 < M(\pi K) < 1.88 \text{ GeV}/c^2$ and $5.27 < M_{bc} < 5.29 \text{ GeV}/c^2$) projections of the two dimensional fit on stream0 (Fig. 57).

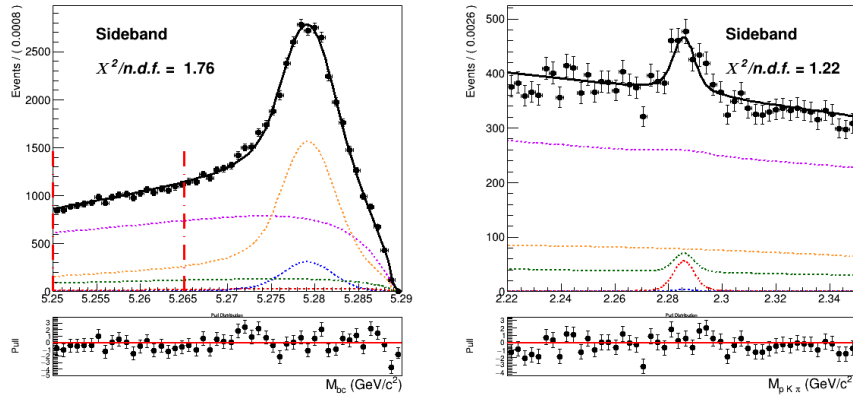


Figure (99) Sideband region of $5.25 < M_{bc} < 5.265 \text{ GeV}/c^2$ projection in $M(\pi K)$ of the two dimensional fit on stream 0.

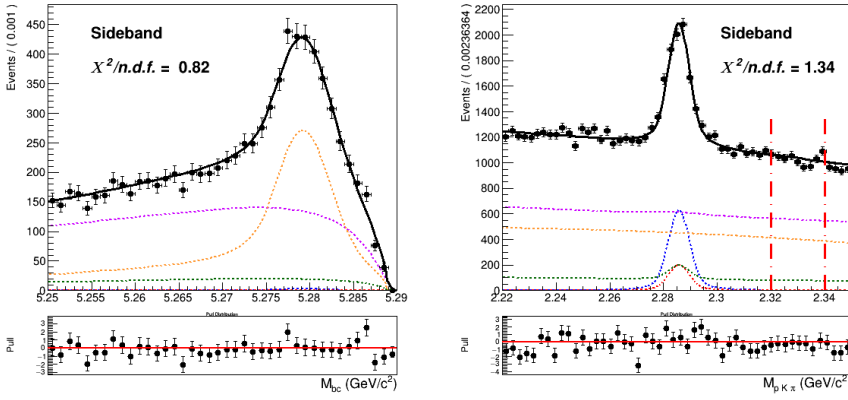


Figure (100) Sideband region of $1.8 < M(\pi K) < 1.84 \text{ GeV}/c^2$ projection in M_{bc} of the two dimensional fit on stream 0.

973 Figs. 101 to 103 show the projections in M_{bc} and in the D^0 invariant mass of the two
974 dimensional fit on data.

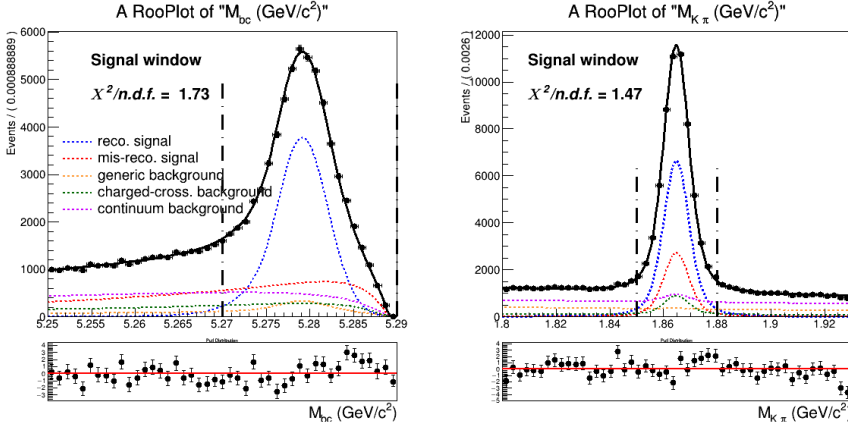


Figure (101) Signal region ($1.85 < M(\pi K) < 1.88 \text{ GeV}/c^2$ and $5.27 < M_{bc} < 5.29 \text{ GeV}/c^2$) projections of the two dimensional fit on data described in Sec. 5.6

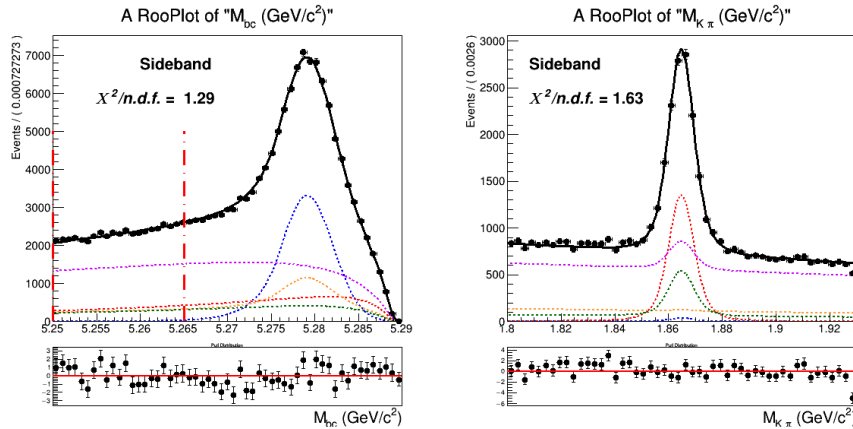


Figure (102) Sideband region of $5.25 < M_{bc} < 5.265 \text{ GeV}/c^2$ projection in $M(\pi K)$ of the two dimensional fit on data

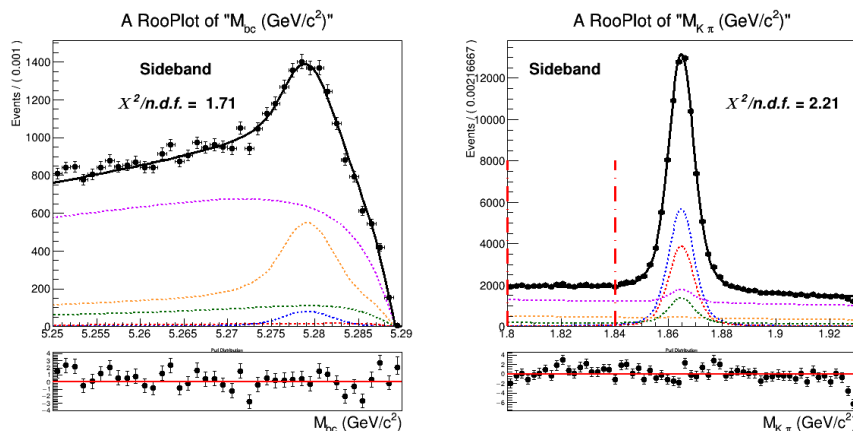


Figure (103) Sideband region of $1.8 < M(\pi K) < 1.84 \text{ GeV}/c^2$ projection in M_{bc} of the two dimensional fit on data.

.3 $B^- \rightarrow \bar{\Lambda}_c^-$ decays: additional plots

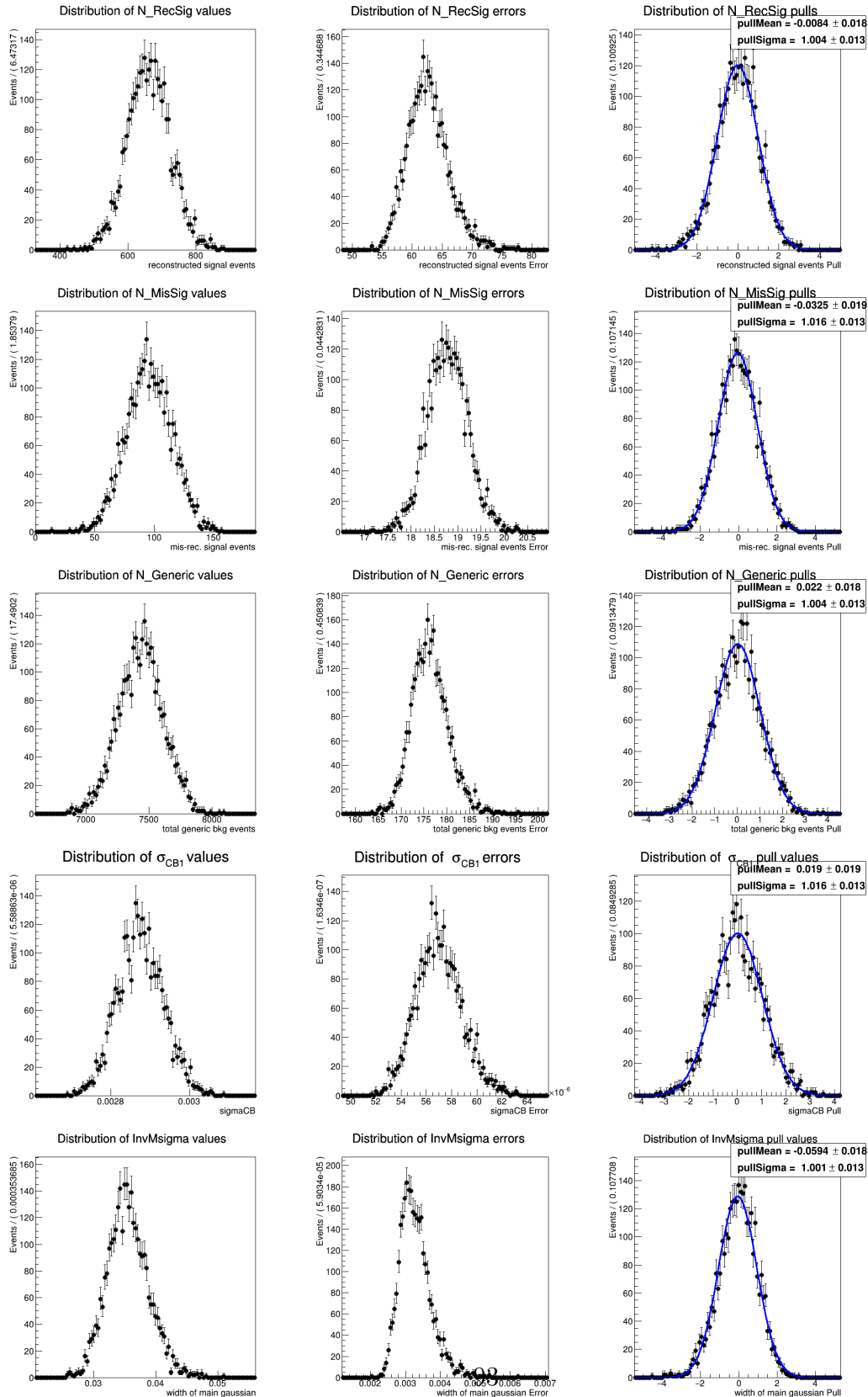


Figure (104) Toy MC study for the two dimensional fit model described in Sec. 6.2

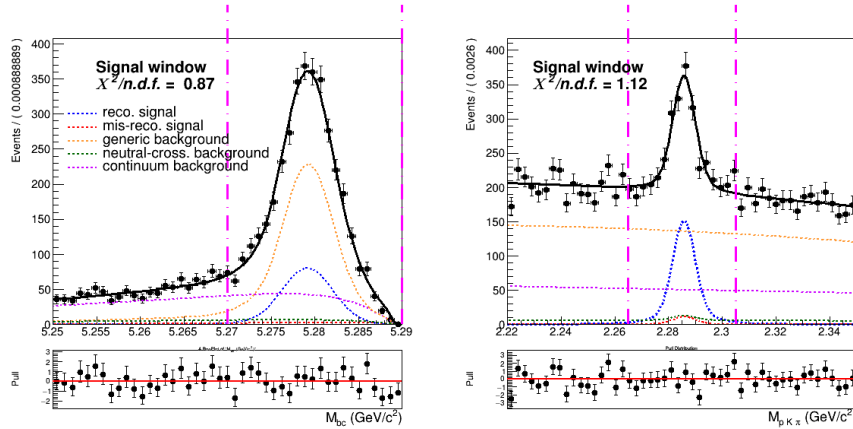


Figure (105) Signal region ($2.22 < M(pK\pi) < 2.35 \text{ GeV}/c^2$ and $5.27 < M_{bc} < 5.29 \text{ GeV}/c^2$) projections of the dimensional fit on stream 0 Monte Carlo simulated data.

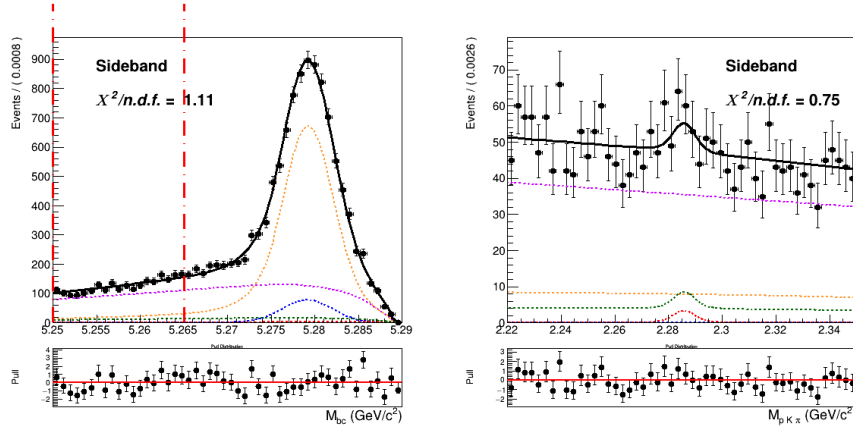


Figure (106) Sideband region of $5.25 < M_{bc} < 5.265 \text{ GeV}/c^2$ projection of the two dimensional fit on stream 0 Monte Carlo simulated data.

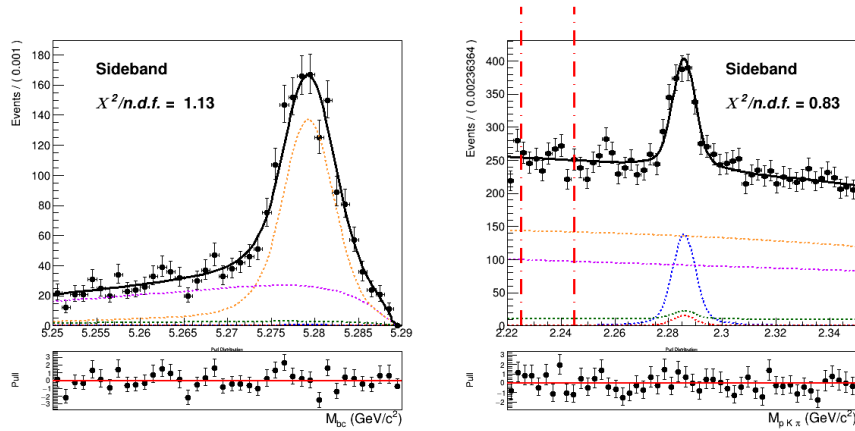


Figure (107) Sideband region of $2.22 < M(pK\pi) < 2.35 \text{ GeV}/c^2$ projection of the two dimensional fit on stream 0 Monte Carlo simulated data.

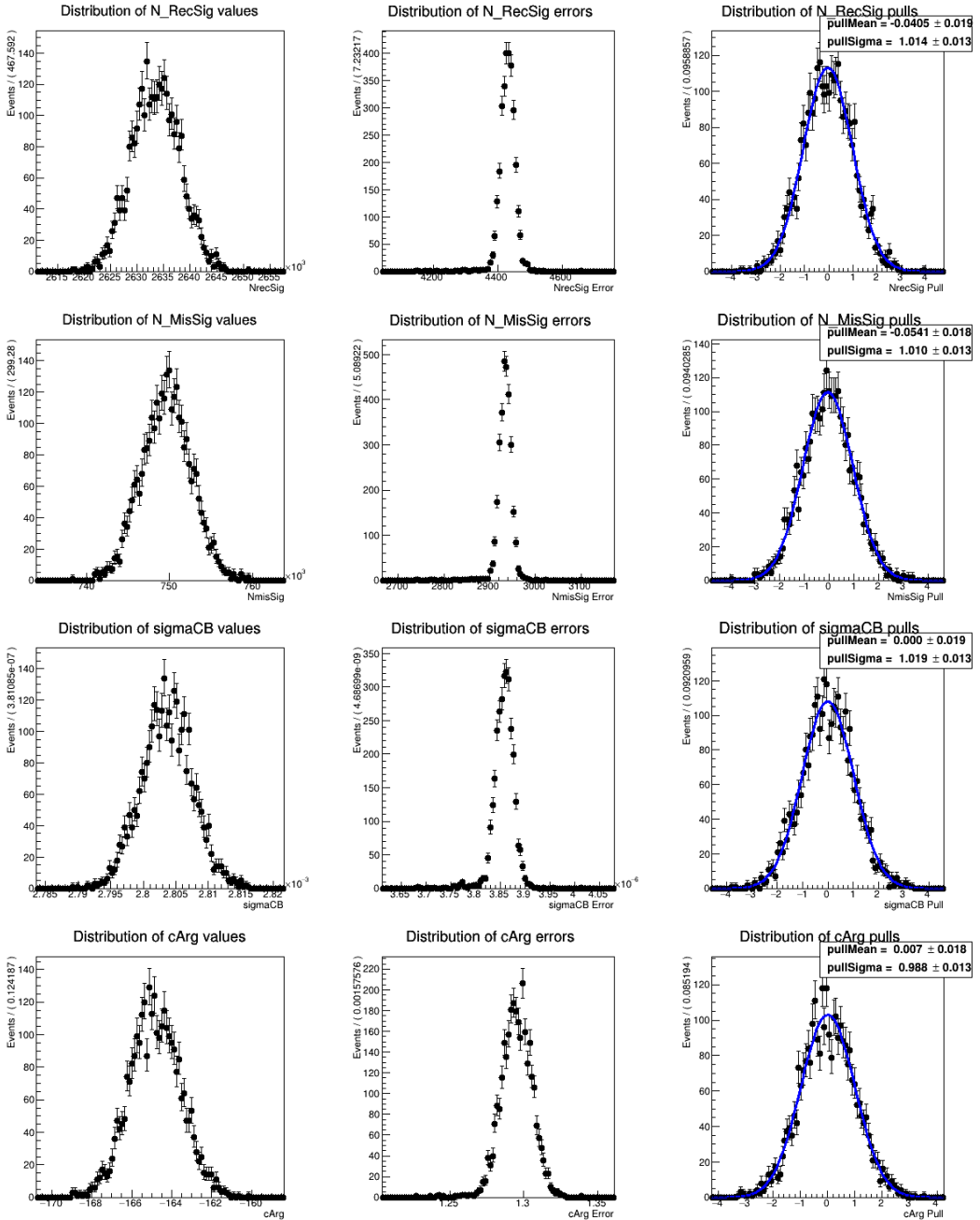


Figure (108) Toy MC study for the B_{tag} fit model described in Sec. 6.4

- 976 **References**
- 977 [1] B. Aubert et al., BaBar, *Study of inclusive B^- and \bar{B}^0 decays to flavor-tagged D , D_s*
978 *and Λ_c^+* , Phys. Rev. D **75** (2007) 072002, [arXiv:hep-ex/0606026](https://arxiv.org/abs/hep-ex/0606026).
- 979 [2] I. Grach, I. Narodetskii, S. Simula, and K. Ter-Martirosyan, *Exclusive and inclusive*
980 *weak decays of the B -meson*, Nuclear Physics B **502** (1997) no. 1-2, 227–248.
- 981 [3] M. Gelb, *Search for the Rare Decay $B^+ \rightarrow \ell^+ \nu_\ell \gamma$ with the Full Event Interpretation at*
982 *the Belle Experiment*. PhD thesis, Karlsruhe Institute of Technology (KIT), 2018.
- 983 [4] J. Schwab, *Calibration of the Full Event Interpretation for the Belle and the Belle II*
984 *Experiment*, Master's thesis, Karlsruhe Institute of Technology (KIT), 2017.
- 985 [5] K.-J. Tien and M.-Z. Wang, *Proton identification efficiency study*, BELLE NOTE 1279.
- 986 [6] S. Nishida, *Study of Kaon and Pion Identification Using Inclusive D^* Sample*, BELLE
987 NOTE 779.